

INFORMATION TO USERS

This manuscript has been reproduced from the microfilm master. UMI films the text directly from the original or copy submitted. Thus, some thesis and dissertation copies are in typewriter face, while others may be from any type of computer printer.

The quality of this reproduction is dependent upon the quality of the copy submitted. Broken or indistinct print, colored or poor quality illustrations and photographs, print bleedthrough, substandard margins, and improper alignment can adversely affect reproduction.

In the unlikely event that the author did not send UMI a complete manuscript and there are missing pages, these will be noted. Also, if unauthorized copyright material had to be removed, a note will indicate the deletion.

Oversize materials (e.g., maps, drawings, charts) are reproduced by sectioning the original, beginning at the upper left-hand corner and continuing from left to right in equal sections with small overlaps.

Photographs included in the original manuscript have been reproduced xerographically in this copy. Higher quality 6" x 9" black and white photographic prints are available for any photographs or illustrations appearing in this copy for an additional charge. Contact UMI directly to order.

ProQuest Information and Learning
300 North Zeeb Road, Ann Arbor, MI 48106-1346 USA
800-521-0600

UMI[®]

Uptake and Efflux of PAHs across Bacterial Cell Membranes

By

Trevor Bugg



**A thesis submitted to the Faculty of Graduate Studies and Research in partial fulfillment
of the requirements for the degree of Master of Science**

Department of Chemical and Materials Engineering and Biological Sciences

Edmonton, Alberta

Spring 2000



National Library
of Canada

Acquisitions and
Bibliographic Services

395 Wellington Street
Ottawa ON K1A 0N4
Canada

Bibliothèque nationale
du Canada

Acquisitions et
services bibliographiques

395, rue Wellington
Ottawa ON K1A 0N4
Canada

Your file *Votre référence*

Our file *Notre référence*

The author has granted a non-exclusive licence allowing the National Library of Canada to reproduce, loan, distribute or sell copies of this thesis in microform, paper or electronic formats.

The author retains ownership of the copyright in this thesis. Neither the thesis nor substantial extracts from it may be printed or otherwise reproduced without the author's permission.

L'auteur a accordé une licence non exclusive permettant à la Bibliothèque nationale du Canada de reproduire, prêter, distribuer ou vendre des copies de cette thèse sous la forme de microfiche/film, de reproduction sur papier ou sur format électronique.

L'auteur conserve la propriété du droit d'auteur qui protège cette thèse. Ni la thèse ni des extraits substantiels de celle-ci ne doivent être imprimés ou autrement reproduits sans son autorisation.

0-612-60096-3

Canada

University of Alberta

Library Release Form

Name of Author: Trevor Bugg

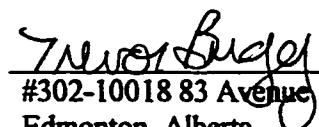
Title of Thesis: Uptake and Efflux of PAHs across Bacterial Cell Membranes

Degree: Master of Science

Year this Degree Granted: 2000

Permission is hereby granted to the University of Alberta Library to reproduce single copies of this thesis and to lend or sell such copies for private, scholarly, or scientific research purposes only.

The author reserves all other publication and other rights in association with the copyright in the thesis, and except as hereinbefore provided, neither the thesis nor any substantial portion thereof may be printed or otherwise reproduced in any material form whatever without the author's prior written permission.

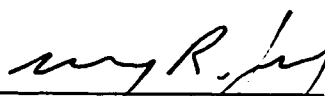

#302-10018 83 Avenue
Edmonton, Alberta
T6E 2C2

January 25, 2000


University of Alberta

Faculty of Graduate Studies and Research

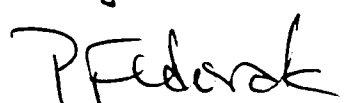
The undersigned certify that they have read, and recommend to the Faculty of Graduate Studies and Research for acceptance, a thesis entitled Uptake and Efflux of PAHs across Bacterial Cell Membranes submitted by Trevor Bugg in partial fulfillment of the requirements for the degree of Master of Science.




Dr. M.R. Gray, supervisor



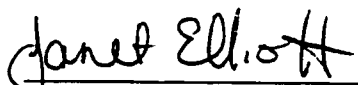
Dr. J. Foght



Dr. P. Fedorak



Dr. M. Pickard



Dr. J. Elliott

January 18, 2000

ABSTRACT

The objective of this study was to determine the mechanisms by which PAHs are transported in *Pseudomonas fluorescens* LP6a, a PAH-degrading bacterium. It was found that there are two conflicting transport mechanisms: uptake by passive diffusion and an energy driven efflux system to transport PAHs out of the cell. The efflux mechanism was found to be chromosomally encoded and constitutively expressed. *P. fluorescens* LP6a demonstrated a lack of saturation for the accumulation of phenanthrene in the cell and a lack of saturation of uptake and active efflux over the concentration range used. The efflux mechanism showed selectivity in that phenanthrene, anthracene and fluoranthene were transported out of the cell, but naphthalene was not. Data obtained on the transport of toluene were inconclusive. A model was developed to describe the transport of PAHs in LP6a. However, insufficient information could be obtained to determine unique parameters.

ACKNOWLEDGEMENTS

I would like to thank my supervisors Dr. M.R. Gray, Dr. P. Fedorak, Dr. J. Foght, and Dr. M.A. Pickard, and for their support and guidance. They provided direction, focus, and insight without which I could not have completed my studies.

I would like to thank Ruth Eckford for her help with the research and Dr. N. Miyata for his work on a related project.

I would like to thank A. Hashimoto and T. Hantos for their help and patience in teaching me microbiology methods and techniques. I would like to thank R. Mah for providing lab space in his already crowded lab.

I am grateful for the financial support of NSERC.

I would also like to express appreciation for the friends that have provided support along the way. They include Patricia Stelmack, Soheila Karimi, Shakir Japanwala, and Andrée Koenig. I would also like to thank the many friends that have helped provide stress relieve on numerous Friday afternoons. Finally, I could not have completed my research without the support of my family Richard, Nancy, and Michelle Bugg.

Table of Contents

1.0 INTRODUCTION	1
2.0 LITERATURE REVIEW	4
2.1 Bioremediation	4
2.1.1 Sources of PAH contamination	4
2.1.2 Toxicology of PAHs	6
2.1.3 Metabolic Pathways	6
2.1.4 Benefits of Bioremediation	10
2.1.5 Limitations of Bioremediation	12
2.2 Transport in Bacteria	16
2.2.1 Membrane Structures	16
2.2.2 Membrane Energetics	19
2.2.3 Passive Transport	22
2.2.4 Active Transport	24
2.2.5 Energy Inhibitors	25
2.3 Transport of Hydrophobic Compounds	27
2.3.1 Membrane Partitioning	28
2.3.2 Membrane Toxicity	31
2.3.3 Transport of PAHs	35
2.3.4 Active Efflux of Organic Solvents and Antibiotics	42
3.0 MATERIALS AND METHODS	46
3.1 Materials	46
3.1.1 Microorganisms	46
3.1.2 Polycyclic Aromatic Hydrocarbons	47
3.1.3 Inhibitors and Uncouplers	47
3.1.4 Other Compounds	47
3.2 Methods	48
3.2.1 Microbial Growth and Harvesting	48

3.2.2 Microbial Characterization	50
3.2.3 Analytical Techniques	52
3.2.4 Method Development	53
3.2.5 Transport of Phenanthrene Experiments	55
3.2.6 Positive and Negative Controls	56
3.2.7 Effect of Azide Concentration	58
3.2.8 Other Inhibitors	58
3.2.9 Partitioning Experiments	59
3.2.10 Transport of Other PAHs	59
3.2.11 Competitive Transport Experiments	60
3.2.12 Induction Experiments	61
3.2.13 Metabolite Extractions	61
3.2.14 Effect of Emulsifying Agent	63
 4.0 RESULTS AND DISCUSSION	 64
4.1 Characterization of Growth of Bacteria	64
4.2 Methodology	67
4.2.1 Treatment of Glassware	67
4.2.2 Filtration	68
4.2.3 Rapid Centrifugation	70
4.3 Positive Control	73
4.4 Uptake of Phenanthrene	76
4.4.1 Abiotic Partitioning	76
4.4.2 Biotic Transport	78
4.4.3 Procedural Evaluation	88
4.4.4 Negative Control	90
4.4.5 Azide Concentrations	93
4.4.6 Other Inhibitors of Electron Transport	95
4.4.7 Adsorption Isotherms	104
4.5 Transport of Other PAHs	108
4.6 Toluene Transport	127

List of Tables

Table 2.1 Aqueous solubilities and Log K_{ow} values for representative hydrophobic compounds (Mackay and Shiu, 1992)	29
Table 4.1 Summary of cell enumeration data for LP6a wild-type and mutant 1-51 strains.	66
Table 4.2 Summary of average liquid phase phenanthrene concentrations and variability in treated erlenmeyer flasks containing an initial concentration of 6.36 $\mu\text{mol/L}$	68
Table 4.3 Summary of the fractional amount of ^{14}C -phenanthrene retained by filters in filtration of abiotic controls.....	69
Table 4.4 Summary of results for rapid centrifugation tests with <i>S. cerevisiae</i> cells.....	72
Table 4.5 Comparison of partition coefficients obtained for LP6a mutant 1-51 strain to those reported by Sikkema et al. (1994) for single membrane liposomes.	138
Table 4.6 Summary of liquid phase phenanthrene concentrations as determined by HPLC	140
Table 4.7 Summary of liquid phase phenanthrene concentrations as determined by UV-visible spectroscopy of extract from supernatant samples	143

List of Figures

Figure 2.1: Molecular structures of representative PAHs	5
Figure 2.2: Pathway for the bacterial metabolism of naphthalene in <i>Pseudomonas putida</i> (Cerniglia, 1984)	8
Figure 2.3: Pathway for bacterial metabolism of anthracene in <i>Pseudomonas putida</i> (Cerniglia, 1984)	9
Figure 2.4: Schematic of phospholipids and phospholipid bilayer	17
Figure 2.5: Schematic of bacterial cell membrane and cell wall structures	19
Figure 2.6: Schematic of chemiosmosis generating the proton motive force.....	21
Figure 2.7: Structures of representative uncouplers	26
Figure 2.8: Structures of compounds that partition into membranes.....	32
Figure 2.9: Structure of polar aromatics subject to active transport.....	42
Figure 3.1 Schematic of filtration apparatus.....	54
Figure 4.1 Change in optical density over time for the LP6a wild-type and mutant 1-51 strains over the last 10 h of a 24-h incubation period.	65
Figure 4.2 Time dependence of a) supernatant phase and b) cell pellet phase isoleucine concentrations for the transport of isoleucine in <i>S. epidermidis</i>	74
Figure 4.3 Liquid phase phenanthrene concentration for partitioning in abiotic control. .	77
Figure 4.4 Time dependence of liquid phase and cell pellet ¹⁴ C concentrations for the transport of phenanthrene in LP6a wild-type strain. The data points are an average of three samples and the error bars represent one standard deviation.	79
Figure 4.5 Time dependence of liquid phase and cell pellet phenanthrene and metabolite concentrations for the transport of phenanthrene in LP6a wild-type.....	80
Figure 4.6 Time dependence of liquid phase and cell pellet ¹⁴ C concentrations for the transport of phenanthrene in LP6a mutant 1-51.....	82
Figure 4.7 Time dependence of liquid phase and cell pellet phenanthrene concentrations for the transport of phenanthrene in LP6a mutant 1-51.....	83

Figure 4.8 Time dependence of liquid phase and cell pellet ^{14}C concentrations for the transport of phenanthrene in LP6a cured strain.	86
Figure 4.9 Time dependence of liquid phase and cell pellet phenanthrene concentrations for the transport of phenanthrene in LP6a cured strain.	87
Figure 4.10 Time dependence of cell pellet ^{14}C concentrations for the transport of phenanthrene in LP6a mutant 1-51 as determined by filtration method.	89
Figure 4.11 Partitioning of phenanthrene between the liquid phase and cell pellet for the transport of phenanthrene in <i>A. vinelandii</i> UW.	91
Figure 4.12 Time dependence for cell pellet phenanthrene concentrations for LP6a mutant 1-51 in the presence of different azide concentrations.	92
Figure 4.13 Time dependence of liquid phase and cell pellet phenanthrene and metabolite concentrations for the transport of phenanthrene in LP6a wild-type in the presence and absence of 10 mM cyanide.	96
Figure 4.14 Time dependence of liquid phase and cell pellet phenanthrene concentrations for the transport of phenanthrene in LP6a mutant 1-51 in the presence and absence of 10 mM cyanide.	97
Figure 4.15 Time dependence of liquid phase and cell pellet phenanthrene and metabolite concentrations for the transport of phenanthrene in LP6a wild-type in the presence and absence of 50 μM CCCP.	98
Figure 4.16 Time dependence of liquid phase and cell pellet phenanthrene concentrations for the transport of phenanthrene in LP6a mutant 1-51 in the presence and absence of 50 μM CCCP.	100
Figure 4.17 Cell pellet phase-liquid phase partitioning isotherm for initial phenanthrene concentrations in LP6a wild-type and steady-state phenanthrene concentrations in LP6a mutant 1-51. The error bars represent the 95% confidence interval on the experimental values.	102
Figure 4.18 Cell pellet phase-liquid phase phenanthrene partitioning isotherm for equilibrium phenanthrene concentrations in LP6a mutant 1-51 in the presence of 120 mM azide. The error bars represent the 95% confidence interval on the experimental values.	103
Figure 4.19 Time dependence of liquid phase ^{14}C concentrations for the transport of anthracene in LP6a wild-type.	109
Figure 4.20 Time dependence of liquid phase and cell pellet anthracene and metabolites concentrations for the transport of anthracene in LP6a wild-type.	110

Figure 4.36 Time dependence of liquid phase and cell pellet toluene concentrations for the transport of toluene in LP6a mutant 1-51	132
Figure 4.37 Relationship between PAH partition coefficients with LP6a mutant 1-51 in the presence of azide and the corresponding K_{ow} (Mackay and Shiu, 1992). The error bars represent a 95% confidence interval on the partition coefficients.	136
Figure 4.38 Time dependence of liquid phase and cell pellet phenanthrene concentrations for the transport of phenanthrene in induced and non-induced LP6a mutant 1-51 cells.	146
Figure 4.39 Effect of anthracene addition on the transport of ^{14}C phenanthrene in LP6a mutant 1-51.	148
Figure 4.40 Effect of fluoranthene addition on the transport of ^{14}C phenanthrene in LP6a mutant 1-51.	149
Figure 4.41 Effect of naphthalene addition on the transport of ^{14}C phenanthrene in LP6a mutant 1-51.	150
Figure 4.42 Schematic of concentration gradients in bacteria and location of important parameters	152
Figure 4.43 Plots of equation 4-26 for a range of values of α and δ	165
Figure 4.44 Plot of α and δ values that give the experimentally obtained value of $f=6.74$ for phenanthrene transport	166
Figure 4.45 Plot of α and δ values that give the experimentally obtained value of $f=5.23$ for fluoranthene transport.....	168
Figure 4.46 Plot of α and δ values that give the experimentally obtained value of $f=2.80$ for anthracene transport	169

List of Nomenclature and Abbreviations

Abiotic: Physical-chemical effects; absence of biological factors.

ACS: Aqueous scintillation fluor.

Amorphous: Random structure.

Aromatic: Chemical structure whereby the electron density is delocalized and distributed evenly amongst the atoms in the structure.

ATP: Adenine triphosphate; a chemical that stores energy in phosphate bonds.

ATP synthase: A transmembrane protein that couples the addition of a phosphate group to ADP to the dissipation of the proton gradient across the cell membrane. Is reversible in that ATP can drive the extrusion of hydrogen ions.

Bioavailable: A measure of the accessibility of a compound to bacteria.

Biosurfactant: A surfactant or surface active agent produced by bacteria.

Biotic: Effects relating specifically to biological processes.

Brownian Motion: The random movement of molecules as a result of their kinetic energy and collisions with other molecules.

BCA: Bicinchoninic Acid

BSA: Bovine serum albumin; a protein used as a calibration standard for protein assays.

CCCP: Carbonyl cyanide m-chlorophenylhydrazone; an uncoupler.

CFU : Colony forming units; the number of cells that grow on agar media.

cpm: Counts per mintue; a measure of radioactivity.

Chemical potential: The energy associated with mass. A gradient in chemical potential drives mass transfer.

Co-metabolize: The degradation of a compound by an organism that does not utilize that compound as an energy source. The organism must rely on other substrates for growth.

Confidence Interval: A statistical range in which the true value is expected to be reside a certain percentage of the time.

Constitutively expressed: Proteins that are produced or transcribed which lack a chemical signal as a pre-requisite to its production.

Cytochrome: Metallo-enzyme structures in the electron transport chains.

Dioxygenase enzymes: The first enzymes in the metabolic cycle of PAH degradation.

DNP: Dinitrophenol; an uncoupler.

dpm: Disintegrations per minute; a measure of radioactivity.

Efflux: The movement of chemicals out of the cell.

Electroneutral: No net change in charge gradient during transport.

Equilibrium: A thermodynamic state in which the chemical potential gradient of the solute is zero.

Fick's Law: A mathematical expression that describes diffusion in bulk phases.

Flavoprotein: A protein containing a derivative of riboflavin. Acts as an electron carrier in the electron transport chain.

Gram-negative: Bacteria that contain two membrane structures: an inner and outer membrane.

Gram-positive: Bacteria that contain one membrane structure.

Glycosidic bonds: Chemical bonds formed between two sugar molecules as a result of a dehydration reaction between two hydroxyl groups.

HPLC: High performance liquid chromatography; an analytical technique.

Hydrophilic: Soluble in water.

Hydrophobic: Not soluble in water; Soluble in organic phases.

In-situ: In place; Treatment of soil and water without its removal from site.

Induction: The production of a protein from a gene sequence as a result of the presence of a specific chemical signal.

Inoculate: To add biological material to a system to initiate a microbial culture.

Inoculum: Biological material used to initiate a microbial culture.

Interface: The boundary between two phases.

Lag phase: A period of time during which there is either no observable changes in substrate concentration or no growth.

LPS: Lipopolysaccharide; a component of the outer cell membrane.

Mass transfer: The movement of molecules from one location to another.

NADH (Nicotineamide adenine dinucleotide): A chemical produced during metabolic cycles that stores energy in the hydrogen bond.

OD₆₀₀: Optical density at 600 nm.

Operon: A cluster of genes relating to a specific function.

Osmotic Balance: Regulation and balance of pressures inside and outside the cell that result from ion gradients and osmosis.

PAH: Polycyclic aromatic hydrocarbons.

Peptide Bonds: A chemical bond between amino acids as a result of a dehydration reaction between an amino group on one amino acid and a carboxyl group on another.

PCA: Plate count agar; a solid, nutrient rich medium.

Plasmid: A segment of DNA located outside of the chromosomal DNA.

Proton motive force: The chemical potential gradient resulting from the ion gradients across the bacterial cell membranes.

Redox reactions: Chemical reactions that involve the oxidation of one compound and the reduction of another.

Saccharides: Sugar molecules.

Stationary phase: A stage in the growth cycle in which exponential growth has ceased.

Steady-state: A dynamic state in which there are no net changes in concentrations over time; differs from equilibrium in that the compound has a non-zero chemical potential gradient.

Surfactant: A chemical that is surface active.

Synergism: The combined effects of two or more organisms, chemicals, etc. are greater than the sum of the independent effects of each.

Terminal electron acceptor: Chemicals that are reduced in the final step of respiratory cycles in cells.

Transition temperature: The temperature at which the membrane changes from a fluid structure to a gel structure.

Transposon: A genetic element with the ability to move from one site on the chromosome to another.

TSB: Tryptic soy broth; a nutrient rich culture medium.

Uniporter: A protein that transports a molecule without coupling its transport to another substrate or energy event.

Uptake: The movement of material into the cell.

UV-vis spectroscopy: UV-visible spectroscopy; an analytical technique.

Van der Waal's forces: electrostatic interactions between molecules as a result of temporary dipole moments.

List of Symbols

α : ratio of outer membrane to inner membrane partition coefficient

A : surface area (m^2)

A_i : surface area of inner membrane(m^2)

A_o : surface area of outer membrane(m^2)

C_c : cytoplasmic substrate concentration ($\mu\text{mol/L}$)

C_{liq} : liquid phase substrate concentration ($\mu\text{mol/L}$)

C'_{liq} : liquid phase substrate concentration at steady-state ($\mu\text{mol/L}$)

C_p : periplasmic substrate concentration ($\mu\text{mol/L}$)

δ : ratio of outer membrane to inner membrane permeability coefficient

F : Faraday's constant

J : flux ($\mu\text{mol/s}$)

K_{avg} : average liquid-cell partition coefficient (L/g dry wt)

K_m : affinity constant ($\mu\text{mol/L}$)

K_{im} : inner membrane partition coefficient (L/L)

K_{om} : outer membrane partition coefficient (L/L)

L : membrane thickness

P : membrane permeability (m/s)

P_{im} : inner membrane permeability (m/s)

P_{om} : outer membrane permeability (m/s)

ΔpH : pH gradient, logarithmic ratio of hydrogen ion concentrations outside and inside the cell.

R : gas Constant; 8.3145 J/mol.K

1.0 INTRODUCTION

Bioremediation provides a cost-effective option for the treatment of contaminated soils. Its versatility has allowed its application to the treatment of a broad range of compounds including hydrocarbons, chlorinated compounds, and heavy metals. Polycyclic aromatic hydrocarbons (PAHs) are one class of compounds on which there has been extensive research on biodegradation. There are numerous complex interactions involved in bioremediation including the PAH-soil interaction, bacterial-PAH interaction, and metabolic pathways that occur within the cell. Each of these can limit the rates and extents of biodegradation. The applicability of bioremediation is impeded by lengthy treatment times and residual concentrations that do not always meet government regulations. Therefore, there is a need to understand all the processes involved with the goal of increasing degradation rates for cost effectiveness and decreasing residual contamination for feasibility.

In bacteria, the enzymes involved in PAH degradation are typically intracellular. Given the high affinity of PAHs for adsorption to soil, the extremely low aqueous solubilities of PAHs, and a need for PAHs to enter bacteria for metabolism, the question arises as to how these compounds are transported across bacterial cell membranes. There has been little research published on the transport of PAHs in bacterial systems. However research with polar aromatics would suggest, there is potential for active transport. Experimentation also indicates that PAHs partition into the membranes of membrane vesicles. Partitioning allows for the possibility of passive transport. In contrast, research

on bacteria which are tolerant to organic solvents reveals the existence of energy mediated efflux pumps to remove toxic hydrophobic compounds from the membranes. Furthermore, there has been evidence linking toluene efflux pumps to antibiotic efflux pumps. The lack of selectivity suggests a generalized efflux pump for hydrophobic compounds. However, this concept conflicts with the metabolic needs of a PAH-degrading bacterium.

The objective of this research was to study the transport of PAHs across bacterial cell membranes. Research using a Gram-negative species, *Pseudomonas fluorescens* LP6a, that has been characterized as a strain capable of degrading and cometabolizing a range of PAHs. A transposon mutant of LP6a, designated 1-51, was also used because of its inability to produce dioxygenase enzymes for PAH metabolism (Foght and Westlake, 1996). The focus of the work was on the mechanisms by which PAHs were transported into the cell and on the presence of an active efflux pump for PAH removal from the bacteria. Using kinetic and partitioning data, a mathematical model describing the transport was sought. Experiments were set up such that data for the time dependence of transport could be obtained. Experiments were conducted both in the presence and absence of energy inhibitors to investigate energy mediated processes. The transport of a range of single PAHs was explored, as well as the transport of multiple PAHs to observe the occurrence of competition effects. Finally, the transport of toluene was studied to investigate a connection between PAH transport and organic solvent tolerance.

Given the low aqueous solubilities of PAHs, it was expected that these compounds would partition readily into membranes. Consequentially, it was hypothesized that uptake would occur by a passive diffusion process. Since LP6a is a PAH-degrading bacterium, the presence of an active efflux mechanism was not anticipated.

2.0 LITERATURE REVIEW

2.1 Bioremediation

Bioremediation is the application of biological agents, typically microbes, to degrade environmental pollutants. It is a natural process whereby microorganisms utilize or degrade the carbon and other nutrients in these compounds. As a result, much interest has been generated in the feasibility of bioremediation as a cost competitive alternative to physical and chemical treatment of contaminated sites. Conventional physical and chemical treatment methods include excavation of soil for landfill disposal or incineration, pumping and treating groundwater, and soil-vapour extraction (Alexander, 1994). Each of these physical and chemical technologies is limited to specific conditions. Bioremediation is a technology that can be used both on excavated soil and *in-situ* on a wide range on contaminants. This gives flexibility in its use.

2.1.1 Sources of PAH contamination

PAHs are aromatic compounds whose structure is comprised of multiple fused aromatic rings (Figure 2.1). They are natural compounds formed as byproducts of incomplete combustion. They are also present in fossil fuels. As a result, the primary sources of natural PAH contamination are forest fires, volcanic activity, and oil seepage. However, these sources are insignificant to generate ecological hazards. Our exploitation of fossil fuels has led to widespread PAH pollution. Anthropogenic sources include emissions from the processing and combustion of coal and oil, accidental spills, and the production

and use of petroleum products (Cerniglia, 1984). Thus, contamination is centered around oil and coal refining sites, gas stations, and creosote wood treatment sites. Extensive PAH pollution is compounded by the high degree of resistance of PAHs to physical, chemical, and biological degradation. As a result, these pollutants accumulate in the environment posing potential toxicity problems.

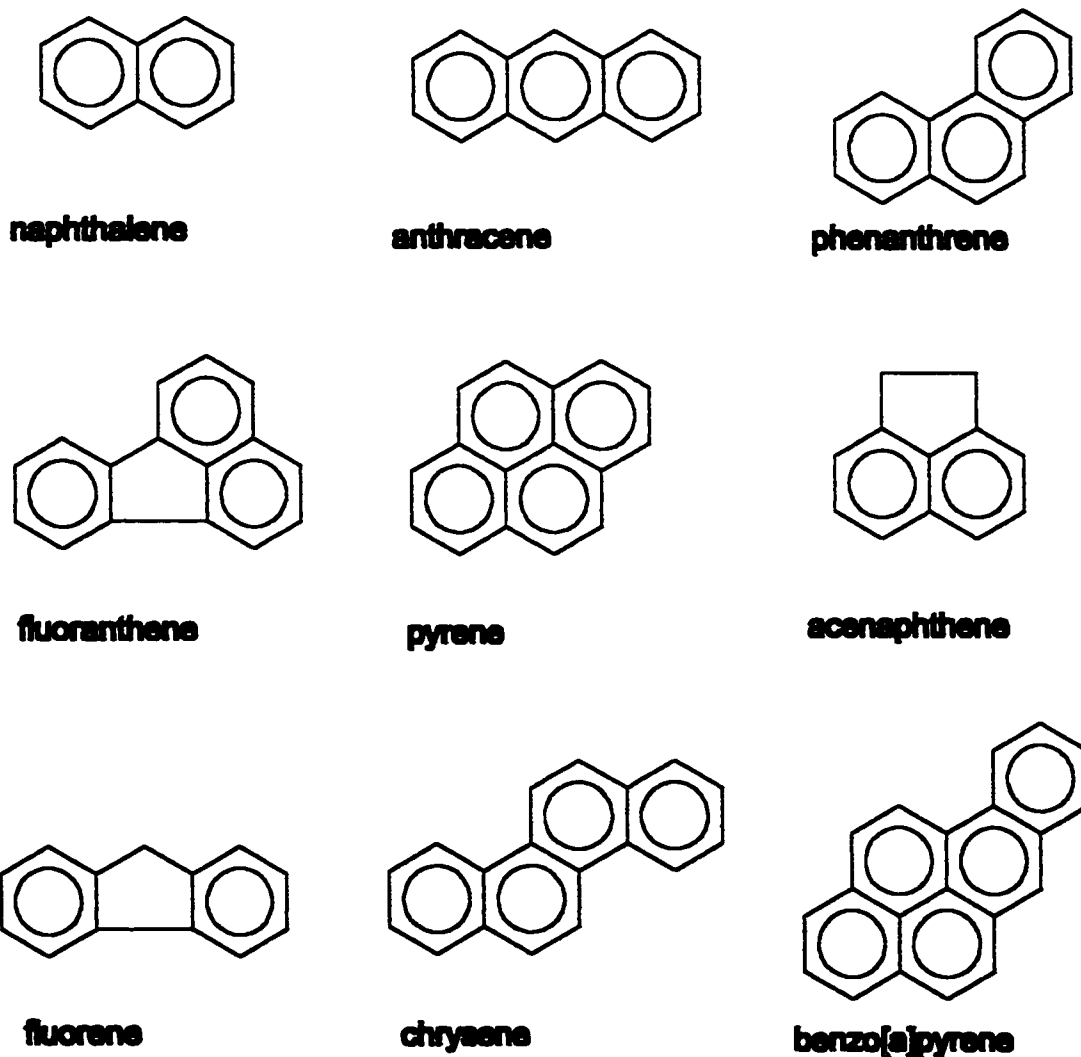


Figure 2.1: Molecular structures of representative PAHs

2.1.2 Toxicology of PAHs

Some PAHs pose health concerns to the human population. While short term, acute exposure is potentially harmful, the primary source of human exposure is long term, low level pollution. A major concern with PAH toxicity is the potential for these compounds to be carcinogenic (Keuth and Rehm, 1991). The carcinogenic effects arise not from the parent compound, but from certain PAH metabolites that are produced in the body. The mammalian oxidation of PAHs can produce organic-soluble metabolites like epoxides, phenols, sulfate esters, quinones, dihydrodiol epoxides, and tetraols (Pothuluri and Cerniglia, 1994). The most extensively studied system is metabolism of benzo[a]pyrene. The two isomers of the 7,8-diol-9,10 epoxide metabolite are mutagenic (Manahan, 1990). Other carcinogenic PAHs include benzo[a]anthracene, 3-methylcholanthrene, fluoranthene and 1-nitropyrene (Pothuluri and Cerniglia, 1994). Naphthalene has slightly different toxicity properties as a result of its volatility. There is the potential for acute exposure whereupon one can suffer from anemia, reductions in red cell count and hemoglobin, skin irritation, and headaches (Manahan, 1990). Due to their resistance to degradation, these compounds accumulate in the environment. Given the importance of fossil fuels in our society, PAH pollution will persist. Consequently, we must focus on means to remediate PAH contaminated sites.

2.1.3 Metabolic Pathways

PAHs are degraded by intracellular enzymes in soil bacteria such as *Pseudomonas*, *Rhodococcus*, *Mycobacterium*, and *Flavobacterium*. As a result, there is a need for the transport of PAHs into cells. There are many different metabolic pathways for the

degradation of PAHs. In bacteria, the conventional aerobic pathway involves the addition of two oxygen atoms onto the aromatic ring to form a dihydrodiol (Cerniglia, 1984). This reaction is carried out by dioxygenase enzymes. This reaction is also stereospecific in that only the *cis* isomer is formed. For naphthalene degradation, naphthalene is converted to *cis*-1,2-dihydroxy-1,2-dihydronaphthalene by naphthalene dioxygenase (Figure 2.2). This initial step imparts two important structural features to the PAH. Firstly, it destabilizes the aromatic structure of the compound, making the compound easier to degrade. Secondly, it renders the compound polar. The change in polarity increases the aqueous solubility of the compound. Thus, the metabolite will not partition into cell membranes and it will not adsorb to organic matter in the soil should it leak across the cell membranes. Following oxidation of the compound, the PAH is reduced by dehydrogenase enzymes to form a diol structure; 1,2-dihydroxy-1,2-dihydronaphthalene is reduced to 1,2-dihydroxynaphthalene. This process returns the aromatic structure to the compound, but the polarity remains. The next step is a ring cleavage step to form *cis*-*o*-hydroxybenzalpyruvic acid, which undergoes a number of conversions to salicylic acid and then to catechol. In three steps, a two ring non-polar structure has been converted to a one ring polar structure. Catechol proceeds to be mineralized starting with ring cleavage. The metabolism of PAHs with a higher number of rings occurs by a similar process with subsequent reduction in the number of rings to reach catechol. As an example, anthracene is attacked by dioxygenase enzymes to form a dihydrodiol (Figure 2.3). The dihydrodiol is converted to a diol and eventually, after ring cleavage, to 2,3-dihydroxynaphthalene (Cerniglia, 1984). This compound is very similar in structure to 1,2-dihydroxynaphthalene in the naphthalene degradation pathway. Thus,

its degradative pathway to catechol will resemble that in the naphthalene degradation pathway. However, since it is a different isomer, the degradation of 2,3-dihydroxynaphthalene may require different enzymes than those needed for the degradation of 1,2-dihydroxynaphthalene. The similarities in metabolic cycles between the different PAHs often allow bacteria to degrade a range of PAHs. However, slight differences in isomers can also restrict that range.

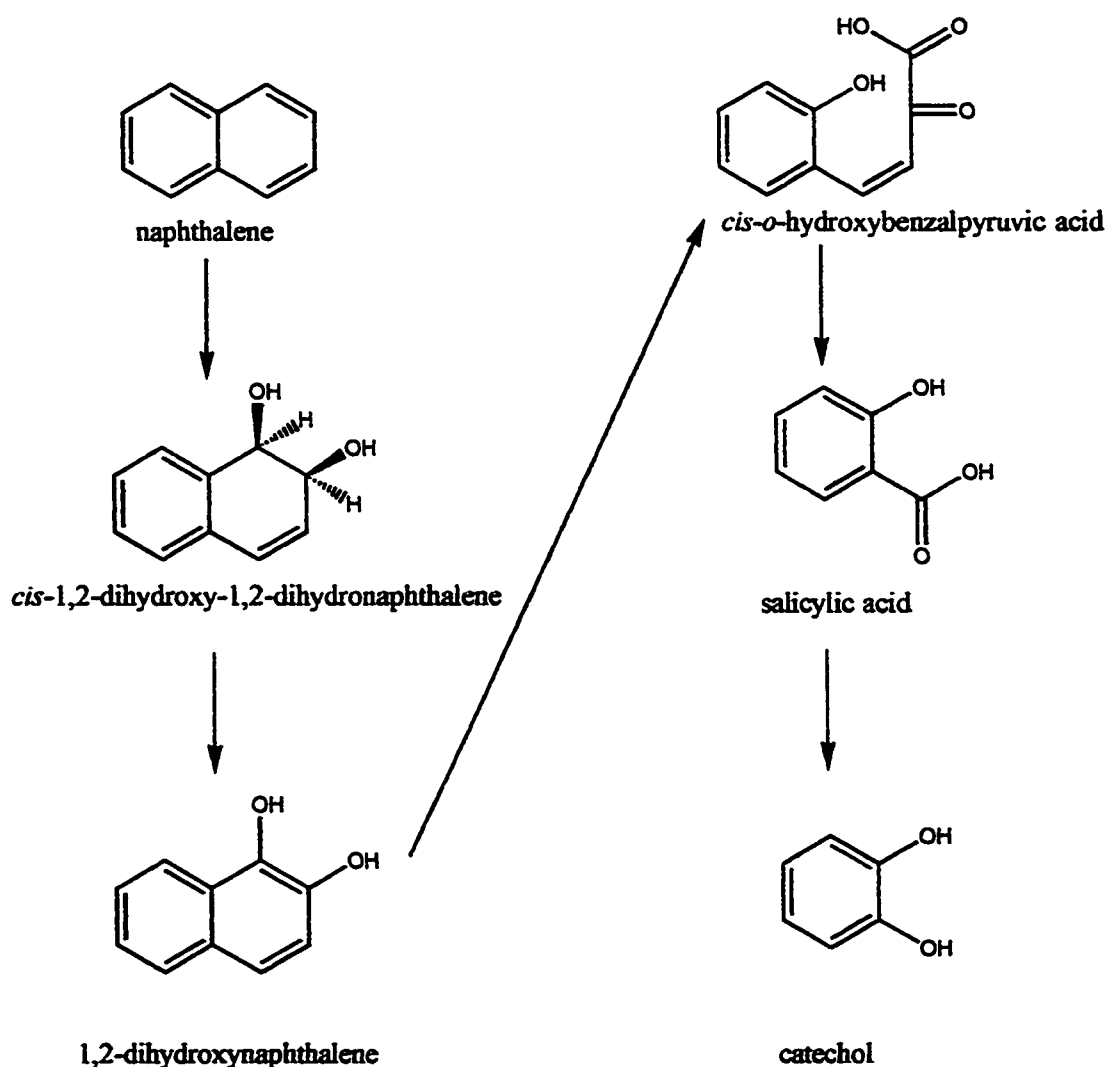


Figure 2.2: Pathway for the bacterial metabolism of naphthalene in *Pseudomonas putida* (Cerniglia, 1984)

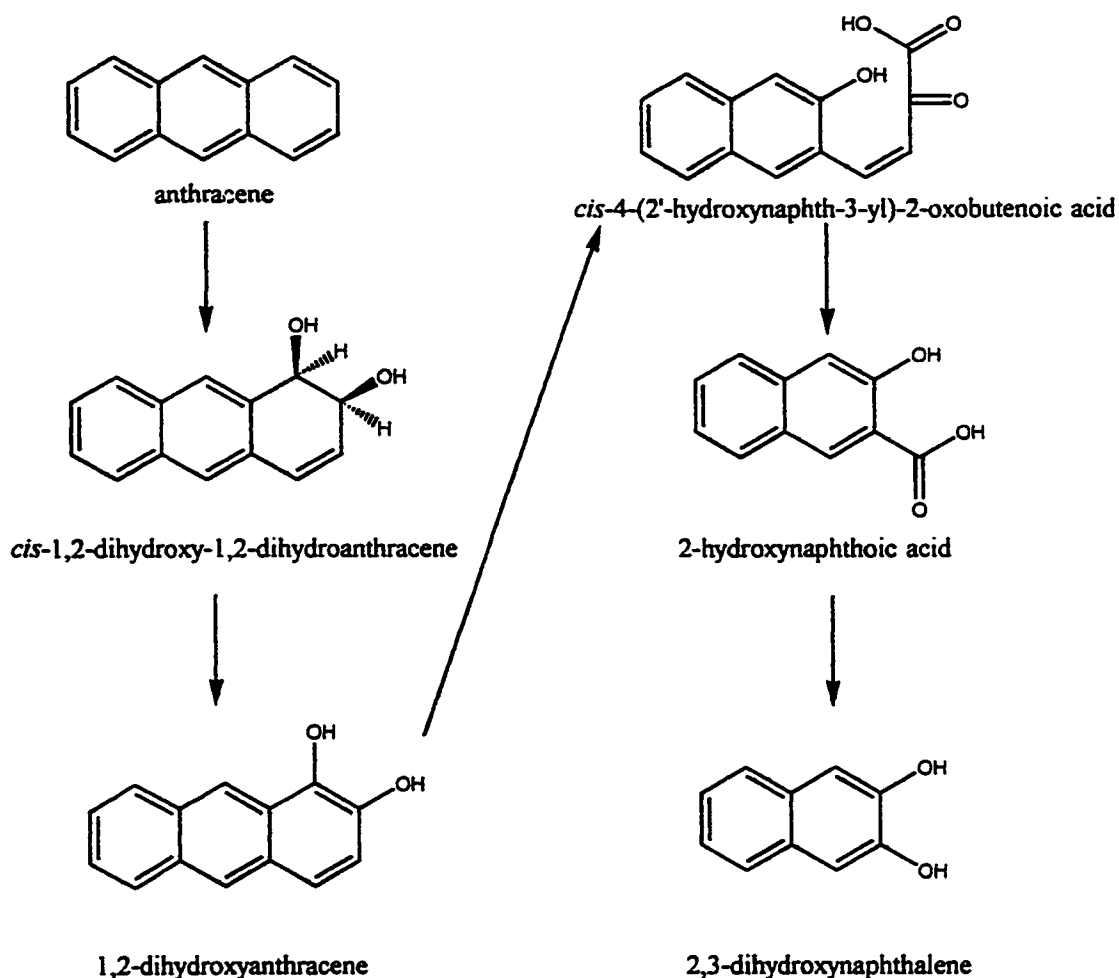


Figure 2.3: Pathway for bacterial metabolism of anthracene in *Pseudomonas putida* (Cerniglia, 1984)

An alternate variation on the phenanthrene degradation pathway begins in a similar direction as the one presented in Figure 2.3. However, 1-hydroxy-2-naphthoic acid is produced instead of the isomer 2-hydroxynaphthoic acid shown in Figure 2.3. This metabolite can then be converted to 1,2-dihydroxynaphthalene and be degraded as shown in the naphthalene pathway (Figure 2.2). It can also undergo ring cleavage to produce a phthalic acid structure (Pothuluri and Cerniglia, 1994). When PAHs have substituent

groups or are more complex in structure, there is greater variety in degradation pathways.

Fluorene (Figure 2.1) can be degraded in an analogous manner naphthalene through dioxygenase enzyme to form a *cis*-dihydrodihydroxy structure. Alternatively, it can be oxidized by monooxygenase enzymes at the 9 position on the central ring to form 9-fluorenol (Cookson, 1995). Similarly, one proposed route for acenaphthene degradation is the addition of a single oxygen by monooxygenase enzymes to the cyclopentane ring to form 1-acenaphthol (Pothuluri and Cerniglia, 1994). With higher molecular weight PAHs, there are numerous sites for enzymes to attack. Benzo[a]anthracene can follow two routes that produce isomeric metabolites of phenanthrene based structures or it can be degraded by a third route that produces metabolites whose structure is based on anthracene (Cookson, 1990).

Fungal oxidation of PAHs differ significantly from bacterial metabolic pathways.

Bacteria make use of monooxygenase enzyme to add an oxygen atom to the PAH and form an epoxide structure. This structure is then hydrated to form *trans* dihydrodiol structures. Fungal monooxygenase enzymes appear less specific in their site of attack and many isomers of metabolites can be produced. Additionally, monooxygenases can continue to attack metabolites, producing tetraol structures (Cookson, 1990).

2.1.4 Benefits of Bioremediation

Bioremediation provides a natural means by which to treat contaminated soil. The presence of indigenous PAH-degrading microflora, nutrients, and water results in the natural biodegradation of contaminants. The goal of engineers in remediating a site is to

stimulate and enhance the rate and extent at which it proceeds. As a result, bioremediation is often a cost effective alternative to the more conventional physical and chemical treatment options like soil excavation for landfill or incineration, pumping and treating of groundwater, and soil-vapour extraction. A survey that compared bioremediation to conventional treatment technologies over a range of 55 contaminated sites in the Tennessee region found that bioremediation was usually either comparable or more effective on a cost basis to conventional treatment technologies. (Davis et al., 1995). In particular, bioremediation was most cost effective in treating smaller volumes of soil and in treating smaller concentrations of contaminants.

Microorganisms show great diversity in degrading a wide range of pollutants. If they are unable to utilize a compound directly as a carbon source, they can often co-metabolize it to an extent. Through co-metabolism, microorganisms work synergistically to degrade otherwise highly resistant and toxic compounds. Bacteria also have great adaptability to different environments. They can operate in extremely cold environments where some chemical treatment technologies might otherwise have problems. In anaerobic environments, there are bacteria that are able to use terminal electron acceptors other than oxygen to initiate biodegradation (Alexander, 1994). Bioremediation offers a natural treatment option that often does not require the addition of chemicals to the soil. Bacteria are ubiquitous in the environment which has given bioremediation extensive flexibility in its application. Furthermore, bioremediation can also be combined with other treatment technologies to provide an optimized remediation solution.

Bioremediation can be applied *in-situ* or *ex-situ*. *In-situ* treatment options include bioaugmentation, biostimulation, intrinsic bioremediation. Bioaugmentation involves inoculating the soil with an active culture that has the ability to degrade the target compounds. Biostimulation is the application of nutrients or alternate carbon sources to stimulate the activity of indigenous bacteria. Intrinsic remediation is the monitoring of natural degradation processes of the target compounds. It is a cost effective option at sites where there may be no time restrictions (King et al., 1998). *Ex-situ* bioremediation options involve the excavation of soil for off-site treatment by such methods as land farming, biopiles, and bioreactors (Cookson, 1995).

2.1.5 Limitations of Bioremediation

Like all technologies, bioremediation has limitations. These limitations often center on the metabolic and physiological requirements of bacteria. One of the main restrictions on the applicability of bioremediation is the time required. Bioremediation often takes more time than other treatment options; particularly soil excavation for landfill or incineration. Also, the end point of bioremediation does not always meet government regulations. Thus, business considerations and site usage may necessitate other treatment options.

Bacteria have metabolic and physiological requirements that can limit biodegradation rates. If the temperature is sub-optimal, as it often is with cool ground temperatures, growth and metabolic rates are decreased. Nutrients or terminal electron acceptors may be limiting. Oxygen addition is often a key component since aerobic degradation proceeds significantly faster than anaerobic degradation. However, mass transfer

problems in getting oxygen to all regions of the soil limit the effectiveness of oxygen addition for *in-situ* treatment. Different modes of oxygen delivery from pumping air, pure oxygen, or hydrogen peroxide have all been explored. Air has the advantages of being inexpensive but it can also be ineffective. Pure oxygen will greatly enhance mass transfer. However, the safety precautions for handling pure oxygen become expensive. Hydrogen peroxide has the advantage that it is water soluble and so its distribution can be controlled by groundwater movement. Furthermore, there is an equilibrium between the peroxide and oxygen. This balance can control oxygen delivery and ensure better distribution of oxygen through the contaminated zone. However, the active bacteria must be resistant to the concentrations of peroxide used (Cookson, 1995).

Two important nutrients for bacteria are nitrogen and phosphorous. Both are important in the synthesis of biochemical molecules for the cell. Additionally, moisture is an important component since ion transport is important in bacteria. Optimal soil moisture content is typically in the range of 10 – 25 % wt (King et al., 1998). The addition of nutrients or oxygen to can increase site remediation costs and may compromise the economical advantage of bioremediation.

There is often a lag phase during bioremediation. The lag phase can be the result of a lack of an active degrading population, a need for induction of enzymes, or an insufficient number of bacteria to create significant changes in contaminant levels. The lag phase can also be caused by the presence of a toxic agent, usually the pollutants in question. Until levels of the pollutant drop below the point at which they are no longer

toxic, there may be limited biodegradation. This problem can often be mitigated by the addition of an active degrading bacterial population to the site (Alexander, 1994).

Another problem limiting biodegradation rates is the presence of a more favourable carbon source. In this situation, biodegradation of the target toxic compounds does not proceed until the more favourable carbon source is removed from the system. In PAH biodegradation this situation may be one cause of sequential PAH degradation. It has been observed that metabolism of higher molecular weight PAHs does not occur until the disappearance of the lower molecular weight ones (Stringfellow and Aitken, 1995). This process can increase the remediation time at sites contaminated by multiple PAHs. In the reverse situation, the compound may be co-metabolized, but biodegradation does not occur because of the lack of a substrate to support growth. In such cases, a carbon source must be added to the system. With the addition of a carbon source or nutrient, there is a requirement to track its concentration and ensure that residual levels following site remediation meet government regulations. As a result, site remediation costs increase. There are a number of factors that can all contribute to sub-optimal rates of metabolism. These factors cause prolonged treatment times and put constraints on the applicability of bioremediation.

Limitations on the extent of pollutant removal can hinder the use of bioremediation. Residual concentrations can sometimes be higher than government regulations, which makes bioremediation unsuitable in certain circumstances. The limited extent of bioremediation is a poorly understood phenomenon. It is believed to be caused primarily

by the lack of availability of the pollutant to the bacteria. There are a number of factors that control bioavailability. Three hypotheses have been developed on how pollutants are made bioavailable: dissolution of the pollutant into the aqueous phase, direct contact between the cell and the pollutant, or microemulsion of the pollutant by surfactants and biosurfactants (Bouchez, et al., 1997). As a result, the interaction of the pollutant with the soil is a key component in controlling the extent of bioremediation. Hydrophobic pollutants like PAHs sorb strongly to clays and organic material in the soil. Thus, they are unlikely to partition into the aqueous phase for degradation. Furthermore, these pollutants tend to be located in tiny pores in the soil that are often too small for bacterial access. Thus, the bacteria are unable to come in contact with the pollutant. As a result, there is a possible role for surfactants in bioremediation. It is believed that surfactants promote the desorption of the pollutant from the soil, allowing its transport to the bacteria. However, surfactants can also affect bacteria. One hypothesis is that they interfere with adhesion between the bacteria and PAH (Stelmack, 1997). Extensive research has been conducted on the role of surfactants. Unfortunately, the reported results on the effectiveness of surfactants are contradictory (Bouchez-Naïtali et al., 1999). Another consideration is that bacterial membranes act as a barrier to the transport of pollutants, a major role of the membrane is to prevent toxic materials from entering the cell. Restricted permeation could limit metabolism. Thus, many factors contribute to limiting extents of biodegradation. As well, much remains unknown about the processes in bioremediation. This lack of knowledge poses the greatest obstacle to its use in industry as a treatment technology.

2.2 Transport in Bacteria

2.2.1 Membrane Structures

Membrane composition and function are critical in regulating the transport of solutes. They must allow the passage of vital nutrients and carbon sources. At the same time, they must prevent the transport of harmful agents like toxic pollutants and antibiotics. Additionally they must maintain osmotic balance by regulating ion flux. These strict requirements have forced membranes to become highly complex structures.

The basic component of membranes is phospholipids. Phospholipids are modified triglycerides with two fatty acids and a modified phosphate group (Figure 2.4). The fatty acid groups typically contain 16 to 18 carbon atoms denoted by 'n'. An example of the substituent 'R' is ethanolamine ($\text{NH}_2^+\text{CH}_2\text{CH}_2$) (Brock et al., 1994). The structure of the phospholipid results in both a hydrophilic and hydrophobic region on the molecule. As a result of this dual polarity, the phospholipids arrange themselves in a bilayer structure forming a membrane. The outside surfaces of the bilayer are hydrophilic, suiting its exposure to the aqueous environment both inside and outside of the cell. The interior of the bilayer is hydrophobic. The hydrophobic interior restricts the free movement of polar compounds across the membrane (Brock et al., 1994). To control the transport of some compounds, as well as carry out other functions, bacteria make use of proteins inserted in the bilayer. These proteins are specialized in function. Some transmembrane proteins act to transport material across the membrane.

Another important bilayer property is its fluidity, which allows the migration of proteins and phospholipids over the surface of the bilayer. Fluidity also imparts a degree of permeability to the membrane. Bacteria have the ability to alter the membrane fluidity to an extent by changing the fatty acyl components of phospholipids or by inserting efflux proteins into the lipid bilayer. These alterations are often done in response to environmental stress (Nikaido, 1990). In altering membrane fluidity, bacteria also alter membrane permeability (Magin et al., 1990). Thus, phospholipid bilayers are complex structures with many features that all affect the transport of hydrophobic compounds.

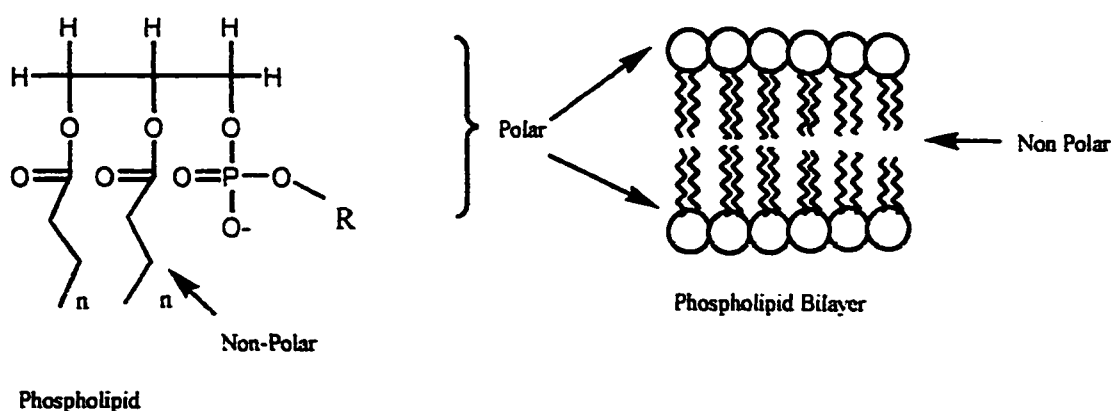


Figure 2.4: Schematic of phospholipids and phospholipid bilayer

Gram-positive bacteria contain a single membrane whose structure is based on a phospholipid bilayer enclosing the cell. This bilayer is protected by a layer of peptidoglycan (Figure 2.5a). Peptidoglycan is composed of repeating disaccharide units of N-acetylglucosamine and N-acetylmuramic acid in parallel chains and crosslinked by a tetra or penta peptide containing the amino acids L-alanine, D-glutamic acid, either lysine or diaminopimelic acid, and D-alanine. The sugar molecules interconnect by glycosidic

bonds and the amino acids are crosslinked by peptide bonds, defining the cell shape. The membranes of Gram-positive bacteria contain numerous layers of peptidoglycan with the amounts varying among species. In addition to peptidoglycan, Gram-positive bacteria also contain teichoic acids. These are glycerol and polyribitol structures with substituent amino acids and sugars. They impart a negative charge to the exterior surface of Gram-positive bacteria, causing the wall to act as a cation exchanger and to sequester magnesium and calcium ions (Brock et al., 1994).

The physiology of Gram-negative bacteria differs from that of Gram-positive bacteria in that Gram-negative bacteria contain two membrane structures: an inner cytoplasmic membrane and an outer membrane (Figure 2.5b). The inner cytoplasmic membrane is a phospholipid bilayer. This layer is insufficient on its own to provide protection against toxins. Thus, an outer membrane surrounds the inner membrane. Between the two membranes is the periplasm, a liquid volume with physical properties similar to a gel (Brock et al., 1994). The outer membrane is also a phospholipid bilayer, however, half of the outer surface of this bilayer is composed of lipopolysaccharide (LPS). LPS is a complex structure made up of a lipid group bound to sugar structures that are highly branched and hydrophilic. The outer membrane is relatively permeable to many small ions as a result of small protein channels called porins. The outer membrane is not permeable to larger compounds (Nikaido, 1990). The current understanding of the outer membrane is that it provides a diffusion barrier to larger molecules that would be potentially harmful to the bacteria.

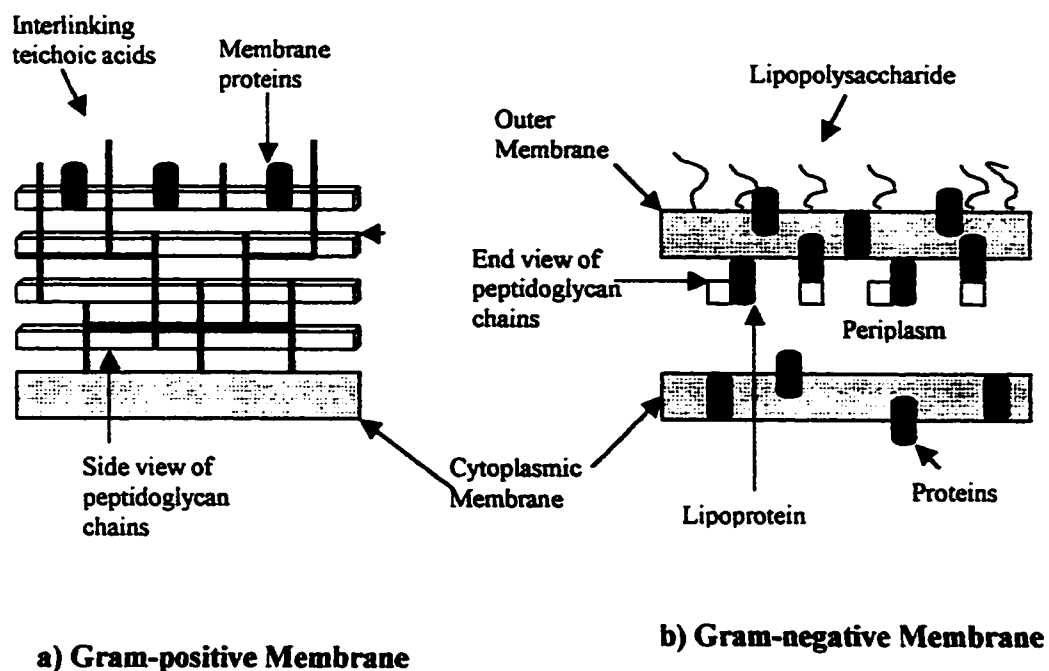


Figure 2.5: Schematic of bacterial cell membrane and cell wall structures

2.2.2 Membrane Energetics

Most processes in bacteria are energy mediated. One mechanism of energy production is the electron transport chain, which is comprised of a series of membrane associated proteins and non-proteins with decreasing reduction potential. They transfer electrons from electron donors like reduced nicotinamide adenine dinucleotide (NADH) to a terminal electron acceptor like oxygen (White, 1995). During this transfer of electrons, hydrogen ions are transported across the cell membrane against a concentration gradient (Figure 2.6). A typical electron transport chain is described below. The first protein,

NADH dehydrogenase, oxidizes NADH to NAD^+ . The resulting hydrogen ions and electrons are passed to a flavoprotein. The flavoprotein transports the hydrogen ions across the membrane and passes the electrons on to an iron-sulphur protein. This non-heme protein reduces a quinone, coenzyme Q, resulting in the uptake of two more hydrogen ions from the cytoplasm. The reduced quinone, QH_2 , transfers the electrons, one at a time, to a cytochrome bc_1 complex. During this transfer, one hydrogen ion is transported across the cell membrane, forming a semiquinone QH. For every two QH complexes, one is oxidized to Q by extrusion of a hydrogen ion out of the cell and one is reduced to QH_2 through the uptake of a proton from the cytoplasm. From cytochrome bc_1 , the electrons are passed sequentially to other cytochromes and finally to oxygen. The reduction of oxygen to form water requires two more hydrogen ions from the cytoplasm for every electron pair (Brock et al., 1994). The electron transport chain creates a pH and charge gradient across the cell membrane as a result of an excess of hydrogen ions outside the cell membrane and an excess of hydroxyl ions within the cytoplasm. Electrons transport chains can differ between bacteria in both the number and type of components present.

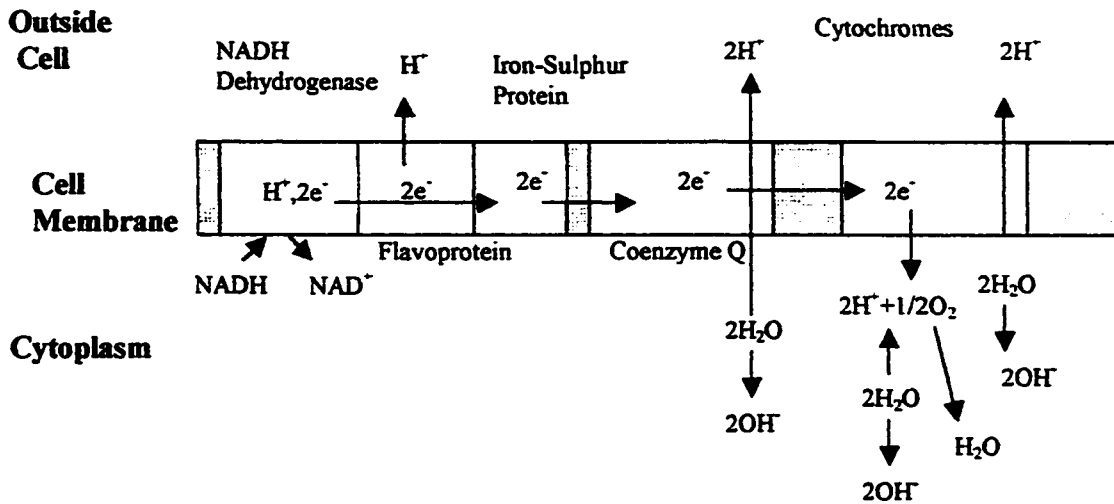


Figure 2.6: Schematic of chemiosmosis generating the proton motive force

The proton gradients established by chemiosmosis can be harnessed for the operation of energy mediated processes within bacteria. The chemical potential gradient ($\Delta\mu$), referred to as the proton motive force, associated with the pH gradient (ΔpH) and the charge gradient ($\Delta\Psi$) is on the order of -120 to -220 mV (equation 2-1) (Kaback, 1976). In this equation, R is the gas constant, T is the temperature in K, and F is Faraday's constant.

$$\Delta\mu = \Delta\Psi - \frac{2.3RT}{F} \Delta\text{pH} \quad (2-1)$$

Furthermore, bacteria routinely transport positive ions, like sodium and potassium ions, outside the cell, adding to the already established charge gradient. Bacteria make use of this chemical potential gradient by controlling the transport of positive ions, particularly

hydrogen ions, back into the cell. A universal example is the phosphorylation of adenosine diphosphate (ADP) to adenosine triphosphate (ATP). ATP serves as the primary source of energy for bacterial processes. A transmembrane complex, ATP synthase, couples the phosphorylation reaction to the transport of hydrogen ions into the cell. ATP stores chemical energy in the terminal phosphate bonds that can be later harvested through its cleavage to form ADP again (Kaback, 1976). Other energy driven processes can then use ATP directly or make use of the proton motive force.

2.2.3 Passive Transport

Passive transport is the spontaneous movement of solutes in or out of cells. It is driven by the chemical potential gradients associated with the solute being transported. As a result, transport can only proceed to an extent governed by the thermodynamic equilibrium of the system. Since many bacteria live in dilute environments, passive transport is not a practical means to acquire most nutrients and substrates. As a result, bacteria rely on active transport for most transport processes. There are two types of passive transport: diffusion and facilitated transport.

Diffusion is the movement of material from an area of high concentration to an area of low concentration by the Brownian motion of the molecules. Rates of diffusion are governed by Fick's Law. However, the non-ideality imposed by the membrane structure makes analysis of transport by Fick's law difficult. Thus, permeability equations are used (equation 2-2). In this equation, J describes the rate of mass transfer in $\mu\text{mol/s}$, P is the permeability constant in m/s for the bacterial membrane, A is the membrane surface

area in m^2 across which mass transfer occurs, and y_1 and y_2 are the concentrations of solute in $\mu\text{mol}/\text{m}^3$ at the exterior and interior membrane interfaces.

$$J=PA(y_1-y_2) \quad (2-2)$$

The permeability coefficient (P) accounts for non-ideality and other factors resulting from a thermodynamic analysis of concentration gradients inside the cell membranes. For diffusion to occur in bacteria, the compound in question must be able to penetrate and diffuse through the hydrophobic interior of the lipid bilayer to reach the cytoplasm (Harold, 1986). For Gram-negative membranes, compounds must diffuse through two membranes. For Gram-positive bacteria, they must penetrate a thick peptidoglycan layer. As a result of the hydrophobicity of the interior of lipid bilayers, it is unlikely for hydrophilic compounds to be transported by diffusion. For hydrophobic compounds, there is greater potential for transport by diffusion as a result of the capacity for these compounds to accumulate in membranes (Marrink and Berendsen, 1996). However, the surfaces of membranes are often charged and the hydrophobic compounds must penetrate these hydrophilic surfaces.

In contrast to diffusion, facilitated transport makes use of transmembrane proteins to move the solute across membranes. This mode of transport is beneficial for hydrophilic compounds that are otherwise unable to diffuse across the membranes. There is no cellular energy expenditure in facilitated transport. Thus, the extent of transport is still limited by the equilibrium of the system. These transport proteins can either be generalized, transporting a wide range of compounds, or highly specific. Frequently

though, they only transport a limited range of structurally similar compounds. Given that there is a limited number of transport proteins in a bacterium for a particular compound, there is the potential for saturation of the system (Rogers et al., 1980). As a result, there is an upper limit (v_{\max}) on the maximum rate of transport for these compounds (equation 2-3). In this equation, J is the rate of mass transfer in $\mu\text{mol/s}$, S is the extracellular solute concentration in $\mu\text{mol/L}$, K_m is an affinity constant in $\mu\text{mol/L}$, and V_{\max} is the maximum rate of mass transfer in $\mu\text{mol/s}$.

$$J = \frac{V_{\max} S}{K_m + S} \quad (2-3)$$

Saturation can be a result of high solute concentrations or competition with other structurally related compounds that are transported by the same protein. Additionally, like diffusion, facilitated transport is not selective in the direction of transport (Stein, 1987).

2.2.4 Active Transport

Active transport makes use of transmembrane proteins and energy to accumulate solutes against a concentration gradient inside or outside the cell. In primary active transport, the energy is obtained from ATP or redox reactions within the cell. In secondary active transport, the energy is obtained from the proton motive force. Typically, the solutes that are transported are unable to diffuse across the membrane to any significant extent. Thus, the bacterial membrane serves as a barrier maintaining concentration gradients

established by active transport. No system is perfect though and there is the slow leakage of material down the concentration gradient by passive means, dissipating the gradients (Harold, 1986).

2.2.5 Energy Inhibitors

Inhibitors and uncouplers are used to study active transport. These compounds disrupt energy production in bacterial systems, effectively preventing active transport mechanisms from operating (Brock et al., 1994). Due to solute leakage, concentration gradients established by active transport are then dissipated. For active uptake, solute leakage results in the release of solute back into the aqueous environment. From an experimental perspective, a decrease in intracellular concentrations and an increase in extracellular concentrations are observed. For active efflux, energy poisons cause an increase in intracellular concentration and a decrease in extracellular concentration is observed.

Inhibitors and uncouplers act by different mechanisms. Inhibitors are a class of compounds that interfere directly with the operation of the electron transport chain. They bind to proteins and prevent the flow of electrons. Disrupting the flow of electrons prevents the transport of hydrogen ions across the membrane and the establishment of a proton motive force. Common inhibitors include azide (N_3^-), cyanide (CN^-), and carbon monoxide (CO) (Brock et al., 1994). Both azide and cyanide complex metals in metallo-enzymes (Dawson et al., 1969). Uncouplers include compounds like 2,4-dinitrophenol (DNP) and carbonyl cyanide m-chlorophenylhydrazone (CCCP) (Figure 2.7). Uncouplers

act in an indirect manner by making membranes permeable to hydrogen ions. The increased permeability allows the equilibration of previously established proton gradients across the membrane. As a result, the proton force is disrupted (White, 1995).

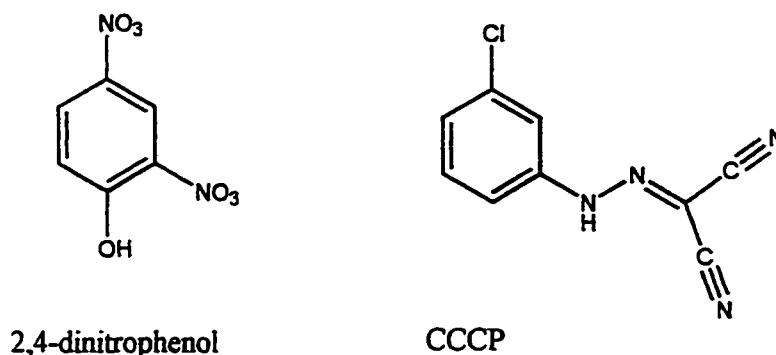


Figure 2.7: Structures of representative uncouplers

The energy source for active transport can be a result of ATP, the pH gradient, or the charge gradient. Ionophores are a class of compounds, which include uncouplers, that make membranes permeable. Many ionophores are selective in which ions become permeable. Judicious use of ionophores along with control of experimental conditions can allow the elucidation of the energy source for active transport. Valinomycin makes membranes permeable to potassium and rubidium ions. Additionally it will allow sodium, lithium and hydrogen ions to permeate to a significantly lesser extent. Nigericin and monensin will also allow potassium and sodium ions to equilibrate across membranes. However, they are electroneutral in their mode of operation. Hence potassium and sodium ion transport is coupled to hydrogen ion countertransport. Gramicidin acts as a uniporter for hydrogen ions and to a lesser extent a few other positive ions (Harold, 1986).

ATP synthesis through the membrane ATP synthase and the pH gradient are inherently coupled. Thus, ATP synthase must be deactivated to study them independently. ATPase can be inactivated by adding N,N'-dicyclohexylcarbodiimide (DCCD). ATP can still be formed in the presence of DCCD by substrate level phosphorylation. Thus, ATP levels can be manipulated by adding a substrate like glucose to promote ATP production or by starving the cells to deplete ATP levels (White, 1995). Distinction can also be made between the different components of the proton motive force. Addition of valinomycin to cells will cause the equilibration of potassium ions across the membrane. If the cells are in environments with high potassium concentrations, this ion will be the primary constituent of the charge gradient and hence $\Delta\psi$ will be collapsed. Nigericin can be used to exchange potassium ions inside the cell for hydrogen ions outside the cell. The exchange eliminates the pH gradient but does not alter the charge gradient (White, 1995). Experimentation with these different ionophores allows the determination of the energy source for active transport.

2.3 Transport of Hydrophobic Compounds

The transport mechanisms and membrane energetics apply equally to hydrophilic and hydrophobic compounds. For hydrophobic compounds, we must consider both the transport into the cell for metabolic needs and the potential for these compounds to accumulate in lipid bilayers. The latter carries with it a potential toxicity concern for bacteria.

2.3.1 Membrane Partitioning

A prerequisite of passive diffusion is the need for compounds to partition into bacterial membranes in order to traverse them. The hydrophobicity of PAHs coupled with the hydrophobic structure of the interior of lipid bilayers creates great potential for these compounds to accumulate in bacterial membranes. As a result, much research has been done on the partitioning behaviour of PAHs and other hydrophobic compounds in membrane vesicles.

Unlike other organic phases, lipid bilayers are highly complex. They have large surface area to volume ratios. As a result, lipid bilayers should not be regarded as homogenous organic phases. Bulk thermodynamics do not apply nor does the assumption of ideality (Marqusee and Dill, 1986). Instead, they should be regarded as interfacial phases where the physical properties vary with distance from the interface (De Young and Dill, 1988). This view is consistent with membrane structures. It also imposes complex thermodynamics on the system. As a result, bulk fluid properties are often used to simplify the system.

The most common measure of hydrophobicity is the octanol-water partition coefficient K_{ow} . Table 2.1 lists aqueous solubilities and K_{ow} values for representative hydrophobic compounds. Correlations have been developed between K_{ow} values for organic compounds and their partitioning into other homogeneous organic phases. There are also correlations between K_{ow} values and partitioning into membranes. However, these correlations differ among bacteria due to the diversity of membrane structures. The

greatest factor in this variability is membrane fluidity. Membrane fluidity can vary among bacteria in similar environments. Furthermore, it can vary within a particular bacterial strain in response to environmental factors (Sikkema et al., 1995). As a result, partitioning into membranes is a complex process.

Table 2.1 Aqueous solubilities and Log K_{ow} values for representative hydrophobic compounds (Mackay and Shiu, 1992).

Compound	Aqueous Solubility (mg/L)	Log K_{ow}
toluene	515	2.69
naphthalene	31.0	3.37
phenanthrene	1.10	4.57
fluoranthene	0.26	5.22
anthracene	0.07	4.54
pyrene	0.13	5.18
benzo[a]pyrene	0.0038	6.04

The chemical structure within the hydrophobic region of bilayers affects the nature and extent of partitioning. There is a volume restriction imposed by the physical dimensions. Also the phospholipids impose ordering constraints on where PAHs can partition in the membrane. The vicinities near the polar head groups of phospholipids are more polar than the rest of the membrane. Thus, they are less favourable regions for hydrophobic compounds. Also, the arrangement of phospholipid tails creates an ordered structure within the membrane. In contrast, the centre of the membrane, where the two phospholipid layers meet, is more amorphous in structure (Weber and de Bont, 1996). Research on the partitioning of alkanes into membranes has shown the effect of membrane structure on partitioning. X-ray diffraction on membrane vesicles exposed to

n-alkanes was able to show changes in bilayer width when various alkanes were added. Partitioning of long chain alkanes, including dodecane, tetradecane, and hexadecane, caused an increase in bilayer width of 0.6 nm. This result was independent of alkane type and concentration. In contrast, experiments with short chain alkanes showed changes in bilayer width that were correlated to changes in concentrations. The rationale for these observed results is that short chain alkanes, being highly unordered, are more likely to accumulate in the amorphous region in the centre of the bilayer. Here there would be a proportional increase in bilayer width with increasing alkane concentration. In contrast, the larger alkanes are more ordered and are more likely to align themselves with the hydrocarbon chains in the phospholipid. As a result, there would be minimal effect on membrane width and no concentration dependence. The observed change of 0.6 nm is believed to be a result of the removal of chain tilt in phospholipid tails to allow the aligning of long chain hydrocarbons (McIntosh et al., 1980). Neutron diffraction experiments on hexane partitioning into liposomes showed that hexane preferentially accumulated in a zone 1 nm in width in the centre of the lipid bilayer. It was found that little hexane accumulated towards the more ordered outer regions of the membrane. Interestingly though, the researchers observed no change in membrane thickness nor were they able to give an explanation for this observation (White et al., 1981). The partitioning into select regions within the bilayer is consistent with the view of membranes as interfacial phases. The equilibrium concentration within the bilayer is not uniform across the bilayer width as it would be in a bulk phase. This idea is further reinforced by research on the partitioning of benzene. X-ray diffraction not only showed that benzene partitioned to the centre of the membrane, but that the extent of partitioning

varied when the surface density of the lipid bilayer was altered (De Young and Dill, 1988). This phenomenon would not be observed in a bulk fluid. In summary, hydrophobic compounds partition readily into membranes with constraints imposed by interfacial properties. From these observations, one can speculate that PAHs are also likely to partition into the centre of membranes. Thus, there is a possibility for diffusion as a means of uptake.

2.3.2 Membrane Toxicity

Despite the fact that bacteria metabolize PAHs and other hydrophobic compounds, the partitioning of these compounds into their membranes can cause toxic effects.

Hydrophobic compounds can alter van der Waals interactions within the bilayer and can cause changes in membrane fluidity and transition temperatures. The primary mechanism for toxicity is the expansion of the cell membrane. Expansion of the membrane has two consequences: disruption of the function of membrane bound proteins and increased membrane permeability (Weber and de Bont, 1996).

Increased membrane permeability interferes with the control of transport processes. The primary casualty is the regulation of ion gradients. Increased proton permeability dissipates the proton motive force thereby interrupting energy driven processes. For example, research on proteoliposomes has shown a concentration dependence between tetralin partitioning and an increase in the flux of protons into liposomes. In turn, this increased flux caused a significant decrease in the pH gradient across the cell membrane. The charge gradient across the membrane was only slightly affected (Sikkema et al.,

1992). Continued work was performed by the same research group on the effect of a range of aromatic hydrocarbons including benzene, ethylbenzene, toluene, *o*-xylene, naphthalene, and other similarly structured compounds (Figure 2.8). Similar to tetralin, they observed that these hydrocarbons increased membrane permeability to hydrogen ions and disrupted the proton motive force. Furthermore, they concluded that the effective concentrations for membrane disruption correlated with the membrane partition coefficients of the different compounds. At higher hydrocarbon concentrations, they also saw a concentration dependent decrease in protein activity. Whether this observation was a result of hydrocarbon-protein interactions or significant disruption of membrane structure could not be determined (Sikkema et al., 1994). Given the structural similarity, one can speculate that PAHs might pose toxicity problems as a result of partitioning.

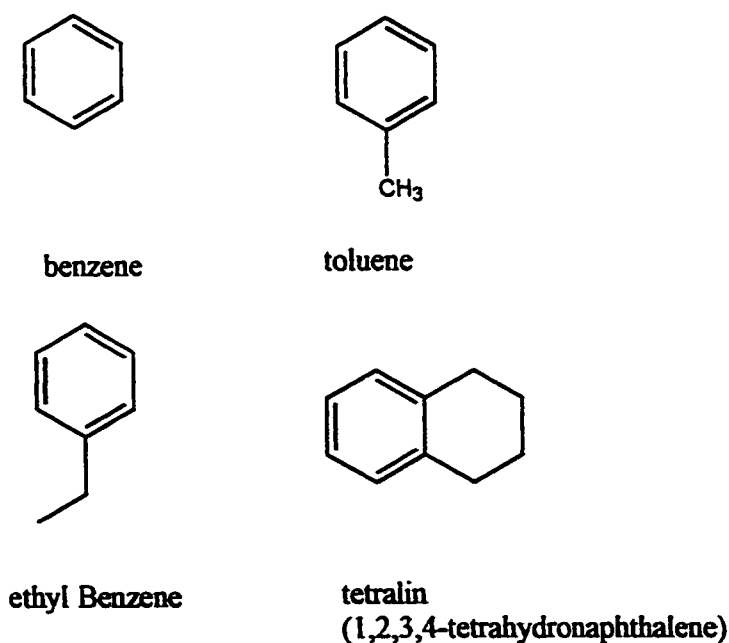


Figure 2.8: Structures of compounds that partition into membranes

Bacteria are able to combat the toxic effects of hydrophobic compounds to an extent through the modification of membrane structures. A frequently observed phenomenon upon exposure to hydrophobic contaminants is the conversion of *cis*-fatty acids to their *trans* isomers. This conversion has a significant effect in decreasing membrane fluidity and hence reducing permeability (de Bont, 1998). Much of the research on changes in membrane composition has been carried out using ethanol as a solvent. As a result, it is uncertain if many of the observed effects also occur upon exposure to more hydrophobic compounds. It has been observed that exposure to ethanol resulted in an increase in protein/lipid ratio in bacterial cell membranes. As a result, the membrane fluidity was decreased (Heipieper et al., 1994). This observation is likely a secondary effect to the insertion of ethanol efflux proteins into the membrane. Additionally, cholesterol, hopanoid, and carotenoid concentrations in the membrane can alter membrane fluidity. Another ethanol-induced change in bacterial membranes is an increase in the amount of unsaturated fatty acids. Unsaturated fatty acids are believed to cause a decrease in the transition temperature of the membrane which is otherwise increased in the presence of ethanol. However, this change wasn't observed in some bacteria (Weber and de Bont, 1996). Research with *Pseudomonas putida* strains and *o*-xylene showed no change in fatty acid composition upon exposure to the more hydrophobic solvent (Pinkart et al., 1995). Thus, there is a question as to what extent bacteria alter membrane composition to reduce PAH permeability.

In Gram-negative bacteria, there is interest in the role of the outer membrane in regulating partitioning and permeability. The LPS layer is highly hydrophilic and is thus

believed to provide a barrier to the permeability of hydrophobic compounds. Upon exposure to organic solvents like toluene, the composition of the outer membrane of *P. putida* S12 was altered, rendering it more hydrophilic (Weber and de Bont, 1996). Experiments with mutant strains, primarily of *Eschericia. coli*, that have altered LPS composition have shown increased sensitivity to a range of hydrophobic compounds. In particular, deep rough mutants, lacking a majority of the saccharides in LPS, are more susceptible to detergents and antibiotics (Nikaido and Vaara, 1985). The hydrated saccharides are one of the compounds that make the LPS more hydrophilic. Another barrier to permeation of hydrophobic compounds is the high concentration of unsaturated fatty acids which impart structural order and rigidity to the outer membrane. Also, LPS molecules are linked to one another through the interaction with divalent cations. Increased sensitivity of Gram-negative bacteria to solvents was observed when EDTA was added to chelate the stabilizing ions. Resistance was regained when more divalent cations were added to the system (Weber and de Bont, 1996). Thus, it is apparent that the structure of the outer and inner membranes are important in controlling permeability.

The hydrophilic nature of the outer membrane and the ability of bacteria to alter membrane composition to increase resistance to solvents pose a barrier to the diffusion of hydrophobic compounds like PAHs. Furthermore, a barrier may be necessary to combat the toxic effects. Thus, the question arises as to a requirement for an active transport mechanism to transport PAHs across bacterial cell membranes.

2.3.3 Transport of PAHs

There is very little research presented in literature specifically on the transport of PAHs. The two articles that report on the transport of naphthalene describe conflicting results. One paper reports the presence of an active uptake mechanism for naphthalene (Whitman et al., 1998). The other found no evidence of energy mediated transport. Rather, they argue that uptake of naphthalene occurs by passive transport (Bateman et al., 1986).

The research conducted by Bateman et al. (1986) gives indirect arguments for the passive uptake of naphthalene. Uptake was studied at room temperature by filtration, centrifugation, flow dialysis, and metabolic activity. For filtration, 2-mL samples of cell suspensions were incubated for 10 min at 30°C on a rotary shaker set at 100 rpm. Naphthalene was added in 20 µL of ethanol, resulting in 1% ethanol in the cell suspension. At timed intervals, 0.2-mL samples were vacuum filtered through 0.2-µm cellulose acetate filters and washed with 10 mL of phosphate buffer. The filters were analyzed for ¹⁴C labeled phenanthrene by liquid scintillation counting. Transport was studied over a 10-min time interval. From the data that were presented, it is obvious that a high amount of material from the abiotic control was retained during filtration. At an initial naphthalene concentration of 2 mM, the abiotic control contained 200 nmol naphthalene/mg dry wt. The naphthalene concentration in the abiotic control was converted to an equivalent dry wt basis for direct comparison with biotic experiments. The biotic sample contained approximately 260 nmol/mg dry wt. The research group argued that more naphthalene was retained on the filters in biotic experiments compared to the abiotic control, allowing interpretation of the results. However, on the presented

graph, the error bars on the naphthalene concentration for the abiotic control span a range from approximately 140 to 300 nmol/mg dry wt. The error bars on the naphthalene concentrations for the biotic samples span a range from approximately 190 to over 350 nmol/mg dry wt. Thus, within experimental error, there is no difference in naphthalene concentrations between abiotic control and biotic samples. These results highlight an inherent problem in sensitivity with this technique. Also, the researchers argued that there was no change in the amount of naphthalene retained by cells when inhibitors were added. This statement is consistent with passive transport, but no evidence was presented in the paper to validate it. Given the sensitivity problems in the experimental technique, it is uncertain if any significant changes could be detected by filtration.

Other evidence given by Bateman et al., 1986 for the passive uptake of naphthalene was the ability of the wild-type strain to metabolize naphthalene in the presence of inhibitors. Cell suspensions were incubated with naphthalene for 5 min then centrifuged to separate the supernatant. The supernatant fraction was analyzed for the presence of the metabolite *cis*-naphthalene dihydrodiol. The data presented indicated that a *cis*-naphthalene dihydrodiol concentration of 1.6 nmol/mg dry wt was found in the abiotic control, 4.4 nmol/g dry wt in the cell suspension with no inhibitors, and concentrations ranging from 4.2 to 8.8 nmol/g dry wt in cell suspensions containing different energy inhibitors. The detection of naphthalene in the abiotic control is likely a result of error in the analytical technique. Given that the enzymes for PAH degradation are intracellular, the PAH must cross the membrane to be degraded. Since the data indicate that the addition of inhibitors had no effect on naphthalene metabolism, it was concluded that naphthalene was

passively transported into the cells. However, this argument does not eliminate the possibility of an active uptake mechanism. Passive uptake will always occur to some extent with its rate controlled by the permeability. The relevant question is whether there is sufficiently low membrane permeability to PAHs to necessitate an active uptake mechanism. The time scale on which the experiments were done does indicate rapid permeability for metabolism to occur in a 5 min time period. Furthermore, over this time period, it would be expected that there would be a noticeable difference between metabolism in inhibited and non-inhibited cells if there were an active transport mechanism present. The data on metabolism provides indirect proof for passive uptake.

The most promising evidence for passive transport is in the experiments conducted by flow dialysis. Bateman et al. (1986) placed naphthalene in a dialysis chamber separated by a membrane from buffer flowing at a rate of 5 mL/min. The buffer, containing partitioned ^{14}C naphthalene, was collected in 2-mL fractions and analyzed by liquid scintillation counting. The comparison between abiotic control and biotic experiments showed a drastic decrease in naphthalene dialysis from 600 counts per minute (cpm) to 200 cpm in approximately a 3-min time period when cells were added to the chamber. Prior to the addition of cells, the rate of decrease in naphthalene dialysis was approximately 45 cpm/min. Thus, the observed change was a result of naphthalene association to the cells. The researchers stated that when inhibitors were added, there was no effect on the dialysis rate. This statement is consistent with passive transport. However, once again, no data were presented to support this claim. An interesting observation was that there was no difference between induced and non-induced cells in

the dialysis experiments (Bateman et al., 1986). This observation would suggest that the transport processes were not sensitive to the presence of a hydrophobic substrate. The research presented by Bateman et al. (1986) states many strong arguments for passive transport, but the data presented in the paper are inconclusive in supporting them.

In contrast, research by Whitman et al. (1998) gives arguments for the active uptake of naphthalene in a *Pseudomonas fluorescens* Uper 1 strain. A mutant strain, *P. fluorescens* TG-5, which is unable to degrade naphthalene, was also used. Uptake was studied by incubating the bacteria with naphthalene in sealed amber gas chromatography vials. The vials were centrifuged and the liquid phase was sampled by syringe and analyzed by liquid scintillation counting. For the cell phase, 1-mL samples were removed from the incubating cultures and applied to a 4/60% w/v discontinuous sucrose gradient. These preparations were then centrifuged and the cells collected at the 4/60% sucrose interface. The primary argument for active uptake is that the amount of ^{14}C associated with the cell pellet fraction was reduced by over 80% in the presence of energy inhibitors. For the cell suspensions to which no azide was added, the cell fraction contained 50 000 cpm/mL. For the azide inhibited suspensions, the cell fraction only contained 10 000 cpm/mL. These observations may very well indicate the inactivation of an active transport mechanism for naphthalene. However, the cell phase analysis was done on a naphthalene degrader after 2 h of incubation. Consequentially, the ^{14}C -label was more likely to be in metabolites rather than in unconverted naphthalene. The results after a long incubation time are likely to be dominated by differences in metabolism rather than transport. Thus, conclusions drawn from the data on the mode of transport may be invalid.

The extent of metabolism of naphthalene in the experiments conducted by Whitman et al. (1998) was determined over a 5-h incubation period. The presented data indicate an increase in cell-phase ^{14}C levels from 1 000 cpm at time zero to nearly 6 000 cpm after 1 h of incubation. The levels in the cell phase remained constant thereafter. In conjunction with this, the liquid phase ^{14}C levels decreased from 190 000 cpm at time zero to approximately 130 000 cpm after 1 h. The liquid phase ^{14}C concentrations also remained constant thereafter. Analysis by gas chromatography indicated that, after 1 h of incubation, the naphthalene concentration in the liquid phase continued to decrease. Thus, the observed plateau is a plateau in the loss of ^{14}C from the liquid and not an endpoint of metabolism. A mass balance on the liquid and cell phases indicates that a substantial portion of the ^{14}C label was lost during the first hour of incubation. Experiments with KOH traps were able to recover 43.9% of the ^{14}C label as trapped carbon dioxide. Thus, there is substantial degradation of the ^{14}C label during the first hour of incubation. These observations confirm that the effect of azide detected in the transport experiments, after a 2-h incubation, was on metabolic factors and not transport factors. Thus, no conclusions can be drawn as to the mode of transport. Similar degradation experiments were conducted with the mutant strain and metabolism or loss of naphthalene was observed. However, no data were presented in the paper on the effect of azide on cell concentrations in this strain. Such experiments would have provided insight into transport processes.

The paper also indicates competition effects for uptake with α -naphthol (Whitman et al., 1998). This result does not conclusively prove active transport either. Facilitated transport, a passive mechanism, is also subject to saturation and competition for uptake. Also, these experiments were conducted with an incubation time of 1 h. Thus, metabolic and not transport effects dominated the results. In summary, no conclusions can be drawn from the research as to the mode of transport of naphthalene in *Pseudomonas fluorescens* Uper-1.

Research on the transport of polar aromatic hydrocarbons (Figure 2.9) has provided conclusive evidence for active transport processes for these compounds. These studies also indicate the need for induction of the transport mechanism and show its dependence on the proton motive force. Experiments on the transport of benzoate in *P. putida* indicated that benzoate was concentrated 150 fold inside the bacteria. The extent of accumulation of benzoate was impeded to different extents through the addition of various inhibitors. Furthermore, the level of inhibition showed no correlation to intracellular ATP levels (Thayer and Wheelis, 1981). This result implies that the proton motive force is the source of energy. Researchers working with mandelate and *P. putida* indicated that the compound equilibrated easily across the membrane. At lower initial mandelate concentrations, the amount in the cell was six times higher in induced cells versus non-induced cells. This high concentration of mandelate decreased after the addition of dinitrophenol. These observations suggest the presence of an inducible active transport mechanism for mandelate (Higgins and Mandelstam, 1971). Research also identified an active transport mechanism for 4-chlorobenzoate in a Coryneform bacterium

NTB-1. Experiments under anaerobic conditions showed negligible levels of 4-chlorobenzoate in this bacterium. Levels of the compound increased when an artificial charge gradient was applied. The levels of 4-chlorobenzoate levels increased even more drastically in the presence of an artificial pH gradient. From these results it was concluded that active transport of 4-chlorobenzoate was coupled primarily to the proton gradient (Groenewegen et al., 1990).

Finally, an active uptake mechanism for 4-toluene sulphonate has been identified in *Comamonas testosteroni* T-2 (Locher et al., 1993). In this bacterium, it was found that CCCP inhibited uptake of the compound completely. Furthermore, work with various inhibitors showed no correlation between the extent of inhibition and ATP levels. This observation once again indicates the dependence of transport on the proton motive force. The researchers also stated that incubation with succinate or acetate, metabolites of 4-toluene sulphonate degradation, increased initial rates of uptake by 2-3 fold. However, they did not provide data to substantiate the statements. From these results, they argued that the uptake mechanism was inducible. The research on polar aromatics identifies the presence of active transport driven by the proton motive force. Furthermore, there appears to be a requirement for induction of the transport mechanism. Whether the transport of polar aromatics provides insight on the transport of PAHs is uncertain. PAHs are significantly more hydrophobic and would partition more readily into membranes than these polar compounds. Nonetheless, given a degree of structural similarity, it may provide corroborating evidence.

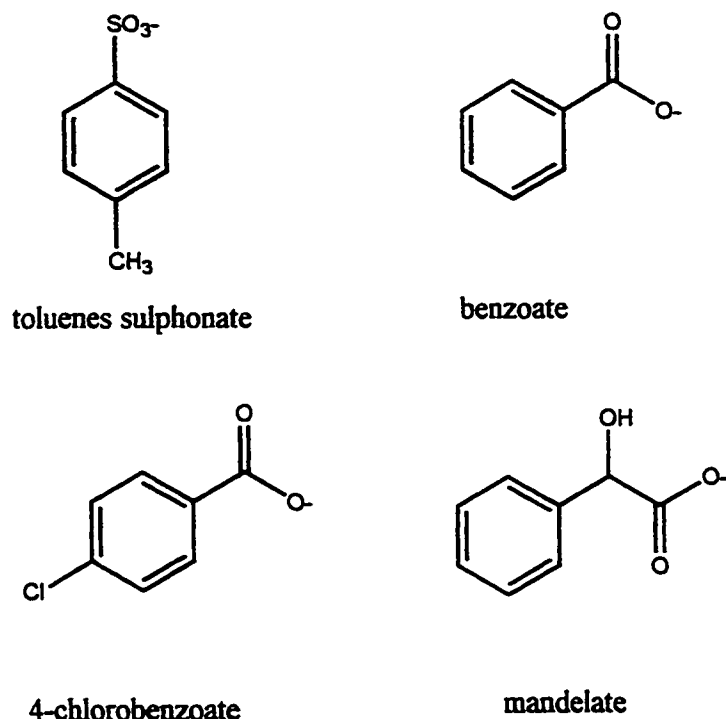


Figure 2.9: Structure of polar aromatics subject to active transport

2.3.4 Active Efflux of Organic Solvents and Antibiotics

The active efflux of antibiotics by bacteria is a phenomenon that has been observed by the medical research community for some time. Recently, the active efflux of organic solvents has also been identified. The function of these efflux pumps is to provide protection to bacteria from the otherwise toxic effects of these compounds. Changes in cell membrane structures may reduce permeability rates, but ultimately they do not prevent the partitioning of hydrophobic compounds. Efflux pumps provide a means to remove these compounds from membranes. However, once outside the bacteria, these compounds can partition back into the membrane. Efflux pumps are faced with a constant battle to maintain low intracellular concentrations of these compounds. Efflux pumps have been identified in Gram-negative bacteria and a link has been shown to exist

between antibiotic resistance and organic solvent tolerance (de Bont, 1998). This observation raises the possibility of a generalized efflux pump for hydrocarbons. It also indicates a potential role for active efflux in the transport of PAHs in Gram-negative bacteria.

Multidrug efflux pumps have been extensively studied for their role in antibiotic resistance. Here it has been found that pumps are not substrate-specific (Li et al., 1998). Rather they transport a broad range of drugs. The most familiar example is multi-drug resistance in *Pseudomonas aeruginosa*, a bacterium with extremely low membrane permeability (Nikaido, 1996). Yet antibiotics partition across its membrane rapidly. The survival of the bacterium depends on a rapid active efflux pump that is able to outcompete transport rates. Experiments have shown that intracellular concentrations of tetracycline, chloramphenicol, norfloxacin, and benzylpenicillin all increased when CCCP was added (Nikaido, 1996). These observations demonstrate the energy dependence of efflux mechanisms. Genetic analysis of these efflux pumps has shown that they are made up of three proteins that, together, span both membranes in Gram-negative bacteria. It is uncertain, though, as to whether these efflux pumps remove the compounds from the cytoplasm or the membranes themselves where the concentrations would be higher (Nikaido, 1996). Multi-drug efflux pumps have been shown to be genetically similar amongst various antibiotic-resistant Gram-negative bacteria. One theory is that these efflux pumps consist of one protein spanning the cytoplasmic membrane and one spanning the outer membrane. The two are connected by a linking protein from the membrane fusion protein family (Nikaido, 1996). These antibiotic

efflux pumps also have a degree of similarity to heavy metal efflux, which would suggest a generic active efflux system for toxins.

Similar to antibiotic-resistant bacteria, organic solvent-tolerant bacteria display resistance to the toxic effects of a broad range of organic solvents. Experiments using *P. putida* S12 showed low levels of toluene in induced cells that increased when energy inhibitors were added (de Bont, 1998). Similarly, research with *P. putida* DOT-T1E indicated increased intracellular concentrations of 1,2,4-trichlorobenzene when CCCP was added (Ramos et al., 1998). These observations argue for the energy dependence of organic solvent efflux pumps. Organic solvent efflux pumps are also subject to induction. Induced cells of *P. putida* S12 accumulated 50% less toluene than their non-induced counterpart.

Additionally, cells pre-exposed to toluene survived toluene shocks whereas those that were not induced did not (de Bont, 1998). Research with *P. putida* S12 also showed that transcription of the *srpABC* operon for solvent efflux was greatly enhanced by the presence of such organic solvents as toluene, benzene, xylene, ethylbenzene, aliphatic solvents, and alcohols. Furthermore, experiments showed that there was a 30-min lag phase between the addition of toluene and induction of this operon (Kieboom et al., 1998). This observation argues for the presence of an inducible organic solvent efflux pump in *P. putida* S12. While efflux is enhanced by induction, there is can also be low levels of constitutively expressed efflux pumps. *P. putida* DOT-T1E was able to transport 1,2,4-trichlorobenzene out of non-induced cells. The addition of toluene appeared to interfere with 1,2,4-trichlorobenzene efflux, resulting in its accumulation in the cell and indicating competition for the same efflux pump. At the same time, toluene efflux in *P.*

putida DOT-T1E was also enhanced by induction. From these results and other work, the researchers argued for the presence of both a constitutively expressed solvent efflux pump and a second inducible efflux pump (Ramos et al., 1998).

Many antibiotic-resistant bacteria are also organic solvent resistant and vice versa. Experiments with *P. aeruginosa* K1112, an antibiotic-resistant strain, showed that this strain was resistant to hexane and *p*-xylene. Resistance to toluene was not immediate, however, following a 72-h incubation with toluene, toluene-resistant colonies developed (Li et al., 1998). Research with the solvent-tolerant *P. putida* S12 strain indicated antibiotic resistance occurred only after induction of the efflux pump with an organic solvent. In conjunction with this, antibiotics alone resulted in only a 2-fold increase in induction of the *srpABC* operon, whereas organic solvents caused a 15-17-fold increase (Kieboom et al., 1998). Other known antibiotic-resistant and organic solvent-tolerant bacteria include *E. coli* and *P. putida* (de Bont, 1998). These observations argue for the similarity between antibiotic resistance and organic solvent tolerance, yet it also indicates slight differences. These differences could potentially be a modification of the process to meet the environment of the bacteria.

3.0 MATERIALS AND METHODS

3.1 Materials

3.1.1 Microorganisms

Pseudomonas fluorescens LP6a was chosen for transport studies. It is a Gram-negative bacterium that is capable of degrading and cometabolizing a broad range of PAHs. The degradative genes are located on a plasmid and extensive research has been done on both the genetics and metabolic pathways (Foght and Westlake, 1996). A variety of mutant strains of LP6a are available. A transposon mutant strain, 1-51, was chosen for study as a result of its inability to produce dioxygenase enzymes. As a result, it is unable to degrade PAHs. The transposon mutant 1-51 was created by the random insertion of a transposon (Tn5) into the plasmid that encodes for PAH degradation. The segment of inserted DNA contained a gene for kanamycin resistance and kanamycin must be added to the medium used to grow the mutant 1-51 strain to prevent the loss of the transposon (Foght and Westlake, 1996). Transport studies for the wild-type and transposon mutant 1-51 were also compared with a cured strain, which lacks the plasmid (Foght and Westlake, 1996). For a negative control, *Azotobacter vinelandii* UW (R. Mah, Department of Biological Sciences, University of Alberta) was used due to its lack of association with PAH degradation. Since isoleucine is known to be actively transported into *Staphylococcus epidermidis* ATCC 155, this strain was used as a positive control to confirm that the methods developed provided accurate transport results.

3.1.2 Polycyclic Aromatic Hydrocarbons

Phenanthrene (99.9 % purity) and fluoranthene (98% purity) were obtained from Aldrich (Milwaukee, USA). Anthracene (98% purity) and naphthalene (99% purity) were obtained from Sigma Chemical Company (St. Louis, MO, USA). Toluene (99.8% purity) was obtained from Fisher Scientific (Fair Lawn, NJ, USA). [9-¹⁴C]-Phenanthrene, [side ring U-¹⁴C]-anthracene, and [methyl ¹⁴C]-toluene were obtained from Amersham (Arlington Heights, Ill, USA). [U-¹⁴C]-Naphthalene and [3-¹⁴C]-fluoranthene were obtained from Sigma Chemical Company.

3.1.3 Inhibitors and Uncouplers

To study the presence of energy mediated transport, two inhibitors and one uncoupler were chosen. Azide and cyanide operate in a nearly identical manner, allowing confirmation of experimental results. CCCP was chosen as a representative compound from the class of uncouplers. Sodium azide was obtained from Fisher Scientific. Potassium cyanide was obtained from Allied Chemical (New York, NY, USA). CCCP was obtained from Sigma Chemical Company.

3.1.4 Other Compounds

Acetonitrile was used for high performance liquid chromatography (HPLC) and was obtained from Fisher Scientific as HPLC grade. Chromerge cleaner, used to treat glassware, was obtained from Fisher Scientific. The sulphuric acid that was mixed with

the Chromerge component was obtained from BDH Inc. (Toronto, ON, CAN). Nitric Acid, which was also used to treat glassware, was obtained from BDH Inc. Methylene chloride was used for liquid-liquid extraction and was obtained from EM Science (Gibbstown, NJ, USA) as HPLC grade. Bicinchoninic acid (BCA) protein assay kit was obtained from Pierce Chemical Company (Rockford, Ill, USA). Tryptic Soy Broth (TSB) and Plate Count agar (PCA) were obtained from Difco Laboratories (Detroit, MI, USA). Kanamycin was obtained from Sigma Chemical Company. Aqueous liquid scintillation fluor (ACS) used for liquid scintillation counting was obtained from Amersham. Proteose peptone, yeast extract, and tryptone used for media formulation were obtained from Difco Laboratories.

3.2 Methods

3.2.1 Microbial Growth and Harvesting

Microbial strains were maintained on agar plates prior to inoculation of liquid cultures for experimental use. The wild-type strain of LP6a was maintained on Bushnell Haas agar (Appendix A) with naphthalene provided in the vapour phase as a carbon source. The mutant I-51 strain was maintained on Luria Bertani (LB) agar (Appendix A) with 25 µg/L kanamycin. The cured strain was maintained on PCA. Following streaking, all plates of LP6a strains were incubated at 30°C for 2 days then stored at 4°C. Cultures were transferred to new plates approximately every 4 weeks. For experimental use, liquid cultures of LP6a strains were inoculated from plates and grown on 100 mL of

sterile TSB. For the mutant 1-51 strain, 25 µg/L of sterile kanamycin was added after autoclaving. The cultures were grown at 30°C for 24 h on a rotary shaker set at 250 rpm. Following the growth period, the cell suspension was centrifuged in sterile centrifuge tubes at 8 000 xg for 15 min on a Sorvall RC-5B refrigerated superspeed centrifuge. The supernatant was decanted and the cells were washed by resuspending in 100 mL of sterile 0.1 M phosphate buffer (pH 7). The cells were centrifuged again at 8 000 xg for 15 min. Once again the supernatant was decanted and the cells resuspended and diluted in 0.1 M sterile phosphate buffer (pH 7) to give an optical density at 600 nm (OD₆₀₀) of 1.

The ability of the LP6a wild-type and mutant 1-51 strains to grow on toluene was tested by incubating cultures on Bushnell Haas agar at 30°C with toluene supplied in the vapour phase. The cultures were incubated over a 1 month period and checked weekly for colony formation.

A. vinelandii UW was grown on sterile Burke's Buffer with glucose and nitrogen (Appendix A). It was incubated at 30°C for 24 h on a rotary shaker set at 250 rpm. The cells were collected and diluted in the same manner as the LP6a strains.

S. epidermidis was used as a positive control to verify the experimental techniques used in transport studies. Sterile TSB was inoculated from cultures grown on PCA. A volume of 100 mL was incubated overnight at 37°C on a rotary shaker set at 250 rpm. This cell suspension was used as the inoculum source for another flask of *S. epidermidis* grown on TSB. An inoculum volume sufficient to give an initial OD₆₀₀ of 0.8 in 200 mL of TSB

was used. This new batch of *S. epidermidis* was incubated at 37°C for 3 h on a rotary shaker set at 250 rpm. After incubation, the cell suspension was washed and resuspended in 33 mM phosphate buffer (pH 7) to an OD₆₀₀ of 2.1. This cell suspension was incubated at 30°C for 3 h on a rotary shaker set at 250 rpm to deplete energy in the cells.

3.2.2 Microbial Characterization

The number of cells at an OD₆₀₀ of 1 was determined for the LP6a wild-type strain and mutant 1-51 strain using dry weight measurements, protein assays, plate counts, and cell counts. Cell counts were performed in a Petroff-Hauser counting chamber under a phase contrast microscope. Five segments of a 25-segment grid were counted and this number was extrapolated to estimate the total number of bacteria. Plate counts were performed by making serial dilutions to a dilution factor of 10⁻⁷. From each dilution, 0.1 mL was spread on PCA plates in replicates of five and grown at 30°C for 24 h. The number of colony forming units (CFU) was determined for the dilution that provided a number between 30 and 300 CFU per plate. Analysis was done in duplicate for each strain with cell suspensions prepared from separate culture flasks.

The amount of protein in the sample was determined using the BCA assay (Smith et al., 1985). This assay was chosen over other assays due to its availability and insensitivity to NaOH which was used to lyse the cells. Protein measurements were performed in triplicate for each cell suspension. Cell suspensions for each strain were also prepared in duplicate from separate culture flasks. For this assay, the cell suspension at OD₆₀₀ of 1 was diluted by a factor of ten. A volume of 1 mL was then centrifuged at 16 000 xg in a

Brinkman 5415 microcentrifuge for 10 min to collect the cell fraction. The supernatant was decanted and the pellet was resuspended in 0.1 mL of 0.1 M sterile NaOH in the 1.5-mL eppendorf centrifuge tube. The samples were incubated at 60°C for 30 min to lyse the cells. The 0.1-mL solutions of lysed cells were then transferred to 5.5-mL test tubes. To the test tubes, 2 mL of copper and BCA reagents were added in a ratio of 1:50 in accordance with the assay protocol (Pierce Chemical Company). The reaction mixtures were incubated at 60°C for 30 min. During this time, the protein reduces the copper, which then reacts with BCA to produce a colour change. Colour changes were detected by a Philips PU 8740 UV-vis Spectrophotometer at a wavelength of 562 nm. In addition to the cell suspensions, 0.1 mL of bovine serum albumin (BSA) standards and a blank of 0.1 mL of 0.1 M NaOH were also tested. The absorbances for the samples were compared to those of the BSA standards and the blank to determine the protein content of the cell suspensions.

Dry weight measurements were performed in triplicate for the same cell suspension. A 120-mL sample of cell suspension at OD₆₀₀ of 1 was centrifuged in sterile centrifuge tubes at 8 000 xg for 15 min on a Sorvall RC-5B refrigerated superspeed centrifuge. The supernatant was decanted and the cells resuspended in 5 mL of sterile 0.05 M phosphate buffer (pH 7). The cell suspension was transferred to numbered aluminum cups tared with an analytical balance, and dried at 70°C for 5 days. A medium blank, consisting of 5 mL of 0.05M buffer, was also dried. After drying, the aluminum cups were weighed.

3.2.3 Analytical Techniques

In experimental work, PAH concentrations were detected by three methods: UV-vis spectroscopy, HPLC, and liquid scintillation counting. A Philips PU 8740 UV-vis spectrophotometer was used at a wavelength of 254 nm, which corresponds to the wavelength of maximum absorbance for phenanthrene. UV-visible spectroscopy (UV-vis) is limited by an inability to distinguish individual compounds in a mixture. It detects all absorbing compounds at that wavelength. The lack of selectivity results in falsely high PAH concentrations when analyzing samples where the PAH may have been partially metabolized. HPLC was also used to determine phenanthrene concentrations. Analysis was performed with a Waters M-45 HPLC pump, with a Waters 75 WISP autosampler, and a Waters 486 tunable absorbance detector set at 254 nm. A Spheri 10 RP-18, 10- μ m, reverse phase column, 100 by 4.6 mm, was used. The mobile phase contained 60% acetonitrile-40% water and the flow rate was 2 mL/min. Comparison with standards allowed for determination of concentrations. The choice of column and mobile phase did not allow the detection of metabolites. UV-vis and HPLC were applied to experiments in which only non-radiolabeled PAHs were used.

The primary analytical technique used in transport experiments was liquid scintillation counting to detect the presence of ^{14}C -radiolabeled compounds. For analysis, 0.5 mL of sample was mixed with 10 mL of ACS and the disintegrations per min (dpm) were determined in a Beckman LS3801 liquid scintillation counter. Liquid scintillation counting detects the ^{14}C label whether it be in a PAH or metabolite molecule. Thus, some caution is required in interpreting data from experiments where there is the

potential for PAH metabolism. For each analysis, a background and a stock sample were analyzed. The background sample allowed correction of the data for background radiation. The stock sample consisted of 0.490 mL of phosphate buffer plus 10 μ L of ^{14}C -labeled PAH.

3.2.4 Method Development

3.2.4.1 Glassware Treatment

Due to non-reproducible, high levels of adsorption of PAH to glassware, a method to treat the glassware was developed. Two approaches were taken: to expose the glass surface to chromerge overnight and to expose the glass to chromerge overnight followed by exposure to nitric acid overnight. After comparison of results, treatment with chromerge followed by treatment with nitric acid was used for all subsequent work.

3.2.4.2 Filtration

Filtration was explored as a possible method to study PAH transport. In this method, a filter was placed in a filter block that was inserted into a vacuum flask and attached to a vacuum pump. The tubing for the vacuum line was set up in such a way that a valve controlled the direction of air suction and thus controlled when the apparatus drew material through the filter (Figure 3.1). Abiotic control experiments were set up with 20 mL of sterile 0.1 M phosphate buffer (pH 7) in 250-mL erlenmeyer flasks. The flasks had been treated with chromerge and nitric acid. To the flasks, a mixture of non-labeled

and ^{14}C -radiolabeled phenanthrene was added to give 100 000 dpm at a concentration of $6.36\ \mu\text{mol/L}$. Prior to sampling, 5 mL of phosphate buffer at 0°C (0.1M, pH 7) were added to the filtration block to dilute the sample and stop transport. At set times, 1-mL samples were taken from the flasks and added to the 5 mL of buffer in the filter apparatus. The valve on the vacuum line was turned to initiate filtration. The filters were then dried and the amount of ^{14}C retained by the filter was determined by liquid scintillation counting. To find a suitable filter for this method, 0.22- μm GVWP, HA, and GS membrane filters and 1.6- μm glass fiber filters (Millipore Corporation, Bedford, MA, USA) were tested

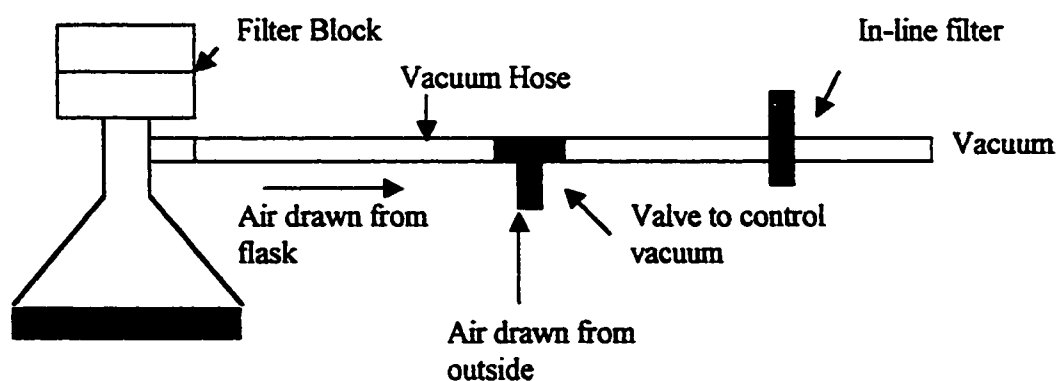


Figure 3.1 Schematic of filtration apparatus

3.2.4.3 Rapid Centrifugation

Rapid centrifugation was also explored as a potential method for transport studies. Both abiotic control and biotic experiments were tested in triplicate. The abiotic control experiments were set up with 20 mL of sterile 0.1M phosphate buffer (pH 7) in 250-mL

erlenmeyer flasks that had been treated with chromerge and nitric acid. For the biotic experiments, 20 mL of a cell suspension of yeast at an OD₆₀₀ of 1 was used. Yeast was used in the initial stages of experimentation as a rapid growing microbe to establish procedures. To both the abiotic control and biotic experiments, ¹⁴C-phenanthrene was added to give 100 000 dpm at a concentration of 6.36 µmol/L. At set time points, 1-mL samples were pipetted into sterile 1.5-mL eppendorf centrifuge tubes and centrifuged in a Brinkman 5415 microcentrifuge at 16 000 xg for 20 seconds with a 15 second deceleration time. A 0.5-mL sample of the supernatant/aqueous phase was pipetted into a liquid scintillation vial. The rest of the supernatant was carefully decanted with pipettes. The pellet was resuspended in 1 mL of 0.1M phosphate buffer (pH 7) and 0.5 mL was sampled for liquid scintillation counting. For the abiotic control flasks, since there is no pellet phase, 1 mL of phosphate buffer was added to the eppendorf tube after the supernatant was removed to look at the extent of desorption of phenanthrene.

3.2.5 Transport of Phenanthrene Experiments

Phenanthrene was used as a representative PAH for most of the experimentation. Non-labeled PAH standards were prepared as concentrated solutions in ethanol. These were mixed with the corresponding ¹⁴C labeled PAH in a ratio that gave, upon dilution into 20 mL of sample, 100 000 dpm per flask at the desired experimental concentration. The dilution of PAH into flasks resulted in the addition of up to 30 µL of ethanol to the flask. The original ¹⁴C-phenanthrene stock was dissolved in benzene and was diluted into ethanol for use, giving a solution that was 91% ethanol-9% benzene. When mixed with non-labeled phenanthrene and added to the flask, it resulted in 45 ppm_v or 1.5 mM

benzene in the flask. Since the benzene and ethanol were added at the same time as the phenanthrene, they were not able to induce any factors that would affect the observed transport of phenanthrene.

Transport studies with phenanthrene were conducted in acid-treated 250-mL erlenmeyer flasks, using the rapid centrifugation method described above. Experiments using 20 mL of cell suspension of the LP6a wild-type strain, mutant 1-51 strain, and cured strain at an OD₆₀₀ of 1 were conducted. An abiotic control experiment was also performed using 20 mL of sterile 0.1 M phosphate buffer (pH 7) in place of a cell suspension. All experiments were done in triplicate with 100 000 dpm of ¹⁴C-phenanthrene at a concentration of 6.36 µmol/L. All transport experiments were conducted at room temperature. Two sets of experiments were conducted for the biotic experiments: one in which 120 mM sodium azide was added at 8.5 min and one where no inhibitors were used. Sodium azide was added as a solid. For the abiotic control, two sets of experiments were conducted: one where the liquid phase was sampled directly from the erlenmeyer flask and another where the liquid phase was sampled after using the rapid centrifugation technique. Also, 120 mM sodium azide was added at 8.5 min for all abiotic control experiments.

3.2.6 Positive and Negative Controls

To determine if the established methods are able to measure transport behaviour, a positive control experiment was done. Since isoleucine is actively transported into *S.*

epidermidis, this compound and strain were used. The cells were suspended to an OD₆₀₀ of 2.1 and starved at 30°C for 3 h. Three experiments were tested at room temperature: a biotic control, a positive control, and an azide inhibited system. For the biotic control, 5 mL of 33 mM phosphate buffer was added to 15 mL of cell suspension in treated 250-mL erlenmeyer flasks at time zero to give a final OD₆₀₀ of 1.6. For the positive control, 5 mL of a 20 mM glucose solution was diluted into 15 mL of cell suspension at time zero to give 5 mM glucose at an OD₆₀₀ of 1.6. The azide inhibited system was set up identically to the positive control and 40 mM azide was added as a solid at 8.5 min. To each flask, ¹⁴C-isoleucine was added at time zero to give 1x10⁶ dpm at a concentration of 0.13 mM

To demonstrate that the observed trends in transport studies with LP6a were a result of transport factors alone, the uptake of phenanthrene in *Azotobacter vinelandii* UW was studied. *A. vinelandii* UW was grown up as previously described and washed and resuspended in sterile 0.1 M phosphate buffer (pH 7) to an OD₆₀₀ of 1. The transport of ¹⁴C-phenanthrene at 6.36 µmol/L was studied in the same manner as it was for the LP6a strains.

3.2.7 Effect of Azide Concentration

To establish complete inhibition of active transport processes, the transport of phenanthrene was studied using a range of azide concentrations. Concentrations of 1.0 mM, 11 mM, 15 mM, 30 mM, and 120 mM were used. For 15 mM, 30 mM, and 120 mM, azide was added as a solid. For 1.0 mM azide, a stock solution of 171 mM was prepared so that a 0.100 mL dilution into the sample would give 1.0 mM azide. For 11 mM azide, a stock solution of 385 mM was prepared so that a 0.5 mL dilution into the sample gave 11 mM azide. For each of these, the dilution factor was taken into account when analyzing data.

3.2.8 Other Inhibitors

To confirm the effects in the presence of azide, the transport of phenanthrene in LP6a wild-type strain and mutant 1-51 strain was studied using inhibitors. The experiments were done in triplicate with a mixture of non-labeled and ^{14}C -radiolabeled phenanthrene at 100 000 dpm and an initial concentration of 6.36 $\mu\text{mol/L}$. Rapid centrifugation was used to study transport in 20 mL of cell suspension in treated 250-mL erlenmeyer flasks. At 8.5 min, 50 $\mu\text{mol/L}$ CCCP or 10 mmol/L potassium cyanide was added. Cyanide was added as a solid. Due to extremely low quantities of CCCP used, a stock solution was prepared in ethanol. From this, 20 μL was diluted into the sample to give 50 $\mu\text{mol/L}$. To confirm that the additional ethanol had no effect, a biotic control was tested where 20 μL of ethanol was added to the LP6a mutant 1-51 strain at 8.5 min. An abiotic control was also tested where 20 μL of CCCP stock solution was added at 8.5 min to 20 mL of phosphate buffer.

3.2.9 Partitioning Experiments

To determine thermodynamic and kinetic parameters, the transport of phenanthrene was studied at different initial phenanthrene conditions. The methods for phenanthrene transport already described were used. Phenanthrene transport was studied in triplicate for each concentration. Parallel experiments were tested with and without azide addition at 8.5 min. A mixture of non-labeled and ^{14}C -radiolabeled phenanthrene was added to give 100 000 dpm and initial phenanthrene concentrations of 2.12 $\mu\text{mol/L}$, 3.54 $\mu\text{mol/L}$, and 4.95 $\mu\text{mol/L}$. These data, in addition to the data collected at 6.36 $\mu\text{mol/L}$, were used to calculate partition coefficients between the aqueous and cell phases with and without azide.

3.2.10 Transport of Other PAHs

Transport studies with other PAHs were conducted in an identical manner to phenanthrene with and without azide addition at 9.5 min. Mixtures of non-labeled and ^{14}C -radiolabeled PAH were diluted into 20 mL of sample to give 100 000 dpm at the desired concentration. Fluoranthene was used at a concentration of 1.16 $\mu\text{mol/L}$, anthracene at a concentration of 0.271 $\mu\text{mol/L}$, naphthalene at a concentration of 5.66 $\mu\text{mol/L}$, and toluene at a concentration of 643.8 $\mu\text{mol/L}$. Transport of fluoranthene and anthracene were conducted in treated 250-mL erlenmeyer flasks with 120 mM azide added as a solid. Due to volatility concerns, the transport of naphthalene and toluene was studied in closed 35-mL serum vials. The vials had also been treated with chromerge and

nitric acid. Rubber stoppers allowed sampling through the use of syringes. For the experiments in closed vials, a stock solution of 1.73 mol/L azide dissolved in buffer was prepared. A volume of 0.3 mL of the stock azide solution was diluted into the serum vial at 9.5 min to give 30 mmol/L azide. Experiments with different azide concentrations indicated that this quantity was sufficient to completely stop active transport. To verify this variation in the method, the transport of phenanthrene was studied in the closed serum vials for comparison with the standard method (Section 3.2.5). The transport of naphthalene was also studied in 250-mL erlenmeyer flasks. Volatilization of naphthalene was taken into account when analyzing this data.

3.2.11 Competitive Transport Experiments

To determine the presence of a saturable uptake or efflux mechanism, the effect of a second PAH on the transport of phenanthrene in the LP6a mutant 1-51 strain was investigated. The choice of second PAH included anthracene, fluoranthene, and naphthalene. To study competition in both passive and active transport, two sets of experiments were conducted for each PAH pair: one with 120 mM solid sodium azide added 30 min prior to the start of transport studies and one where no inhibitors were used. These experiments allowed investigation of competition on both passive and active transport. The experiments were done in triplicate using rapid centrifugation and 20 mL of cell suspension in 250-mL treated erlenmeyer flasks. At the start of the experiment, a mixture of non-labeled and ^{14}C -radiolabeled phenanthrene was diluted into the sample to give 100 000 dpm at a concentration of 6.36 $\mu\text{mol/L}$. At 9.5 min, the non-labeled second PAH was added. Naphthalene was used at a concentration of 5.66 $\mu\text{mol/L}$, anthracene at

a concentration of 0.271 $\mu\text{mol/L}$, and fluoranthene at a concentration of 1.16 $\mu\text{mol/L}$.

Once again, due to volatility concerns, experiments were conducted in the 35-mL serum vials when naphthalene was used as the second PAH.

3.2.12 Induction Experiments

Previous research on the active efflux of antibiotics and organic solvents suggested the need for induction of active efflux pumps. To observe the effect of induction on transport, the LP6a mutant 1-51 strain was grown on sterile TSB, washed, and resuspended in 0.1 M sterile phosphate buffer (pH 7). The cell suspension was diluted to provide 100 mL at an OD_{600} of 1.5 in a 500-mL erlenmeyer flask. To this suspension, non-labeled phenanthrene was added to give an initial concentration at solubility (7 μM). After 2 h of incubation at room temperature, the cell suspension was once again centrifuged, washed, and resuspended in 0.1 M sterile phosphate buffer (pH 7) to an OD_{600} of 1. The transport of phenanthrene was studied in triplicate by rapid centrifugation using 20 mL of cell suspension in 250-mL treated erlenmeyer flasks. A mixture of non-labeled and ^{14}C -radiolabeled phenanthrene was added to give 100 000 dpm and an initial concentration of 6.36 $\mu\text{mol/L}$. Results were compared to those for the non-induced LP6a mutant 1-51 cells.

3.2.13 Metabolite Extractions

To confirm that the observed trends for phenanthrene transport in the LP6a wild-type strain were a result of metabolism, the supernatant was analyzed for evidence of

metabolites. Biotic experiments were tested with both the LP6a mutant 1-51 strain and wild-type strain. A volume of 20 mL of cell suspension, at an OD₆₀₀ of 1, in treated 250-mL erlenmeyer flasks was used. An abiotic control, using 20 mL of sterile 0.1 M phosphate buffer (pH 7) in place of a cell suspension, was also tested. The abiotic control experiments were done in triplicate and biotic experiments in replicates of five. Non-labeled phenanthrene was added to the flasks to give an initial liquid phase concentration of 6.36 $\mu\text{mol/L}$. The flasks were allowed to sit for 25 min. Following this, the 20-mL volume was transferred to sterile centrifuge tubes and centrifuged at 5 900 xg on a Sorvall RC-5B refrigerated superspeed centrifuge for 15 min. A 10-mL volume of the supernatant was then carefully pipetted into a separatory flask along with 3 mL of methylene chloride for liquid-liquid extraction. The two liquids were well mixed and allowed to settle and equilibrate for 10 min. After equilibration, the methylene chloride phase was transferred to a test tube. Liquid-liquid extraction was repeated on the aqueous phase using another 3 mL of methylene chloride, which was also transferred to a second test tube. In addition, the contents of the centrifuge tube were disposed of and the tube rinsed once with water to remove all cells. The tube was then rinsed with 3 mL of methylene chloride to extract phenanthrene that had adsorbed to the walls. Of this 3 mL, a volume of 2 mL was transferred to a test tube. The methylene chloride was allowed to evaporate for 2 days at room temperature. The remaining solid residue was dissolved in 0.5 mL of acetonitrile for analysis. Phenanthrene was analyzed by HPLC using a UV-vis detector set at 254 nm. Extractions were also repeated for analysis by UV-vis spectroscopy. For UV-vis, two sets of experiments were tested in parallel. One set was extracted as described above at pH 7. To the other set, the supernatant was acidified to

pH 2 using 10 M sulphuric acid (H_2SO_4). The sulphuric acid was added to the aqueous phase in the separatory funnel prior to the addition of methylene chloride.

3.2.14 Effect of Emulsifying Agent

During extractions, material was present that was able to emulsify the organic methylene chloride phase. Preliminary work in the presence and absence of phenanthrene indicated that its presence was not affected by exposure of the cell to phenanthrene. Experiments were conducted to determine if the material had a role in PAH transport. Three flasks of 40 mL of LP6a mutant 1-51 strain cell suspension at an OD_{600} of 1 were allowed to sit for 30 min to ensure the presence of the material in question. The cell suspension was then centrifuged at 8 000 $\times g$ on a Sorvall RC-5B refrigerated superspeed centrifuge for 15 min to separate the supernatant and cell pellet phase. Experiments with 20 mL of this supernatant were tested in parallel with 20 mL of sterile 0.1 M phosphate buffer (pH 7) in 250-mL treated erlenmeyer flasks. Experiments were done in triplicate for each. To the solutions, ^{14}C -phenanthrene was added to give 100 000 dpm and an initial concentration of 6.36 $\mu\text{mol/L}$. The solutions were allowed to sit for 30 min to establish equilibrium. After equilibrium, a volume of 0.5 mL was sampled directly from the flasks for analysis by liquid scintillation counting.

4.0 RESULTS AND DISCUSSION

The objective of this research was to study the mechanisms by which PAHs are transported across bacterial cell membranes. This study focused on one PAH-degrading bacterium, *P. fluorescens* LP6a. A transposon mutant of LP6a, which is blocked in its ability to produce dioxygenase enzymes, was also used. Lacking this enzyme, the mutant 1-51 strain is unable to degrade PAHs and its use allowed the study of transport in the absence of metabolism. Sample calculations are given in Appendix B, and statistical analysis is presented in Appendix C.

4.1 Characterization of Growth of Bacteria

To understand the transport data, it was first necessary to understand the nature of the bacterium under the conditions used. Figure 4.1 gives the change in optical density for the LP6a and mutant 1-51 strains during the last 10 h of a 24-h incubation. The data plotted are an average of two samples. Only the last 10 h of incubation was monitored so as to understand the behaviour of the bacteria prior to use for transport studies. Since the cultures were inoculated from plates, the absolute values varied between batches. Figure 4.1 shows a linear stage of growth for both the wild-type and mutant 1-51 strain over a large part of the time period. At the end of the 24-h period, the mutant 1-51 strain exhibited a leveling off of the optical density. These trends indicated that the cells were in stationary phase.

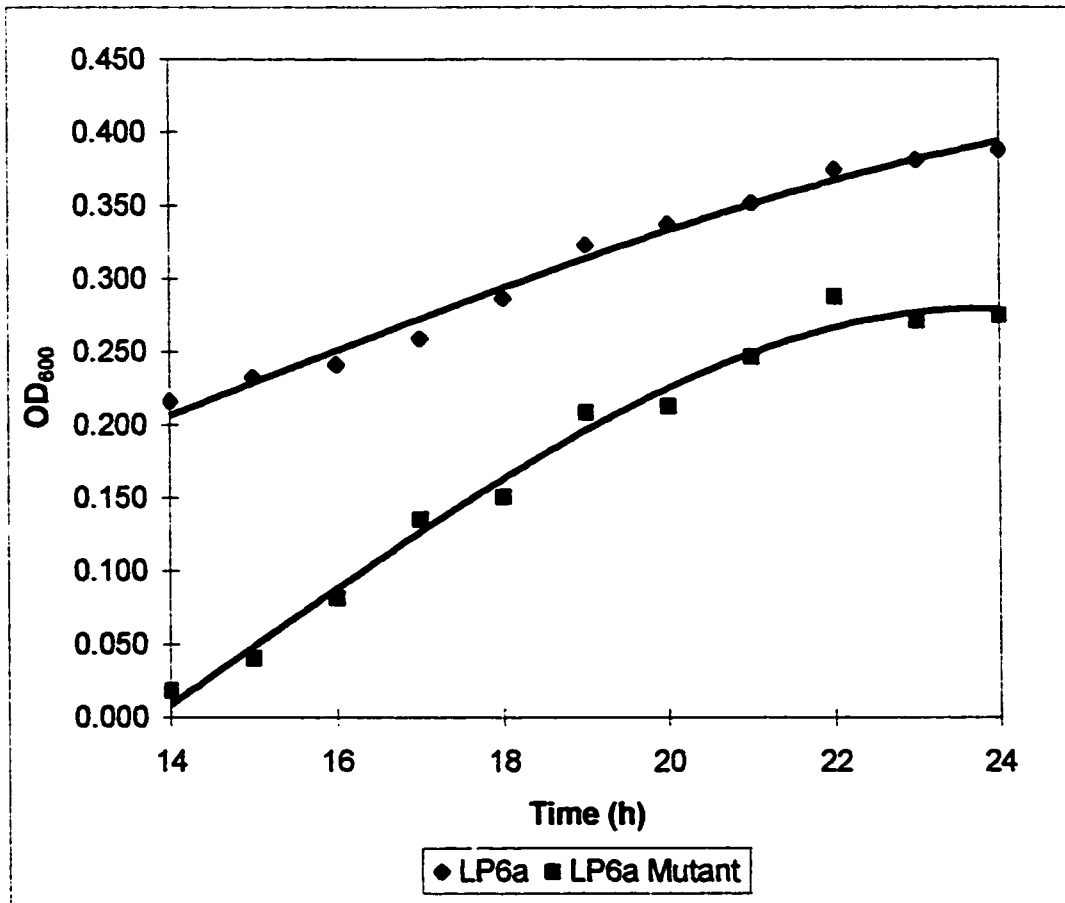


Figure 4.1 Change in optical density over time for the LP6a wild-type and mutant 1-51 strains over the last 10 h of a 24-h incubation period.

To give the data in transport studies significance, quantification of the number of cells used in an experiment was necessary. The dry weight, protein content, and number of cells for a cell suspension at an OD₆₀₀ of 1 is tabulated in Table 4.1. A comparison of the data for the wild-type to that of the mutant 1-51 strain shows similarities between the two. The similarity was expected since there should be no significant cultural differences. Both have nearly identical dry weight, protein, and plate count measurements. The largest difference lies in the cell counts. A larger variability was expected between the two though, given that only one measurement was taken. Another contributing factor was the method of counting whereby five sections of the Petroff-Hauser counting chamber were counted and this number extrapolated to estimate the total number of cells in the 25 section grid. Despite these factors, the two numbers obtained for the cell counts, 2.22×10^9 cells/mL for the mutant 1-51 strain and 1.49×10^9 cells/mL for the wild-type strain, are within the 95% confidence interval of the plate counts for both strains.

Table 4.1 Summary of cell enumeration data for LP6a wild-type and mutant 1-51 strains.

	LP6a		LP6a Mutant 1-51		Conversion factor to convert experimental results from dry weight basis
	Average	Std Dev	Average	Std Dev	
Plate Count (CFU/mL)	1.93×10^9	2×10^8	1.95×10^9	4×10^8	5.16×10^6
Cell Counts per mL	1.5×10^9		2.2×10^9		4.93×10^6
Protein (μg/mL)	187	15	186	15	0.498
Dry Weight (μg/mL)	374	25	377	28	1

4.2 Methodology

4.2.1 Treatment of Glassware

In order to study transport, a reproducible methodology needed to be established. A significant problem that was observed was the loss of PAH from the liquid phase to the glass surface of the erlenmeyer flasks. Other researchers have observed the loss of hydrophobic compounds to glass surfaces. Research with taxol, a hydrophobic drug, showed that 73% of the compound was lost in a 24-h period. However, when 9% BSA was added to the solution no loss was observed (Song et al., 1996). To eliminate PAH loss, two approaches were taken to pre-treat the flasks: exposure to chromerge overnight or to chromerge overnight followed by nitric acid overnight. Chromerge is a very strong acidic liquid composed of sulphuric and chromic acid. It reacts with and dissolves organic materials on the glass surface. Nitric acid is a very strong oxidizing agent that oxidizes reactive surfaces. These two glass treatment methods were compared to no treatment of the glassware in their ability to reduce variability in the amount of phenanthrene adsorbed. For each method, three flasks were treated and abiotic experiments were run with 20 mL of phosphate buffer. To each flask, phenanthrene was added to give an initial liquid phase phenanthrene concentration of 6.36 $\mu\text{mol/L}$. The flasks remained stationary for a 1-h time interval, after which the liquid phase phenanthrene concentration for each flask was determined by HPLC. The results are tabulated in Table 4.2. Abiotic transport experiments later confirmed that 1 h was sufficient to establish equilibrium.

Table 4.2 Summary of average liquid phase phenanthrene concentrations and variability in treated erlenmeyer flasks containing an initial concentration of 6.36 $\mu\text{mol/L}$.

Treatment Method	Concentration ($\mu\text{mol/L}$)	
	Average	Standard Dev.
None	3.03	0.53
Chromerge	3.81	0.30
Chromerge and Nitric Acid	3.73	0.07

It is apparent from Table 4.2 that treating the flasks reduced the extent of adsorption but did not eliminate it. Other potential sources of abiotic loss include volatilization. However, the vapour pressure of phenanthrene is 0.113 Pa. Thus, volatilization will not generate significant losses. In comparing the concentrations and standard deviations for each method, it can be concluded that treating the flasks with chromerge overnight followed by nitric acid treatment overnight was able to reduce the variability in abiotic losses of PAH to an acceptable level. It is important to note that treatment with chromerge alone produced one outlier out of three samples. Whether this result was human error or real variability was never explored. It is possible that chromerge treatment alone was sufficient to minimize variability in abiotic losses; but this issue was never pursued. Treatment of glassware with chromerge and nitric acid was used for all subsequent work.

4.2.2 Filtration

One method to study transport in bacteria is filtration. In this method, cell suspensions incubation with radiolabeled substrate are sampled at various times and the samples are then filtered by vacuum filtration. Analysis of the filter by liquid scintillation counting

along with comparison to appropriate controls gives the concentration of substrate trapped in the cell fraction. Abiotic control experiments were conducted whereby ^{14}C -radiolabeled phenanthrene was added to 20 mL of buffer in 250-mL erlenmeyer flasks to give 100 000 dpm at an initial liquid phase concentration of 6.36 $\mu\text{mol/L}$. At timed intervals, 1-mL samples were diluted into 5 mL of phosphate buffer in a filter apparatus and filtered through four different types of filters. The fractional amount of ^{14}C retained by each filter is reported in Table 4.3.

Table 4.3 Summary of the fractional amount of ^{14}C -phenanthrene retained by filters in filtration of abiotic controls.

Type of Membrane	Additions to Buffer	Fractional Amount of ^{14}C Retained
HA		77%
GS		73%
GVWP		89%
GVWP	Phenanthrene	87%
GVWP	Acetonitrile	33%
Glass Fiber 1.6 μm		40%
Glass Fiber 1.6 μm	Phenanthrene	36%

HA and GS cellulose acetate filters and GVWP hydrophillic polyvinylidene fluoride filters are membrane filters with a 0.22- μm pore size. From the data in Table 4.3, it is apparent that these filters retained 73% to 89% of the total phenanthrene in the abiotic controls. In an effort to reduce the amount of material adsorbed, two approaches were taken: addition of phenanthrene to the buffer to pre-saturate the filter and addition of acetonitrile to the buffer to increase the hydrophobicity of the liquid and decrease the amount adsorbed from the aqueous phase. For the GVWP filter, adding phenanthrene to

the dilution buffer resulted in the adsorption of 87% of the sampled compared to 89% for no phenanthrene presaturation. The lack of reduction in the amount of material adsorbed from the abiotic control indicated that the filter was not saturated and had a significant capacity for adsorption of phenanthrene. The addition of acetonitrile did decrease the amount adsorbed to 33%. However, the use of acetonitrile raises concerns about leaching PAH from bacteria during filtration. Leaching would give falsely low cell concentrations. Thus, this approach was never pursued. Experiments were also conducted with glass fiber filters. From the data in Table 4.3, the amount of phenanthrene retained by glass fiber filters was 36–40%. However, the smallest pore size filters that are commercially available are 1.6 μm . This size is too large to retain all the cells in the sample. As a result, glass fiber filters were unsuitable for quantification of amounts of PAH in bacteria. From the data in Table 4.3 it can be concluded that filtration is not a suitable method for studying the transport of highly hydrophobic compounds.

4.2.3 Rapid Centrifugation

A second approach for studying transport was to use a rapid centrifugation method. In this method, 1-mL samples were centrifuged at 16 000 $\times g$ in 1.5-mL eppendorf tubes. This method allowed for sampling of the aqueous phase concentration, as well as the cell associated concentration. The eppendorf tubes are polymer materials and may be susceptible to adsorption of PAHs. As a result, centrifuging times were adjusted to reduce adsorption but allow sufficient time to collect as many cells as possible. For this purpose, a centrifuge time of 20 s was chosen, with a deceleration time of 15 s. A biotic

experiment was set up with 20 mL of LP6a wild-type cell suspension at an $OD_{600}=1$ in a 250-mL erlenmeyer flask. A volume of 1 mL of the cell suspension was centrifuged for 20 s and the OD_{600} of the supernatant phase was measured. Comparison of the optical density of the supernatant to that of the cell suspension indicated that this method collected approximately 95% of the cells in the pellet phase. Thus, there will be a small overestimate of the supernatant PAH concentrations and an underestimate of the cell pellet PAH concentrations by this method. An additional consideration was the amount of liquid trapped in the cell pellet. Given the short centrifuge times, the cell pellet was not densely packed. However, the fraction of liquid in the cell pellet was not determined and gave a bias in the measurements. Thus, the actual cell concentration was always slightly lower than the reported values.

To determine the reproducibility of rapid centrifugation, samples from an abiotic control flask of phosphate buffer and a biotic flask of a *Saccharomyces cerevisiae* cell suspension at OD_{600} of 1 were analyzed using this method. An initial phenanthrene concentration of $6.36 \mu\text{mol/L}$ was used for each flask. *S. cerevisiae* was used as a trial organism in the initial states of experimentation to establish a procedure. From each flask, three samples were taken and analyzed. The average liquid phase concentration and standard deviation after equilibrium was reached is reported in Table 4.4. For the abiotic control, $76.4 \pm 3.1\%$ of the phenanthrene was retained in the aqueous phases. The remainder of the phenanthrene is assumed to be adsorbed to the equipment. Since phenanthrene has a vapour pressure of 0.113 Pa, phenanthrene is not expected to be lost by evaporation (Mackay and Shiu, 1992). The rapid centrifugation method also shows

very good reproducibility for the supernatant and cell pellet fractions. The supernatant concentration was $27.7 \pm 0.1\%$ and the cell pellet concentration was $53.3 \pm 4.4\%$. There was a larger variance associated with the cell pellet fraction, but this error was expected given the difficulty in not disturbing the cell pellet during the decanting of the supernatant. The sampling of the cell pellet required decanting the remaining supernatant and resuspending the pellet in phosphate buffer. As a result, there was concern about the possibility of desorption of PAH from the eppendorf tube, giving false elevated pellet concentrations. To determine if abiotic factors affect phenanthrene concentration in the cell pellet phase, 1 mL of phosphate buffer was added to the eppendorf tube of the abiotic control after the supernatant had been sampled and decanted. The amount of phenanthrene that desorbed was 0.6% of the total amount added. Given other sources of error, this amount is negligible. Thus, there were no abiotic contributions to the reported pellet concentrations. From all the data in Table 4.4, it can be concluded that rapid centrifugation gives highly reproducible results for studying the transport of PAHs.

Table 4.4 Summary of results for rapid centrifugation tests with *S. cerevisiae* cells.

	Phenanthrene Concentration (% of total phenanthrene)		
	Average	Standard Dev.	Total Measured
Abiotic Supernatant	76.4	3.1	77.0
Desorbed from Tube	0.6	0.1	
Biotic Supernatant	27.7	0.001	81.0
Biotic Pellet Fraction	53.3	0.044	

4.3 Positive Control

To verify that the rapid centrifugation method gave valid results, the transport of isoleucine in *S. epidermidis* was studied. Isoleucine is known to be actively transported into this bacterium (Microb 313 Laboratory manual, Department of Biological Sciences, University of Alberta, 1999). Experiments were set up with 20 mL of cell suspension at an OD₆₀₀ of 1.6 in treated 250-mL erlenmeyer flasks. The cells had been starved to deplete energy reserves. For this experiment, three tests were conducted: a biotic control, a positive control where 5 mM glucose was added at time zero, and an experiment with azide where 5 mM glucose was added at time zero and 40 mM azide added at 8.5 min. For each experiment, 0.13 mM ¹⁴C-isoleucine was added at time zero.

The supernatant and cell pellet concentrations of isoleucine for each of the experiments are given in Figure 4.2. For the biotic control, there was a slight increase in pellet concentration and a slight decrease in supernatant concentration over time. Since the cells had been starved, there was no energy source for active transport. The observed results were due to the slow passive uptake of isoleucine. For the experiments without azide, the addition of glucose allowed for the production of energy in the cells.

Consequently, isoleucine was actively transported into the cells. This process is seen in Figure 4.2 where there was a drastic increase in the pellet isoleucine concentration with time. At the end of the 45-min time period, the fractional amount of isoleucine in the pellet was 43.1% for the experiments without azide versus 10.3% for the biotic control. In conjunction with this trend, there was a drastic decrease in supernatant

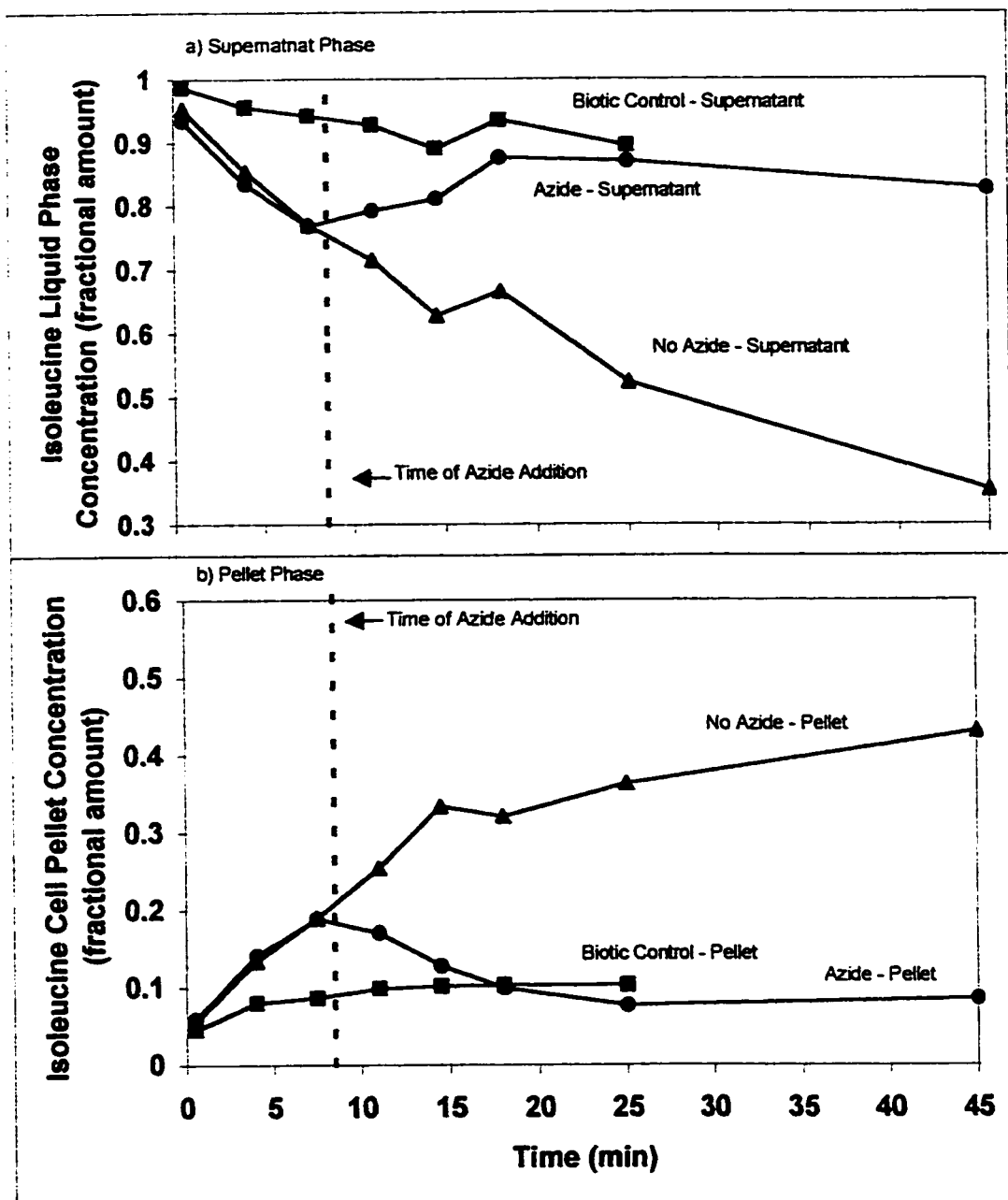


Figure 4.2 Time dependence of a) supernatant phase and b) cell pellet phase isoleucine concentrations for the transport of isoleucine in *S. epidermidis*.

isoleucine concentration for the experiments without azide to levels significantly below the biotic control.

Rapid centrifugation was also able to detect inhibition of the active uptake of isoleucine. In Figure 4.2, for the experiments with azide, there was an increase in the cell pellet isoleucine concentration and decrease in supernatant isoleucine concentration for the first three sample points. These values are comparable with those obtained in the experiments without azide. Thus, during the first 7.5 min, isoleucine was actively transported inside the cells to levels higher than equilibrium. However, when 40 mM azide was added at 8.5 min, there was a decrease in cell pellet concentration and a corresponding increase in supernatant concentration. This observation was a result of the dissipation of the established isoleucine gradient. When active uptake was inhibited, cell pellet and supernatant isoleucine concentrations returned to equilibrium levels. At the end of the sampling period, the pellet phase isoleucine concentration was 8.56% in the experiments with azide. This value was similar to the isoleucine concentration of 10.3% for the biotic control.

The trends for active uptake and inhibition in *S. epidermidis* are identical to those observed for other active uptake processes studied by other researchers. For example, the active transport of 4-toluene sulphonate into *C. testosteroni* T-2 cells displayed an accumulation of this substrate over time. When uptake was inhibited with CCCP, the cell concentration drastically decreased (Locker et al., 1993). Thus, it can be concluded that

rapid centrifugation is able to detect active transport and inhibition of active transport of the highly water soluble substrate isoleucine.

Another observation for all three tests was that at any point during sampling, the sum of the isoleucine in the pellet and liquid fractions corresponded to 100% recovery of the ^{14}C -isoleucine. Thus, the rapid centrifugation method is also an accurate method for the recovery of hydrophilic substrates.

4.4 Uptake of Phenanthrene

A significant portion of the research was conducted using phenanthrene as a model compound. Phenanthrene was chosen because the compound is not volatile and has a high molar absorptivity for analysis by UV-vis and HPLC. These properties allowed for easy analysis in experiments that did not require radiolabeled substrates.

4.4.1 Abiotic Partitioning

To gain a better understanding of the data for the transport of PAHs in bacteria, it was first necessary to understand the abiotic behaviour. Figures 4.3 and 4.4 shows the liquid phase phenanthrene concentration over time for abiotic controls on a fractional and absolute scale respectively. Two sets of experiments were conducted: one where samples were taken directly from the flask and one where samples were taken after using the rapid centrifugation method. All experiments were done at an initial phenanthrene concentration of $6.36\ \mu\text{mol/L}$. This concentration was determined from the ^{14}C activity of the phenanthrene stock solution, which was diluted into the flasks. Thus, an accurate

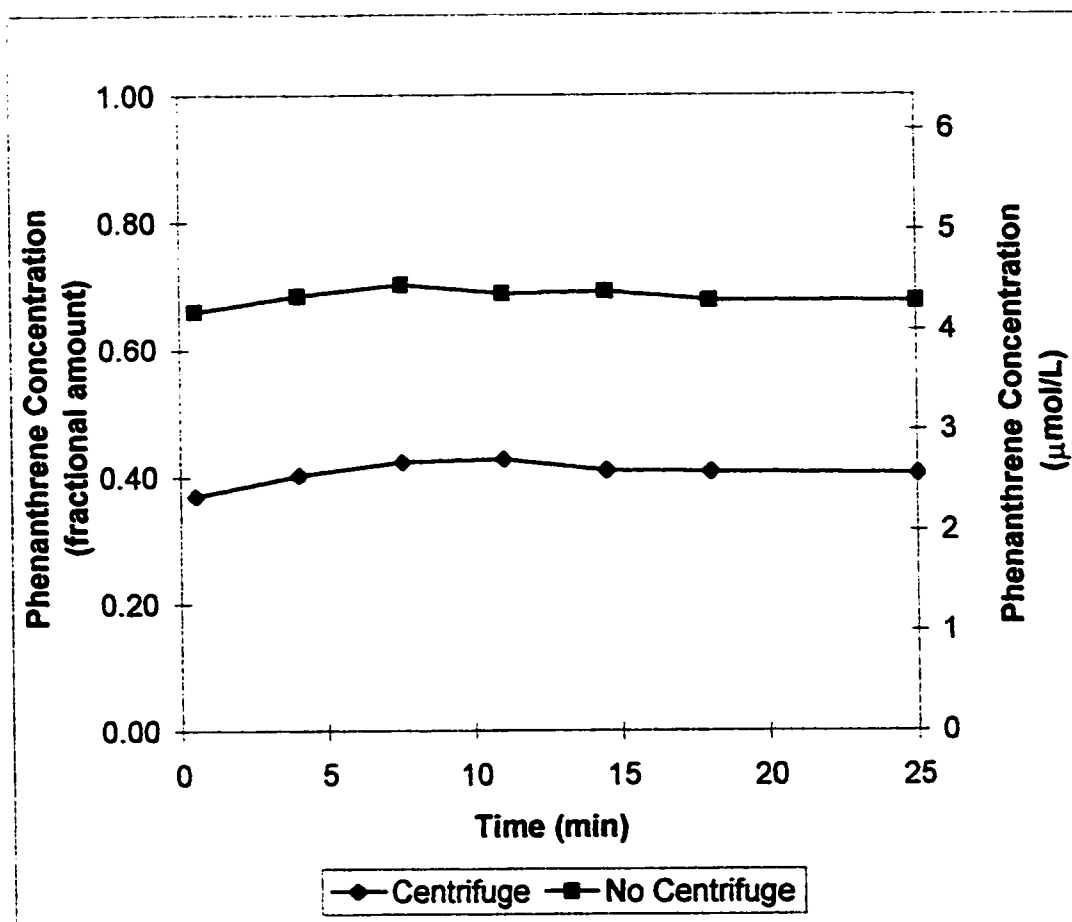


Figure 4.3 Liquid phase phenanthrene concentration for partitioning in abiotic control.

determination of the total phenanthrene added was possible. For all experiments, 120 mM sodium azide was added at 8.5 min. These graphs indicate that there was an immediate partitioning of phenanthrene to the glass surface of the flask and to the plastic walls of the centrifuge tubes that remained constant over time for both tests. Thus, there are no physical or chemical processes that alter the liquid phase phenanthrene concentration of the 25-min time period. The graphs also suggest that the partitioning was very rapid and that the methodology was not fast enough to study the initial unsteady-state behaviour. These results highlight a limitation in the method used. Also, Figure 4.3 indicates that the total amount of material lost after centrifugation was 59%. Although this is a significant portion, it was reproducible and allowed for accurate analysis of biotic data. An important distinction is that phenanthrene was lost to all equipment used: the flask, the eppendorf tube, and the pipette tips used to transfer the sample.

4.4.2 Biotic Transport

The transport of phenanthrene was studied in 20 mL of cell suspension of LP6a wild-type, mutant 1-51, and cured strains at an OD_{600} of 1. An initial liquid phase concentration of 6.36 $\mu\text{mol/L}$ of radiolabeled phenanthrene was used. To determine if transport is active or passive, parallel experiments were tested with and without 120 mM sodium azide addition at 8.5 min. Figures 4.4 and 4.5 show the concentrations in the cell pellet and supernatant for the transport of phenanthrene in LP6a wild-type on a fractional and absolute scale respectively. For the case without azide, there was a continuous increase in supernatant concentration over time (Figure 4.5). At the endpoint of the

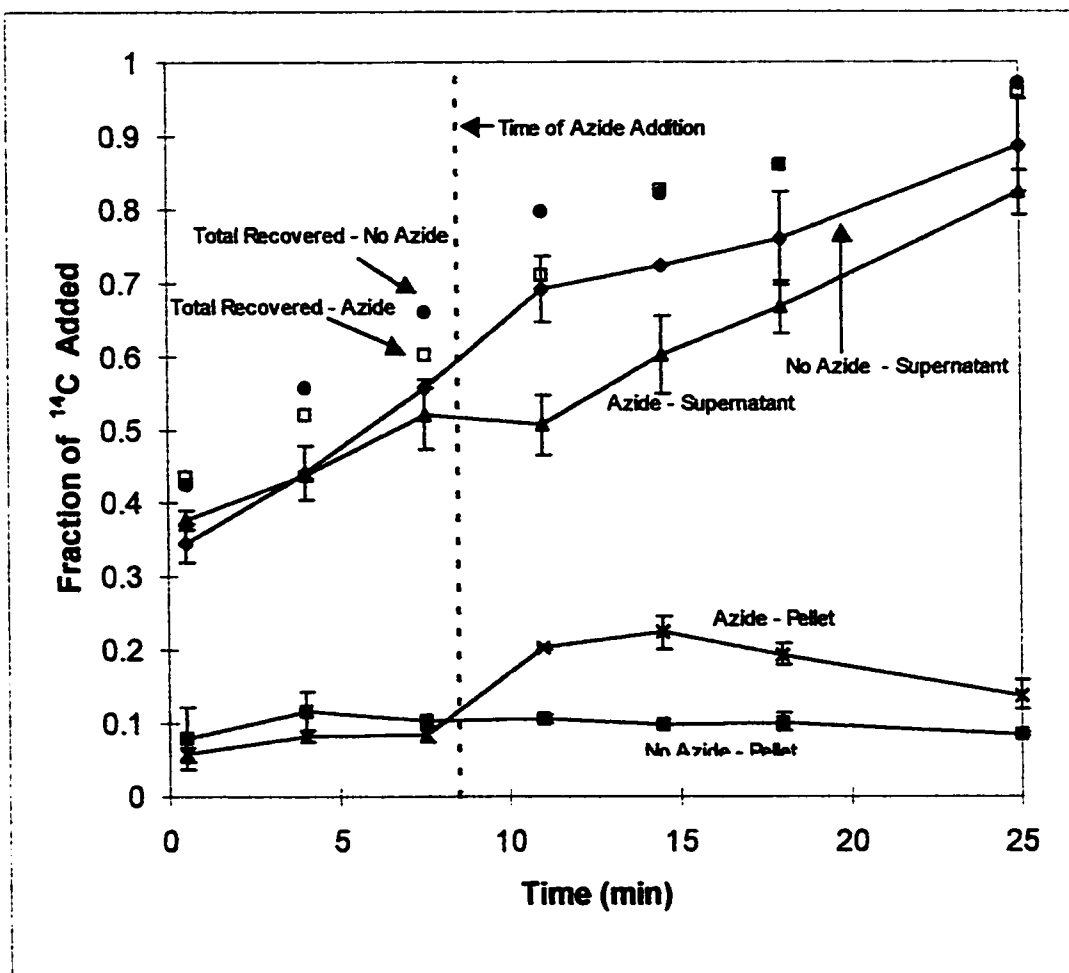


Figure 4.4 Time dependence of liquid phase and cell pellet ^{14}C concentrations for the transport of phenanthrene in LP6a wild-type strain. The data points are an average of three samples and the error bars represent one standard deviation.

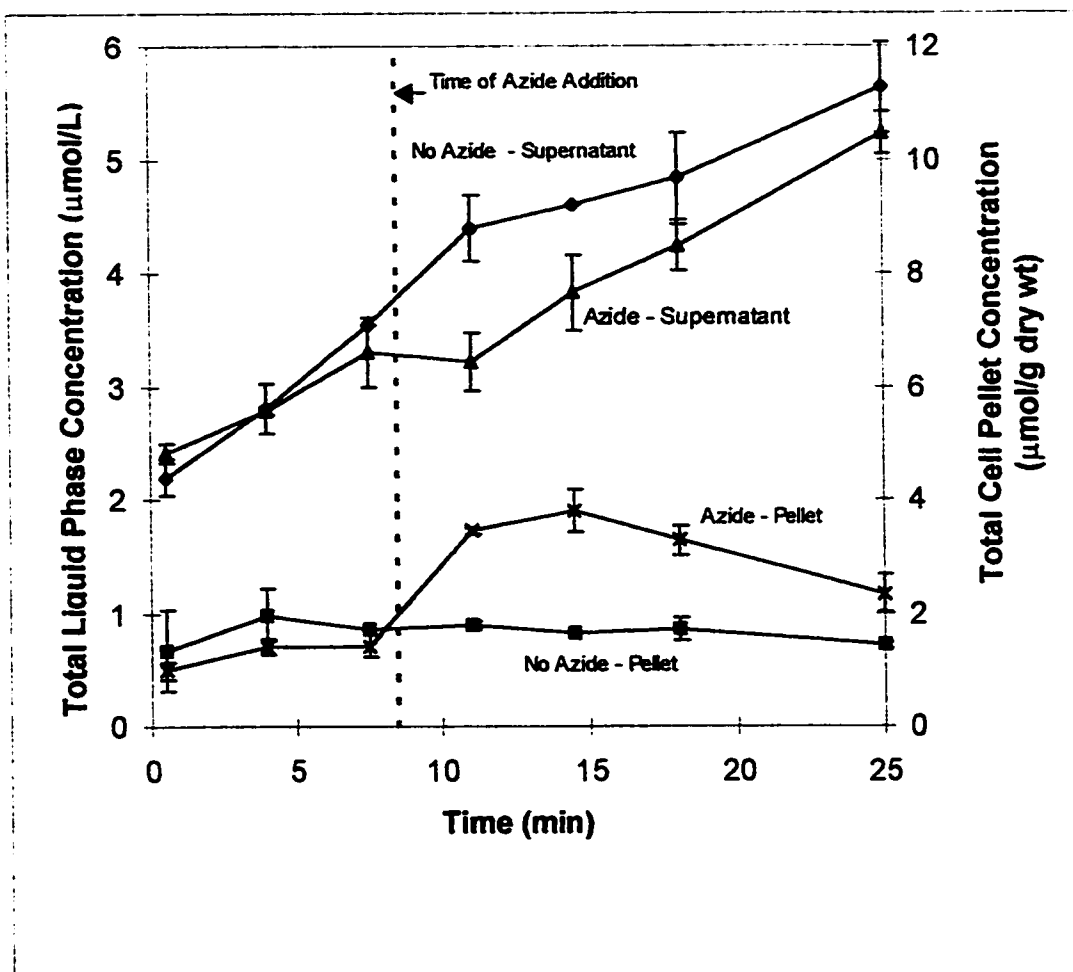


Figure 4.5 Time dependence of liquid phase and cell pellet phenanthrene and metabolite concentrations for the transport of phenanthrene in LP6a wild-type.

experiment, the sum of the amount of ^{14}C in the pellet and supernatant indicates 97.0% recovery of the ^{14}C -label. Liquid scintillation counting detects the ^{14}C label regardless of modification to the compound. It does not detect phenanthrene itself. Thus, the observed increase ^{14}C levels in the supernatant can be explained by metabolism of phenanthrene by LP6a. As the compound was metabolized, polar intermediates were produced which did not adsorb to the equipment. Furthermore, as the compound was metabolized, the supernatant concentration of phenanthrene decreased and phenanthrene that was adsorbed to the flask desorbed into the liquid. Thus, it is possible for there to be 100% recovery of ^{14}C label. The high degree of recovery confirms that the observed losses in Figure 4.3 are a result of adsorption and not volatilization of phenanthrene.

From the graphs, it appears that the metabolites are being released quickly into the medium. One possible explanation is that the metabolites are subject to active efflux as well. The initial metabolites of phenanthrene degradation are similar in structure to the parent compound and could be transported out of the cell along with phenanthrene. However, the increase in liquid phase ^{14}C levels continues after azide is added. It may be that in the presence of the energy poison, the active efflux pump operates as a facilitated pump. In such case, the metabolites would continue to be transported out of the cell. Metabolism would ensure that equilibrium is never established.

Due to metabolism, it is difficult to interpret the results in Figure 4.4 without comparison to the data for the mutant 1-51 strain. Figures 4.6 and 4.7 show the transport of phenanthrene in the LP6a mutant 1-51 on a fractional and absolute scale respectively. In

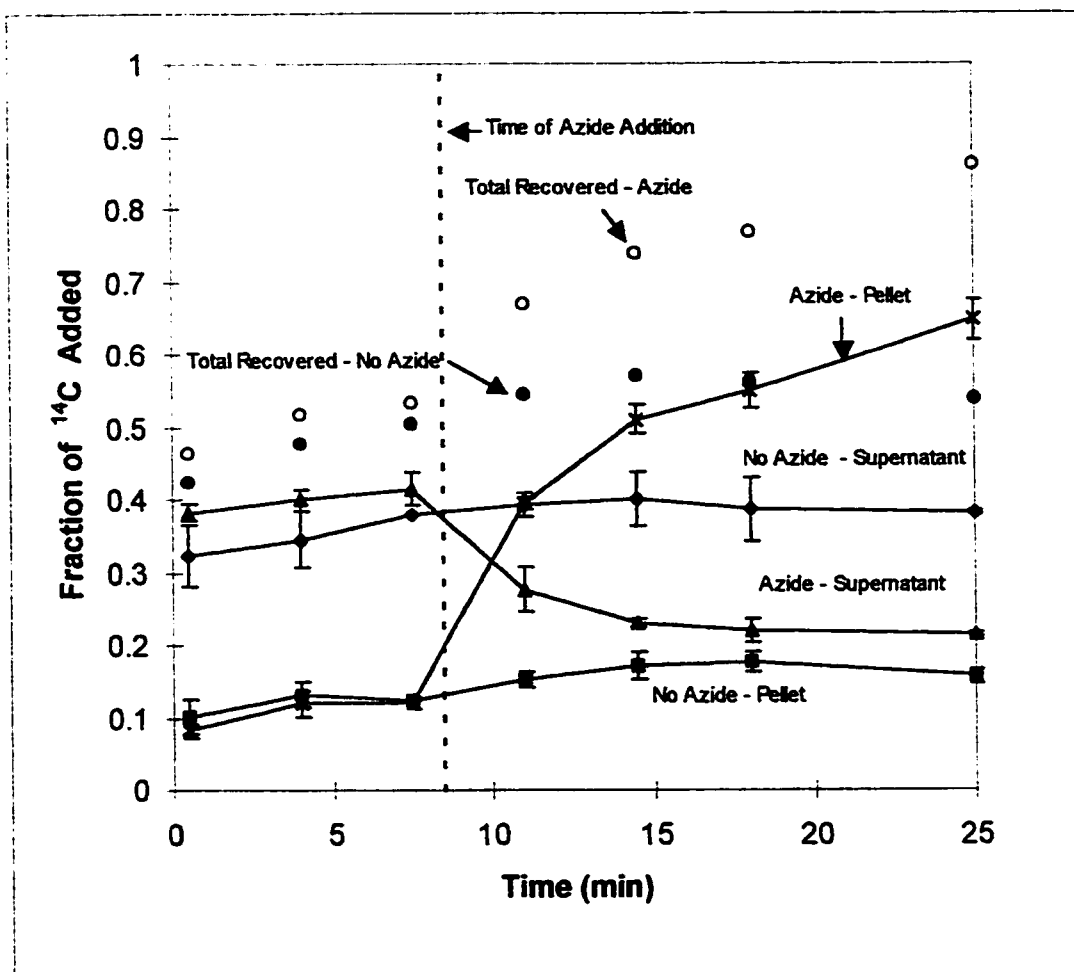


Figure 4.6 Time dependence of liquid phase and cell pellet ^{14}C concentrations for the transport of phenanthrene in LP6a mutant 1-51.

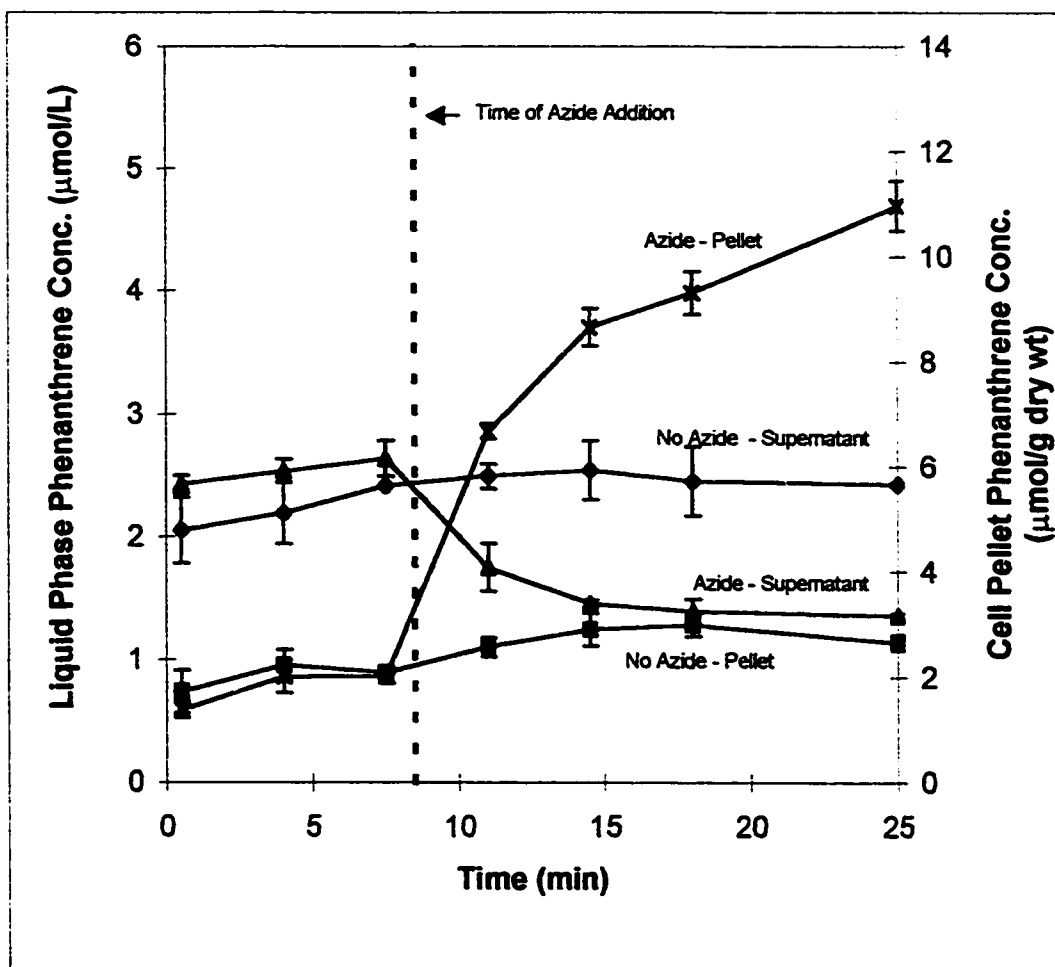


Figure 4.7 Time dependence of liquid phase and cell pellet phenanthrene concentrations for the transport of phenanthrene in LP6a mutant 1-51.

the case without azide, there was a constant cell pellet and supernatant concentration over time. The phenanthrene concentration in the supernatant was $2.5 \pm 0.2 \mu\text{mol/L}$ and the concentration in the cell pellet was $2.8 \pm 0.3 \mu\text{mol/(g dry wt)}$. The lack of change in supernatant and cell pellet concentrations over time indicate that steady-state had already been achieved by the time the first sample was processed. It is important to remember that although the data points are plotted at the time the sample was taken, there was a period of 2.5 min during which the sample was being centrifuged and each fraction sampled. Thus, it is understandable that the method wasn't rapid enough to detect the unsteady-state portion of this rapid partitioning.

For the experiments with azide, there was an immediate increase in cell pellet concentration and a decrease in supernatant concentration when azide was added. After equilibrium was reached, the supernatant phenanthrene concentration was $1.4 \pm 0.1 \mu\text{mol/L}$ and the cell pellet concentration was $11.0 \pm 0.5 \mu\text{mol/g dry wt}$. This trend is the reverse of that seen for the active uptake of isoleucine in *S. epidermidis*. What these data suggest is that phenanthrene is passively transported into the bacterium and transported back out by an active efflux pump. The efflux mechanism maintains the intracellular phenanthrene concentration below its equilibrium level. When this pump is shut down, phenanthrene can then be passively transported into cell until equilibrium is reached. This same trend is observed in research on efflux pumps in other bacteria. For example, when active efflux in a multi-drug resistant *P. Aeruginosa* strain was inhibited with CCCP, the cell concentration of drugs increased drastically (Nikaido, 1996). Thus, the thermodynamic partitioning is represented by the equilibrium values after azide addition.

Efflux can also be seen to an extent in the wild-type data (Figure 4.4 and 4.5). When azide was added, there was a slight decrease in supernatant concentration and a slight increase in cell pellet concentration. Azide only interferes with the electron transport chain and active processes (Brock et al., 1994). The enzymes for phenanthrene metabolism are already present and will continue to degrade the substrate regardless of the presence of azide. As metabolism continued, the cell pellet concentration decreased and the supernatant concentration continued to increase. The effect of azide addition was less pronounced because of metabolism. Presumably a smaller portion of the ^{14}C label was unaltered phenanthrene because of its metabolism. Hence, a smaller portion of the ^{14}C accumulated in the cell after azide addition.

In looking at Figure 4.4 and 4.6, which show the data on a fractional amount for LP6a wild-type and mutant 1-51 strains, it is apparent that phenanthrene entered the cells very easily. There was a rapid initial partitioning of material into the cell prior to the first data point. The rate at which it occurred in the absence of azide was too high to be studied by the centrifugation method. This fact is further emphasized by the rate at which it accumulated in the mutant 1-51 strain after azide addition. There was also an extremely high extent of partitioning into the cells. The volume of the cells was less than 1% of the total volume of the system. Yet in the mutant 1-51 strain, after azide addition, 65% of the total phenanthrene was localized in the cell fraction. This high partitioning reflects the extremely hydrophobic nature of PAHs. It also illustrates potential toxicity concerns posed by high PAH concentrations at contaminated sites.

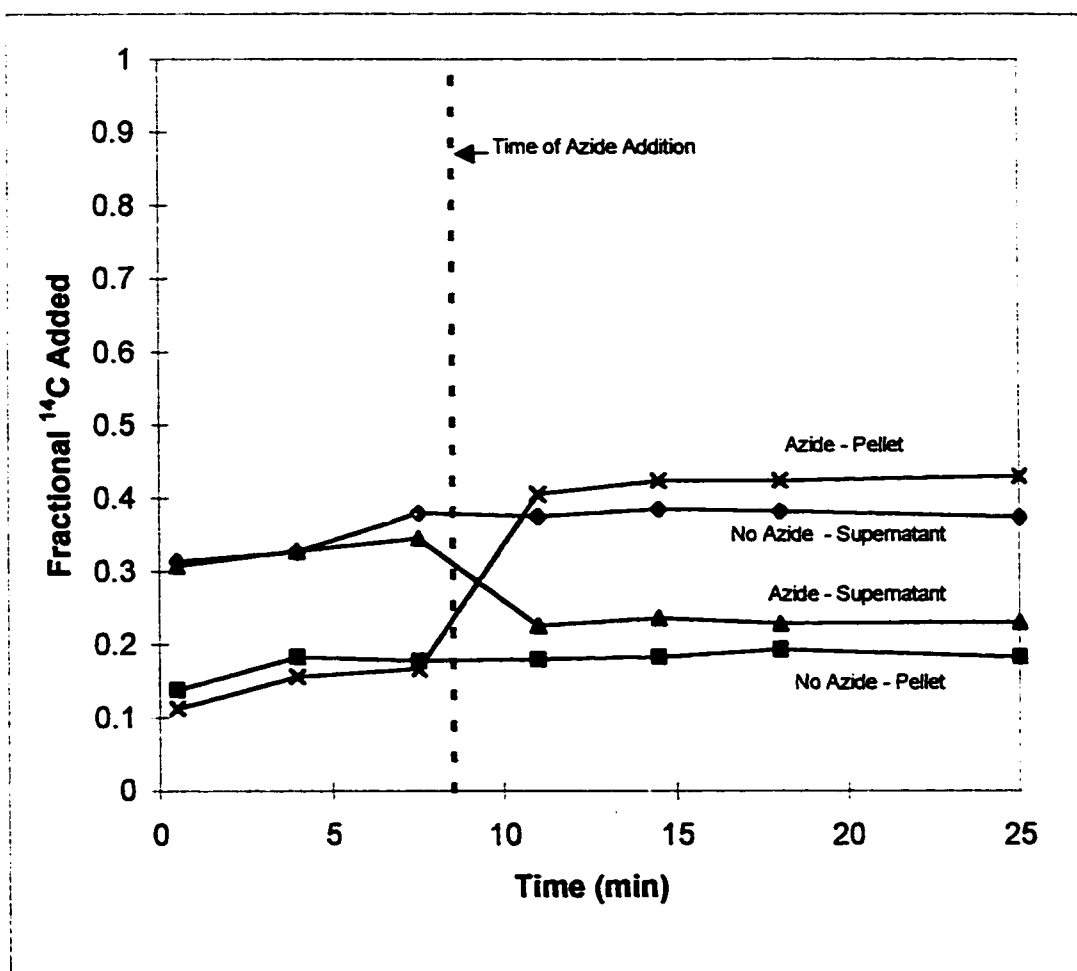


Figure 4.8 Time dependence of liquid phase and cell pellet phenanthrene concentrations for the transport of phenanthrene in LP6a cured strain.

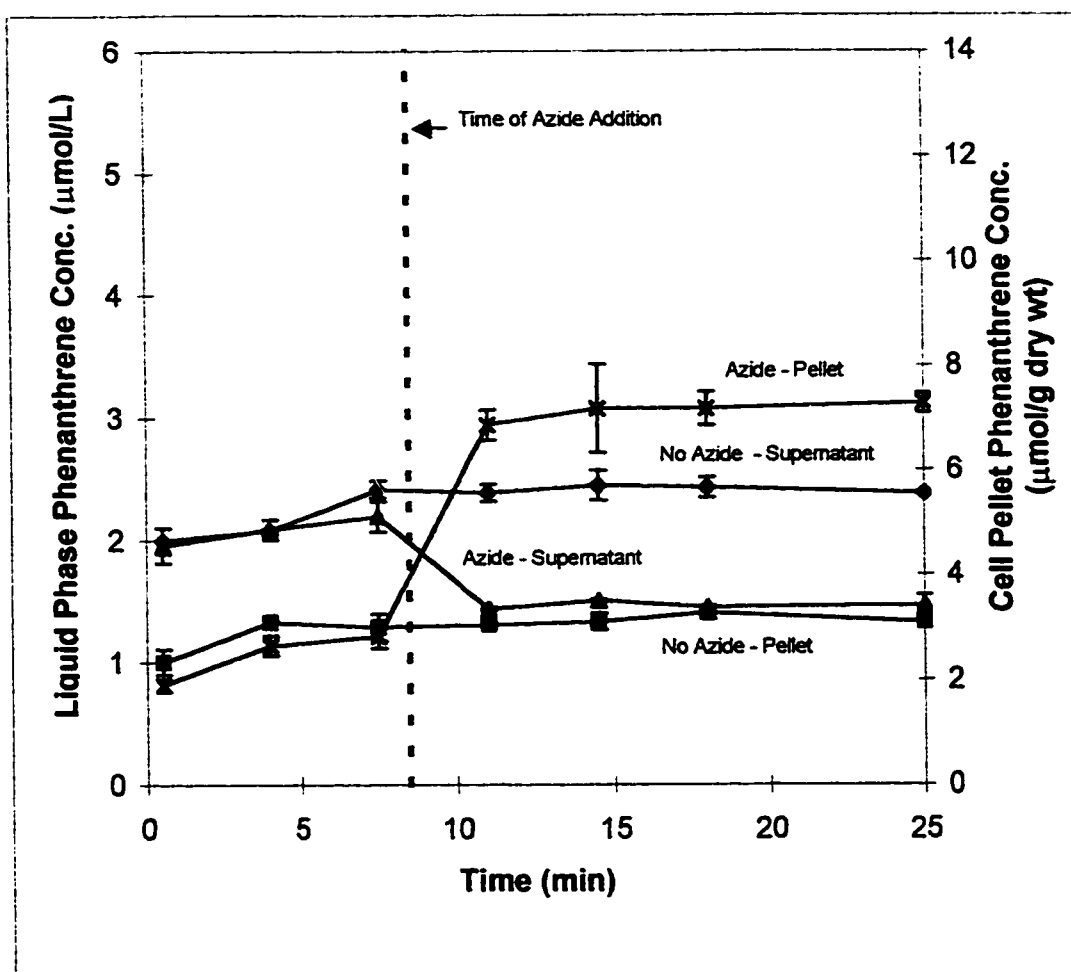


Figure 4.9 Time dependence of liquid phase and cell pellet phenanthrene concentrations for the transport of phenanthrene in LP6a cured strain.

The genes for metabolism of PAHs in LP6a are located on a plasmid (Foght and Westlake, 1996). The question arises as to whether the genes encoding this efflux pump are also located on the plasmid. Transport studies were performed on a cured strain of LP6a, lacking the plasmid responsible for PAH degradation. Figure 4.8 and 4.9 show the transport of phenanthrene in the LP6a cured strain on a fractional and absolute scale respectively. The experiment in the presence of 120 mM azide indicated that the efflux behaviour is also present in the cured strain. When azide was added, the supernatant phenanthrene concentration decreased from $2.4 \pm 0.1 \mu\text{mol/L}$ to $1.5 \pm 0.1 \mu\text{mol/L}$. The cell pellet concentration increased from $3.1 \pm 0.2 \mu\text{mol/(g dry wt)}$ to $7.2 \pm 0.5 \mu\text{mol/(g dry wt)}$. For the experiments without azide, the concentrations remained constant over time. The lack of the plasmid in the cured strain suggests that the efflux mechanism is chromosomally encoded and not related to the biodegradation of PAHs. These observed trends in LP6a cured strain are also similar to those in LP6a mutant 1-51 strain which confirms uptake and efflux of phenanthrene in the absence of metabolism.

4.4.3 Procedural Evaluation

To confirm that results obtained by rapid centrifugation method are valid, the transport of PAHs in the LP6a mutant 1-51 strain with and without 120 mM azide was studied by filtration using glass fiber filters. As was previously discussed, the most significant problem with using glass fiber filters is the large pore size of $1.6 \mu\text{m}$. As a result, it can be assumed that the filter will not retain a majority of the cells in the sample. Nonetheless, it is still possible to observe trends if the changes in concentration are large enough. In Figure 4.10 the difference between the abiotic control and biotic samples

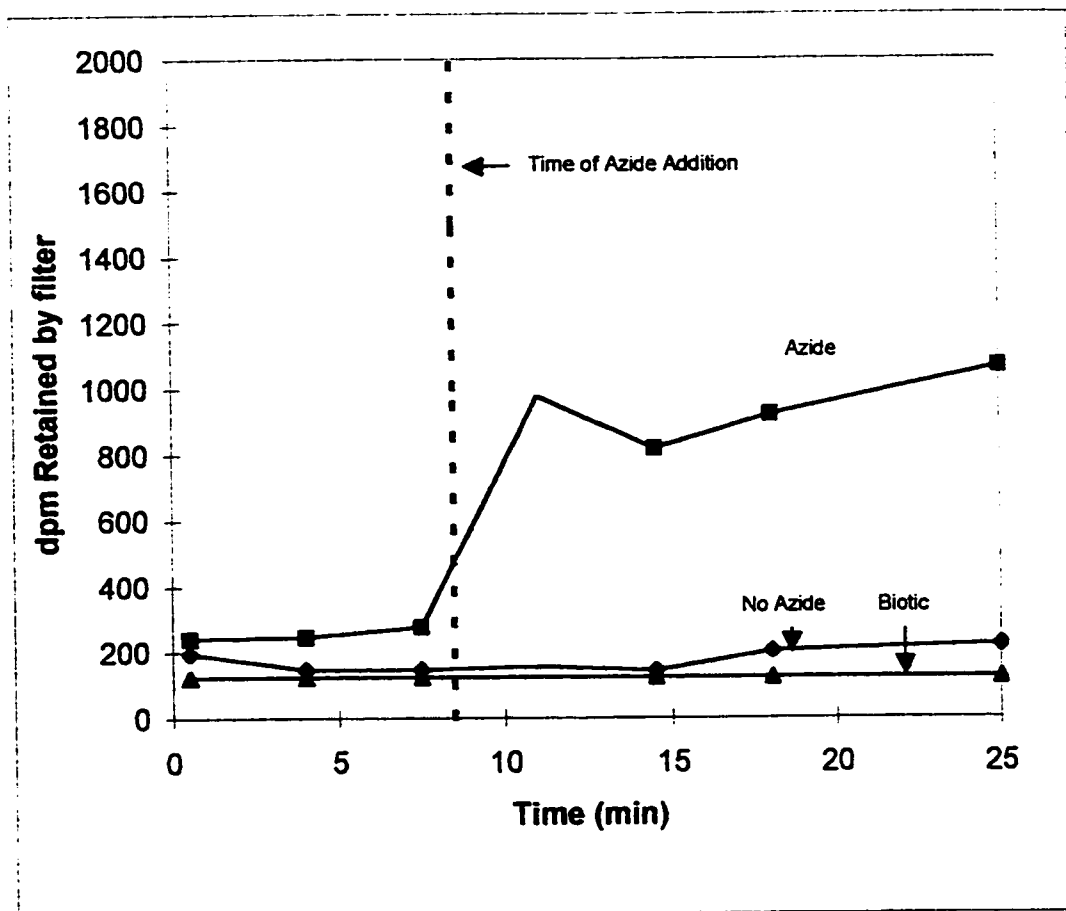


Figure 4.10 Time dependence of cell pellet ^{14}C concentrations for the transport of phenanthrene in LP6a mutant 1-51 as determined by filtration method.

without azide are imperceptible due to poor retention of cells and low amounts of PAH associated with the cell. When azide was added there was an obvious and significant increase in the amount of radioactivity retained by the filter. The filter retained an average of 260 dpm prior to azide addition and 945 dpm after azide addition, an increase by a factor of 3.6. This trend is once again evidence of an active efflux mechanism in LP6a. From these results, it can be concluded that the method of rapid centrifugation is producing valid results for the transport of PAHs in LP6a.

4.4.4 Negative Control

To confirm that the observed changes in phenanthrene concentrations were a result of transport, a negative control was necessary. As a result of possible similarities between PAH efflux and multidrug efflux many *Pseudomonas* strains are poor choices for a negative control as many of these bacteria, particularly *P. putida* strains, exhibit solvent tolerance and antibiotic resistance (Kieboom et al., 1998). *A. vinelandii* UW was chosen as the control bacterium and experiments on the transport of phenanthrene were conducted. For these experiments, one test was conducted in the absence of azide and two test were done in the presence of 120 mM azide added at 8.5 min. The data in Figure 4.11 indicate that, upon addition of azide, there was no change in cell pellet or supernatant phenanthrene concentrations. Thus, there is no active uptake or efflux of phenanthrene in *A. vinelandii* UW. These results confirm that the trends observed for the transport of phenanthrene in LP6a are a result of active efflux and not an unknown factor.

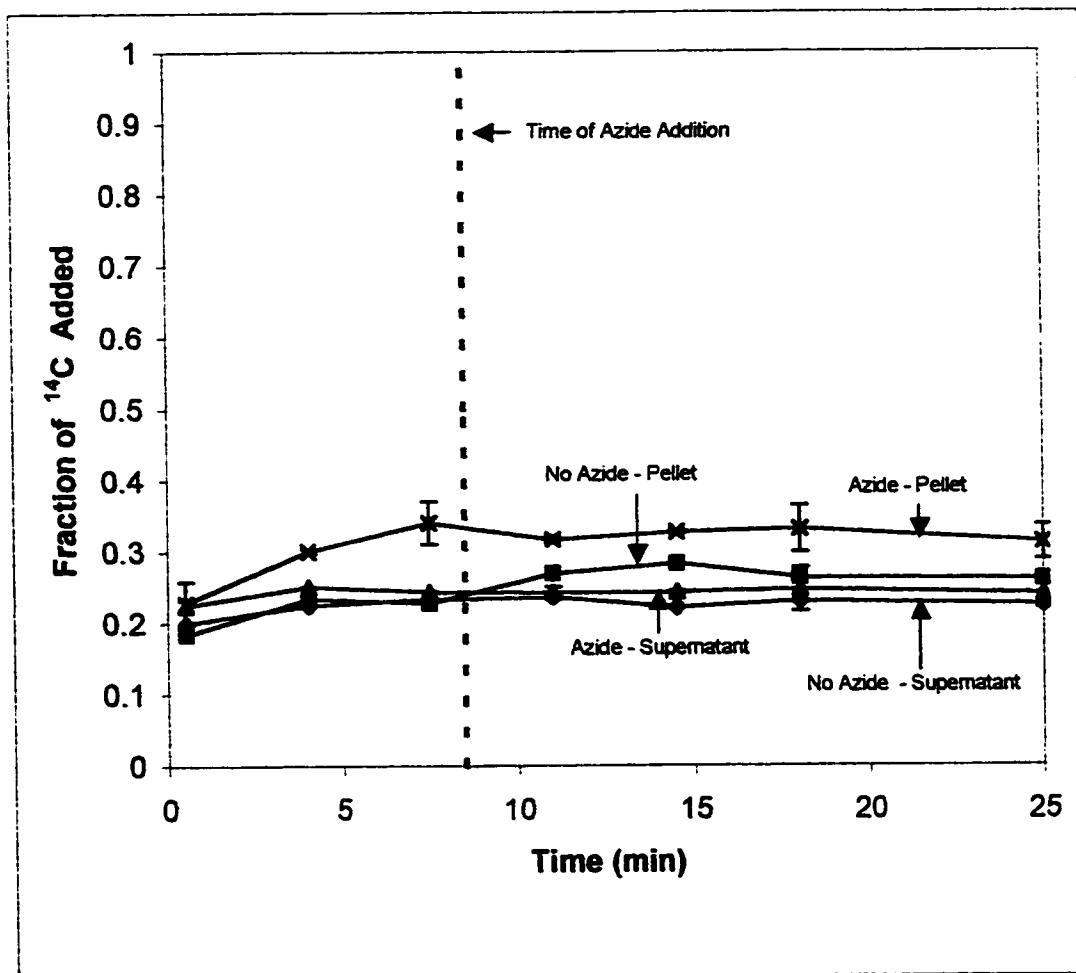


Figure 4.11 Partitioning of phenanthrene between the liquid phase and cell pellet for the transport of phenanthrene in *A. vinelandii* UW.

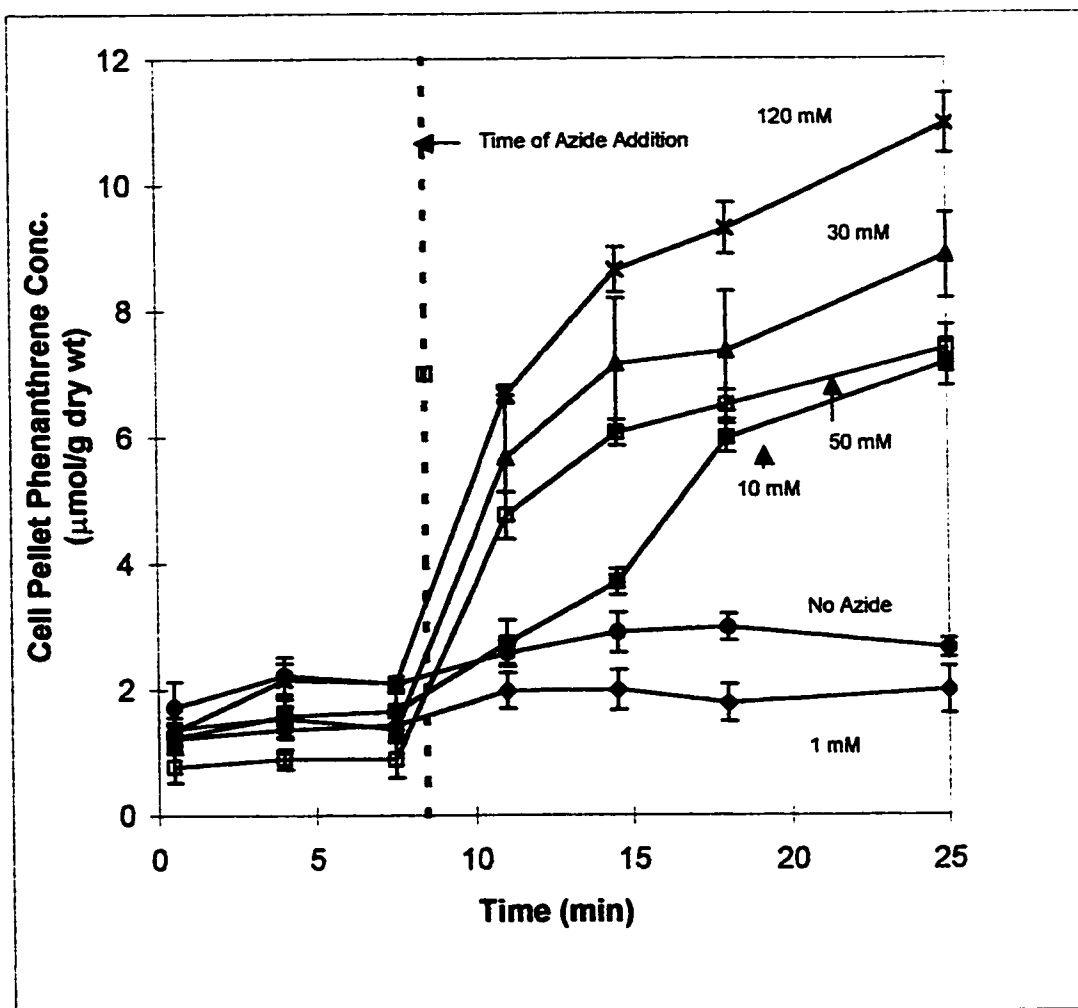


Figure 4.12 Time dependence for cell pellet phenanthrene concentrations for LP6a mutant 1-51 in the presence of different azide concentrations.

4.4.5 Azide Concentrations

To verify the necessary azide concentration for complete inhibition, the transport of phenanthrene in LP6a mutant 1-51 was studied at five different azide concentrations ranging from 1 mM to 120 mM. The concentration of phenanthrene in the cell pellet with time is shown in Figure 4.12. From the graph it is not apparent if cell pellet concentrations have ceased to increase at the end of the 25-min time period. A comparison between the initial rates of phenanthrene uptake after azide addition indicate that there is little difference between 30 mM, 50 mM and 120 mM azide. Additionally, it is apparent that there was little difference in the final cell pellet concentrations after azide addition between the experiments conducted with 30 mM and 50 mM azide. After 25 minutes, the pellet concentration in the experiments with 30 mM azide was 8.9 ± 0.7 $\mu\text{mol}/(\text{g dry wt})$ and 7.4 ± 0.4 $\mu\text{mol}/(\text{g dry wt})$ for the experiments with 50 mM azide. The difference between these two numbers at a 95% confidence limit is 1.5 ± 1.2 . Given that the range on this difference is near zero and that the cell pellet concentration is lower for the experiments with 50 mM azide versus that for 30 mM azide, it can be concluded that the cell pellet concentrations after 25 minutes for the experiments at 50 mM azide and at 30 mM azide are not significantly different. Thus, it can be concluded that a concentration of 30 mM azide or greater is sufficient to almost completely inhibit active transport. In Figure 4.12, there is no change in cell pellet concentration after the addition of 1 mM azide. Also, there was very little difference between the cell pellet concentrations for the experiments without azide and with 1 mM azide. After equilibrium was reached, the pellet concentration was 2.8 ± 0.3 $\mu\text{mol}/(\text{g dry wt})$ without azide and 1.9 ± 0.3 $\mu\text{mol}/(\text{g dry wt})$ with 1 mM azide. The difference between these two endpoint

values at a 95% confidence limit is -0.84 ± 0.23 . Thus, these two values are also significantly different. However, the fact that the average cell pellet concentration in the experiments with 1 mM azide was lower than that for the experiments with no azide indicates that the actual error was much larger than what is indicated by the values for the standard deviation. When 11 mM azide was added at 8.5 minutes, there was an increase in cell pellet phenanthrene concentration at a rate less than that at 30 mM azide. After the 25-min sampling period, the phenanthrene concentration in the experiments with 11 mM was $7.18 \pm 0.37 \mu\text{mol}/(\text{g dry wt})$ whereas it was $2.77 \pm 0.25 \mu\text{mol}/(\text{g dry wt})$ for those without azide. These two endpoints are significantly different. Thus, a minimum azide concentration between 1 and 11 mM is required in LP6a to have an inhibitory effect on phenanthrene transport. The minimum and maximum azide concentrations that produced effects were an order of magnitude larger than what has been observed in other systems. Previous research indicated that azide concentrations in the range of 0.1-1 mM were sufficient to disrupt active transport (Dawson et al., 1969). Also, numerous researchers like Thayer and Wheelis, (1982), and Bateman et al., (1986) routinely use 10 mM azide to completely inhibit active transport. It is uncertain as to why there is a discrepancy.

The data obtained on the transport of phenanthrene in LP6a mutant 1-51 (Figure 4.6) show very rapid initial partitioning of phenanthrene into cells. Accounting for the time period to centrifuge samples, it can be assumed that steady-state is established in a maximum time period of 2 min. Figure 4.12 shows that the concentration of phenanthrene in LP6a mutant 1-51 cells after azide addition takes at least 15 min to reach equilibrium. Furthermore, the rate of uptake of phenanthrene after azide addition is

proportional to the azide concentration. Thus, it can be concluded that the rate of uptake of phenanthrene after azide addition is controlled by the kinetics of azide inhibition of chemiosmosis. It cannot be assumed that the effects of azide are instantaneous. Thus, these data are unsuitable for modeling uptake kinetics.

4.4.6 Other Inhibitors of Electron Transport

To verify the presence of an active efflux mechanism in LP6a, transport studies were conducted in the wild-type and mutant 1-51 strains using cyanide and CCCP to disrupt active transport. Cyanide operates in a very similar manner to azide and provides direct validation of the data obtained with azide. For the wild-type strain, the transport of phenanthrene with and without 10 mM cyanide added at 8.5 min is shown in Figure 4.13. Transport in the mutant 1-51 strain is shown in Figure 4.14. For the mutant 1-51 strain, there was an increase in cell pellet concentration and a decrease in supernatant concentration when cyanide was added. Prior to cyanide addition, the steady-state pellet concentration was $2.6 \pm 0.6 \mu\text{mol}/(\text{g dry wt})$. In the presence of 10 mM cyanide, it was $6.4 \pm 0.8 \mu\text{mol}/(\text{g dry wt})$. Within experimental error, the value of $6.4 \pm 0.8 \mu\text{mol}/(\text{g dry wt})$ is similar to the equilibrium pellet concentration of $7.2 \pm 0.4 \mu\text{mol}/(\text{g dry wt})$ obtained in the presence of 11 mM azide (Figure 4.13). The similarity in values reflects the similarity in mode of action of azide and cyanide. An increase in cell pellet concentration was not observed in the wild-type (Figure 4.13) as a result of low inhibitor concentration and metabolism of the substrate. In Figure 4.4, only a marginal effect on the transport of phenanthrene was observed when 120 mM azide was added to the wild-

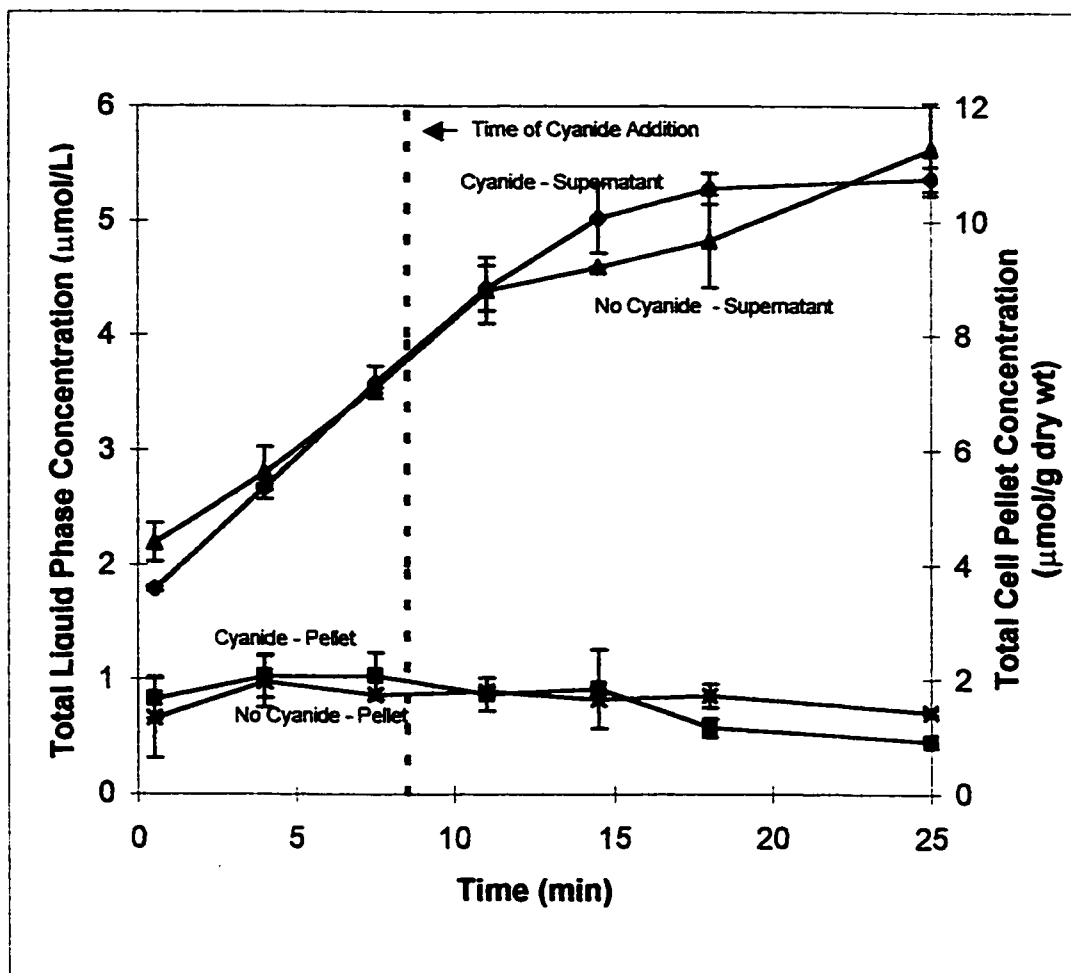


Figure 4.13 Time dependence of liquid phase and cell pellet phenanthrene and metabolite concentrations for the transport of phenanthrene in LP6a wild-type in the presence and absence of 10 mM cyanide.

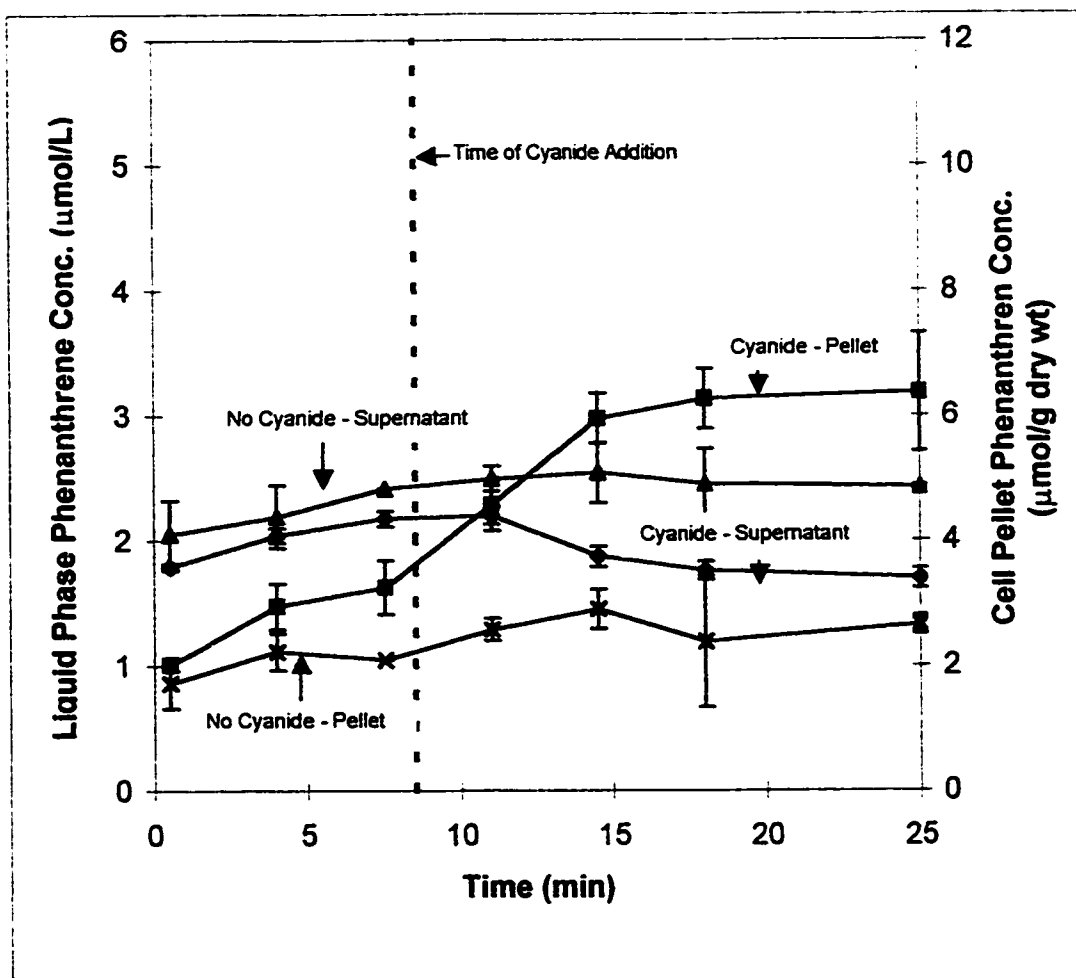


Figure 4.14 Time dependence of liquid phase and cell pellet phenanthrene concentrations for the transport of phenanthrene in LP6a mutant 1-51 in the presence and absence of 10 mM cyanide.

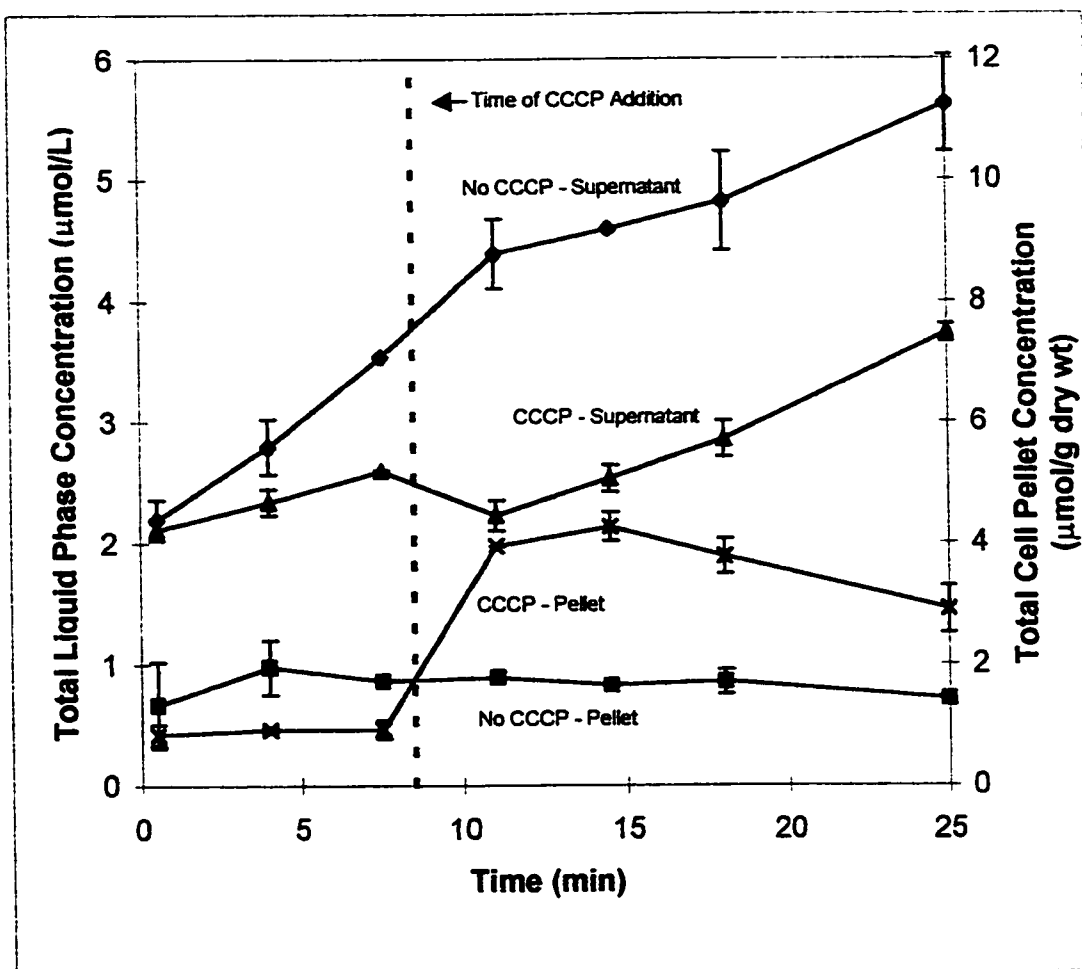


Figure 4.15 Time dependence of liquid phase and cell pellet phenanthrene and metabolite concentrations for the transport of phenanthrene in LP6a wild-type in the presence and absence of 50 μ M CCCP.

type strain. Thus, it is not surprising that no effect was observed at a cyanide concentration one tenth that of the azide concentration used.

The effect of CCCP addition was more pronounced than that of cyanide. In Figure 4.15, it is apparent that upon CCCP addition to the wild-type strain, there was a decrease in supernatant and an increase in cell pellet phase ^{14}C concentrations. Following CCCP addition, the pellet phase concentration continued to decrease as more phenanthrene was metabolized. This trend correlates with a resumed increase in supernatant ^{14}C levels. This trend is also identical to that observed for the wild-type strain when 120 mM azide was added (Figure 4.4). However, it is also apparent that the data points for the experiments in the absence of azide differ from those for the experiments in the presence of azide prior to azide addition. These experiments were not run in parallel and the differences are a result of variability in metabolic activity between the two cultures. Despite this problem, it is still evident that there are sudden changes in phenanthrene concentration in both the liquid and cell pellet phase when azide is added. These changes are not observed in the experiments that lack azide.

For the mutant 1-51 strain, Figure 4.16 shows significantly greater changes in ^{14}C concentrations when CCCP was added due to the lack of metabolism. The steady-state pellet concentration prior to CCCP addition was $1.5 \pm 0.2 \mu\text{mol}/(\text{g dry wt})$ and after the equilibrium concentration after the addition of $50 \mu\text{M}$ CCCP was $10 \pm 1 \mu\text{mol}/(\text{g dry wt})$. The value of $10 \pm 1 \mu\text{mol}/(\text{g dry wt})$ is comparable to the equilibrium pellet concentration of $11 \pm 1 \mu\text{mol}/(\text{g dry wt})$ obtained in the presence of 120 mM azide. Thus, at $50 \mu\text{M}$

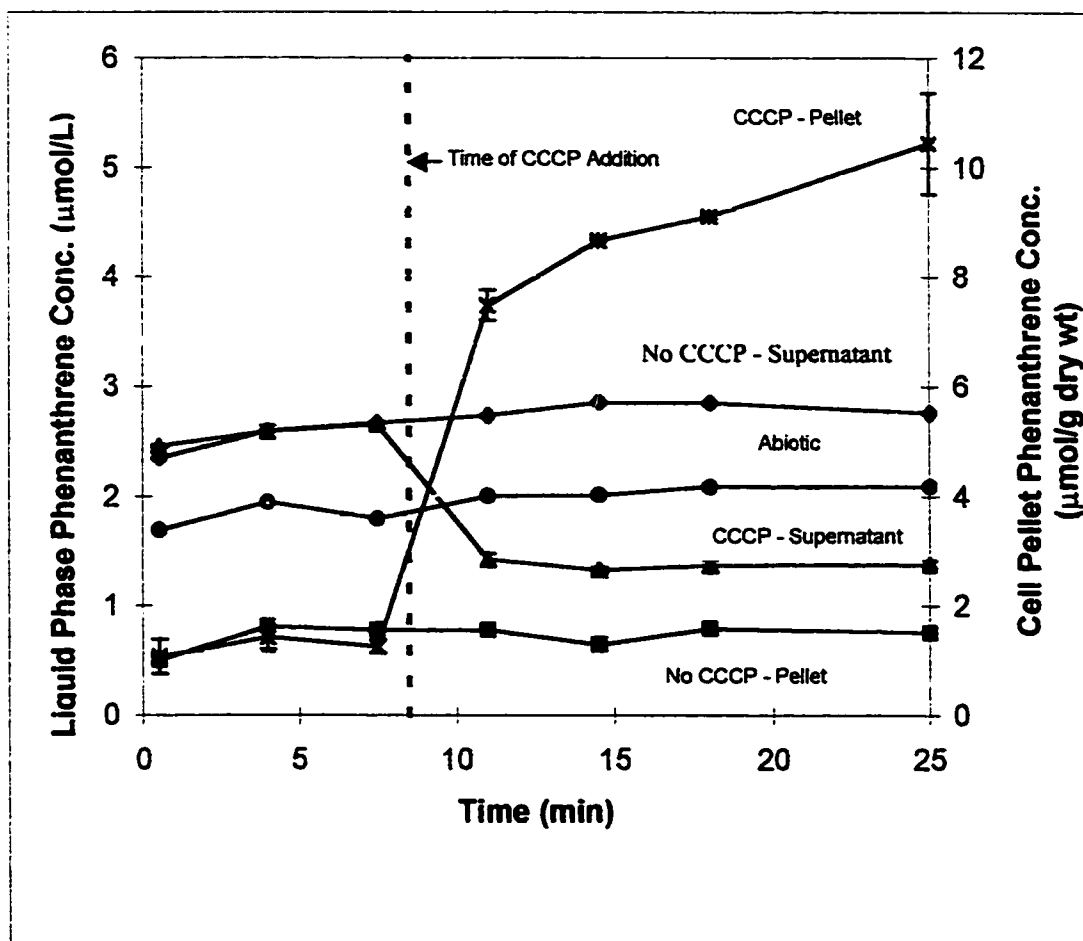


Figure 4.16 Time dependence of liquid phase and cell pellet phenanthrene concentrations for the transport of phenanthrene in LP6a mutant 1-51 in the presence and absence of 50 μ M CCCP.

CCCP, there is complete inhibition of active efflux. From the data on azide, cyanide and CCCP inhibition, one can conclude that there is an energy mediated efflux mechanism for phenanthrene transport in LP6a.

The presence of an active efflux pump in LP6a conflicts with the requirements of PAH metabolism. The goal of an efflux pump is to minimize substrate concentrations in the cell. From the Michealis-Menton equation for enzyme kinetics, it can be rationalized that higher metabolic rates are achieved by higher intracellular substrate concentrations (Brock et al., 1994). Hence, the efflux pumps could limit the rate of metabolism unless the metabolic enzymes have a much higher affinity for the substrate than the efflux pump. Despite this fact though, very rapid metabolism of phenanthrene was observed for the wild-type strain (Figure 4.5). Thus, there must be rapid transport of phenanthrene into the cell. The question remains, if active efflux can be removed, will LP6a become a more efficient degrader as a result of higher intracellular PAH concentrations and thus higher metabolic rates? The fact that efflux is chromosomally encoded suggests that the two processes are unrelated. An argument can be made that this was a bacterium resistant to PAHs that later inherited the ability to degrade PAHs through inheriting the plasmid. Alternatively, does the active efflux mechanism play an important role in providing resistance to toxicity of hydrophobic compounds by minimizing intracellular and membrane concentrations? It may be that the efflux mechanism is required for cell survival and as a result, LP6a must cope with these two conflicting mechanisms.

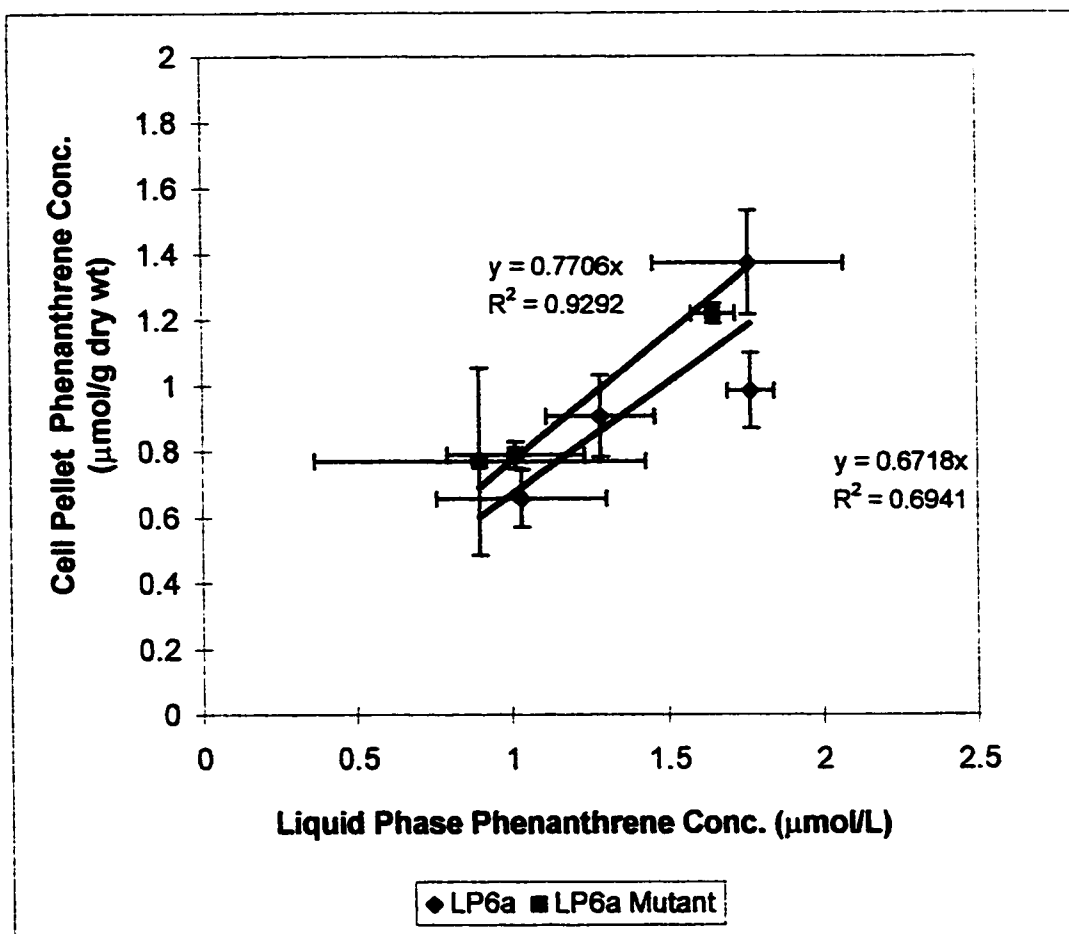


Figure 4.17 Cell pellet phase-liquid phase partitioning isotherm for initial phenanthrene concentrations in LP6a wild-type and steady-state phenanthrene concentrations in LP6a mutant 1-51. The error bars represent the 95% confidence interval on the experimental values.

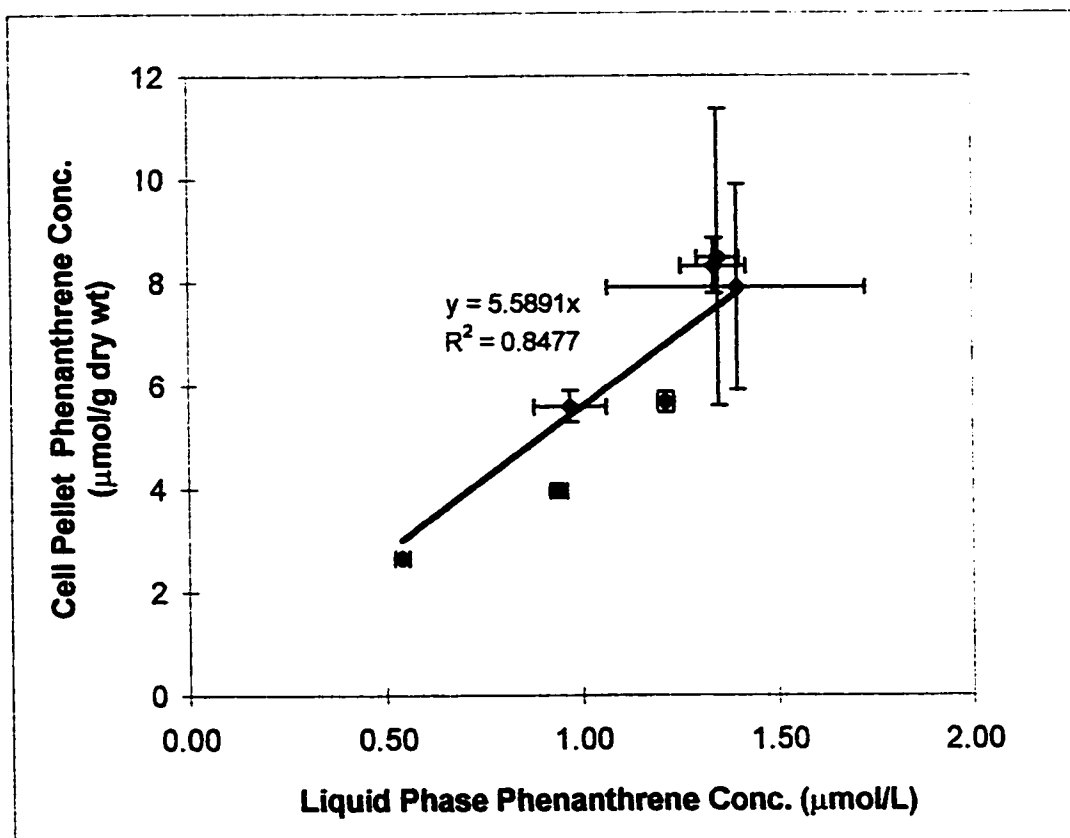


Figure 4.18 Cell pellet phase-liquid phase phenanthrene partitioning isotherm for equilibrium phenanthrene concentrations in LP6a mutant 1-51 in the presence of 120 mM azide. The error bars represent the 95% confidence interval on the experimental values.

4.4.7 Adsorption Isotherms

Experimentation at different phenanthrene concentrations allowed for the determination of thermodynamic parameters. Partition coefficients for phenanthrene between the aqueous phase and total cell pellet phase concentrations were obtained for the LP6a wild-type and mutant 1-51 strain in the absence of azide (Figure 4.17). A partition coefficient was also obtained for the mutant 1-51 strain in the presence of inhibitory levels of azide (Figure 4.18). In these graphs, the equilibrium or steady-state cell pellet concentration was plotted against the liquid phase concentration. For the wild-type strain, supernatant and cell pellet phase concentrations were extrapolated to time zero so as to obtain initial partitioning prior to metabolism of phenanthrene. For the mutant 1-51 strain, an average concentration, after steady-state or equilibrium was reached, was used.

The extent of partitioning between the cell pellet and liquid phase for the wild-type and mutant 1-51 strain in the absence of azide is presented in Figure 4.17. From Figure 4.17, it is apparent that there is a linear relationship between cell pellet and supernatant phenanthrene concentrations for both the wild-type and mutant 1-51 strains. A value of 0.78 ± 0.14 (g dry wt)/L was obtained for the LP6a mutant 1-51 strain and 0.68 ± 0.18 (g dry wt)/L for the LP6a wild-type strain. The variability in the data points and poor correlations are a result of low pellet concentrations and inaccuracies in sampling the pellet phase. In the experiments with LP6a wild-type strain, the plotted data are for an extrapolation to time zero so as to measure initial partitioning in the absence of metabolism. Thus, the similarity in initial partitioning between the mutant 1-51 and wild-type strain was expected.

For partitioning in the mutant 1-51 strain in the presence of azide (Figure 4.18), two sets of data are plotted on the same curve: one in which transport was studied at an OD_{600} of 1 and one in which it was studied at an OD_{600} of 0.2 to try to increase the amount of phenanthrene per cell. However, studying transport at OD_{600} of 0.2 resulted in a large degree of variance in results. This variability is manifested as large error bars on the graph for these samples. The increased error was a result of a minimal amount of cells. It was more difficult to separate the majority of the cells. Also slight variations in technique at an OD_{600} of 1, like disturbing the cell pellet during decanting of the supernatant, would be magnified 5-fold at an OD_{600} of 0.2. Despite the large variance, the collected data points at OD_{600} of 0.2 fit a linear relationship with the data points collected at an OD_{600} of 1. Despite efforts to increase the amount of phenanthrene per cell, only marginal increases were obtained at the lower optical density. Thus the adsorption isotherm in Figure 4.18 is restricted to a narrow range of phenanthrene concentrations.

The data in Figure 4.18 for the mutant 1-51 strain in the presence of inhibitory levels of azide indicate a linear relationship between cell pellet phenanthrene concentrations and supernatant phenanthrene concentrations. A partition coefficient of 5.6 ± 0.7 (g dry wt)/L or $1.2 \times 10^4 \pm 2 \times 10^3$ L (membrane volume)/L (aqueous volume) was obtained for the mutant 1-51 strain. The conversion between the two units was done by assuming a typical bacterium cell is a cylinder 1 μm in diameter and 3 μm in length. Each membrane thickness and the periplasm thickness was assumed to be 4 nm each. From this a

membrane volume per cell can be calculated. Using dry weight measurements from data in Table 4.1 and a liquid volume of 20 mL it can be estimated that there is 2.2×10^3 g dry cell wt/L (membrane volume). This value is used as a conversion factor to convert the units on the partition coefficient. In comparison, Sikkema et al. (1994) gives a phenanthrene partition coefficient of 4937 ± 86 L/L in single membrane liposomes. The liposomes were prepared from *E. Coli* phospholipids. The value obtained from Figure 4.20 is 2.5 times that reported by Sikkema et al. (1994). However, there are two membranes in LP6a versus one in single membrane vesicles. If it is assumed that partitioning in LP6a would be approximately twice that of a single membrane system, it can be concluded that these two values are similar.

Decreasing the cell density was not an effective means to observe saturation of partitioning. A possible approach would be to add more phenanthrene after equilibrium is established. Such an approach would increase the amount of material in the liquid and cell phase. Phenanthrene addition can be repeated after the new equilibrium is established until a liquid phase phenanthrene concentration equal to the solubility of phenanthrene is reached. Analysis at each new equilibrium would allow identification of saturation if it exists within the solubility range. This same approach can be used in the absence of azide to identify a possible saturation of uptake and active efflux.

For the mutant 1-51 strain in the presence of inhibitory levels of azide, the partition coefficient was a thermodynamic partition coefficient as a result of the absence of active efflux. The linear adsorption isotherm indicates that the cells were not near saturation for

phenanthrene partitioning. Thus, LP6a has a high capacity for accumulating phenanthrene relative to the aqueous solubility. The observed results beg the question as to how much material can partition into the cell before saturation. However, there are limitations imposed by low aqueous solubilities and a high degree of partitioning to glassware. For the wild-type and mutant 1-51 strain in the absence of azide, the effective partition coefficient is a measure of the effectiveness of active efflux. The values of 0.78 and 0.67 (g dry wt)/L for partitioning in the presence of active efflux are significantly lower than the thermodynamic partition coefficient of 5.6 (g dry wt)/L. The extent of reduction gives an indication as to the high efficiency of the efflux pump. A comparison of these data indicates that for a fixed liquid phase concentration, the cell pellet phenanthrene concentration is reduced by approximately a factor of 7 in the presence of active efflux. The ratio of the pellet concentration after azide addition to that prior to azide addition is only 3.6. The discrepancy is a result of a changing liquid phenanthrene concentration when azide is added. Since there was a fixed amount of material in the system, the liquid phase phenanthrene concentration must decrease while the cell pellet phenanthrene concentration increases. In conjunction with an increase in pellet phenanthrene concentration by a factor of 3.62 after azide addition, the liquid phase phenanthrene concentration was decreased by nearly a factor of 2. The combination of these two numbers gives the factor of 7 obtained from the adsorption isotherms.

The linear relationship observed in Figure 4.18 for the adsorption isotherm in the absence of azide indicates that both the uptake and active efflux are not saturated at the phenanthrene concentrations tested. For uptake, this trend is consistent with diffusion

where there are no transport proteins to saturate. However, it does not disprove facilitated transport if concentrations are well below saturation and are in the linear regime. For active efflux, this trend indicates that the pump has a significantly higher capacity relative to the low solubility of these compounds. This argument may indicate another use or origin for the efflux pump such as transport of more water-soluble organic solvents or antibiotics. Conversely, it may be a necessity given the extremely fast partitioning of phenanthrene into the cells. The efflux pump may require a high capacity to maintain high transport rates to prevent toxic effects. Another possibility is that in the environment, there may be higher intracellular phenanthrene concentrations as a result of such scenarios as direct contact between the cell and solid PAH.

4.5 Transport of Other PAHs

The transport of other PAHs was studied in a similar manner to that of phenanthrene. Anthracene, fluoranthene, and naphthalene were chosen for study. Both anthracene and fluoranthene are less water-soluble than phenanthrene. Naphthalene is significantly more soluble in water. Thus, transport could be studied through a range of solubilities. Like phenanthrene, anthracene is metabolized by the LP6a wild-type strain. The transport of anthracene in LP6a wild-type is given in Figure 4.19 and 4.20 on a fractional and absolute scale respectively. Similar to the graphs for the transport of phenanthrene in the wild-type strain (Figure 4.4 and 4.5), there was an increase in liquid phase concentration over time. At the start of the transport experiment, the recovery of the ^{14}C -label between the cell pellet and supernatant was 51%. At the end of the experiment, it was 80%. Thus, as anthracene was metabolized, polar intermediates were produced that did not adsorb

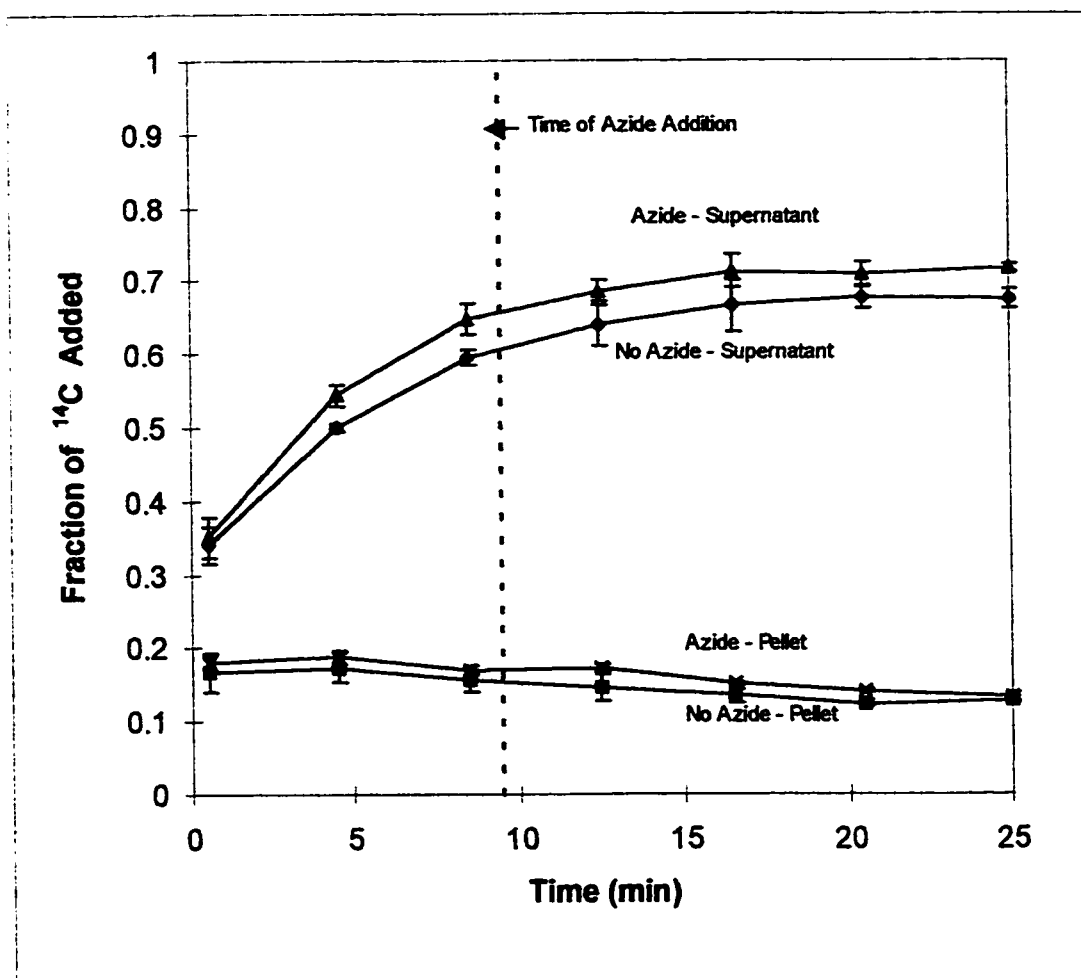


Figure 4.19 Time dependence of liquid phase ^{14}C concentrations for the transport of anthracene in LP6a wild-type.

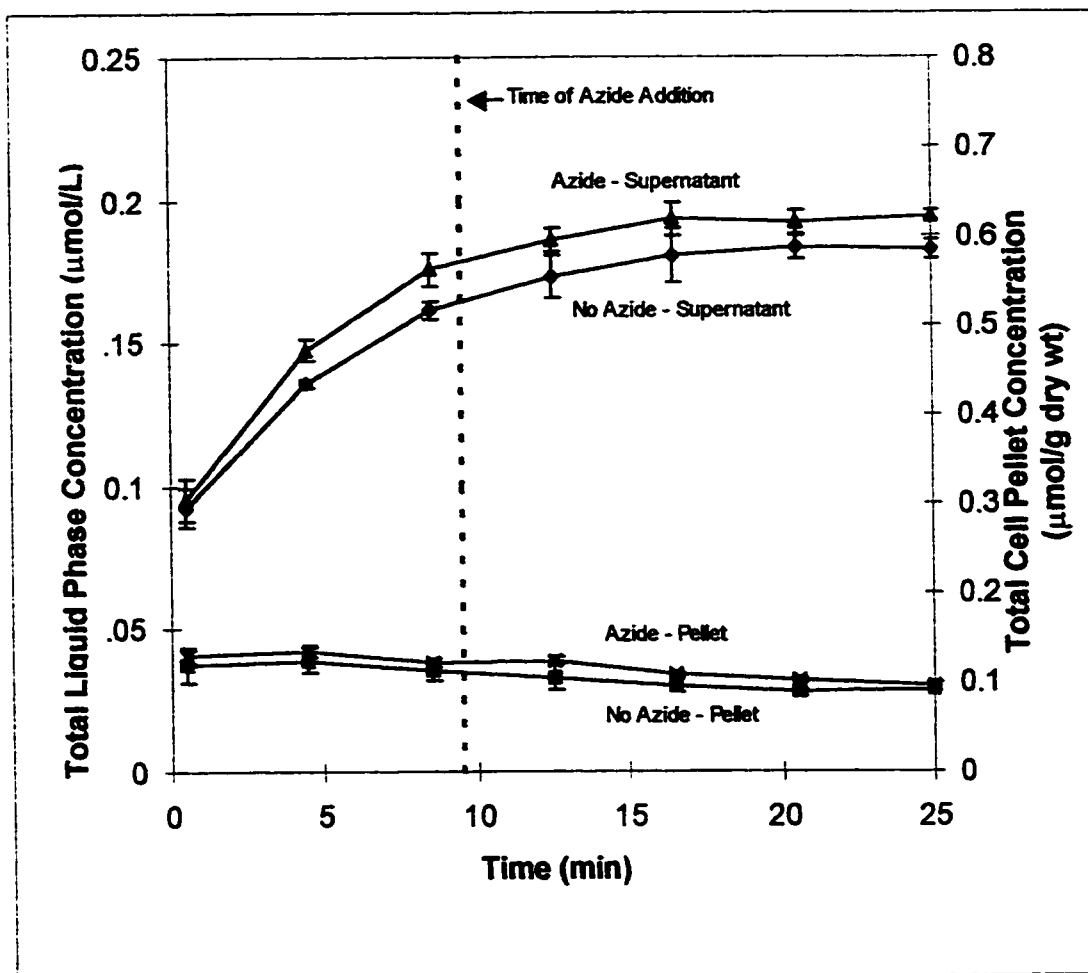


Figure 4.20 Time dependence of liquid phase and cell pellet anthracene and metabolites concentrations for the transport of anthracene in LP6a wild-type.

strongly to the glassware. Also, as the supernatant anthracene concentration was depleted, the anthracene lost to the equipment desorbed. These factors resulted in an increase in total ^{14}C recovery over time. In contrast to phenanthrene transport in the wild-type strain, there was no observed effect when 120 mM azide was added at 8.5 min. Curves for both the experiments with and without azide are essentially identical. This observation is most likely due to the extremely low solubility of anthracene and the high metabolic activity of the bacterium. The small amount of material that was added was most likely already converted to polar metabolites by the time azide was added.

Addition of 120 mM azide to the mutant 1-51 strain, however, produced an effect (Figures 4.21 and 4.22). Similar to the transport of phenanthrene in the mutant 1-51 strain, there was an increase in cell pellet concentration and decrease in supernatant concentration upon the addition of azide. The steady-state anthracene concentration in the cell pellet prior to azide addition was $0.11 \pm 0.01 \mu\text{mol}/(\text{g dry wt})$. The equilibrium concentration after azide addition was $0.21 \pm 0.02 \mu\text{mol}/(\text{g dry wt})$. The supernatant concentration was $0.096 \pm 0.006 \mu\text{mol}/\text{L}$ prior to azide addition and $0.062 \pm 0.003 \mu\text{mol}/\text{L}$ after azide addition. From the data in Figures 4.21 and 4.22, it can be concluded that anthracene is subject to active efflux.

In contrast to anthracene and phenanthrene, the transport of fluoranthene in the LP6a wild-type strain produced a different profile (Figures 4.23 and 4.24). LP6a was not able to grow on fluoranthene as a sole carbon source. As a result, it is unlikely that the LP6a wild-type strain would be able to metabolize fluoranthene during the transport

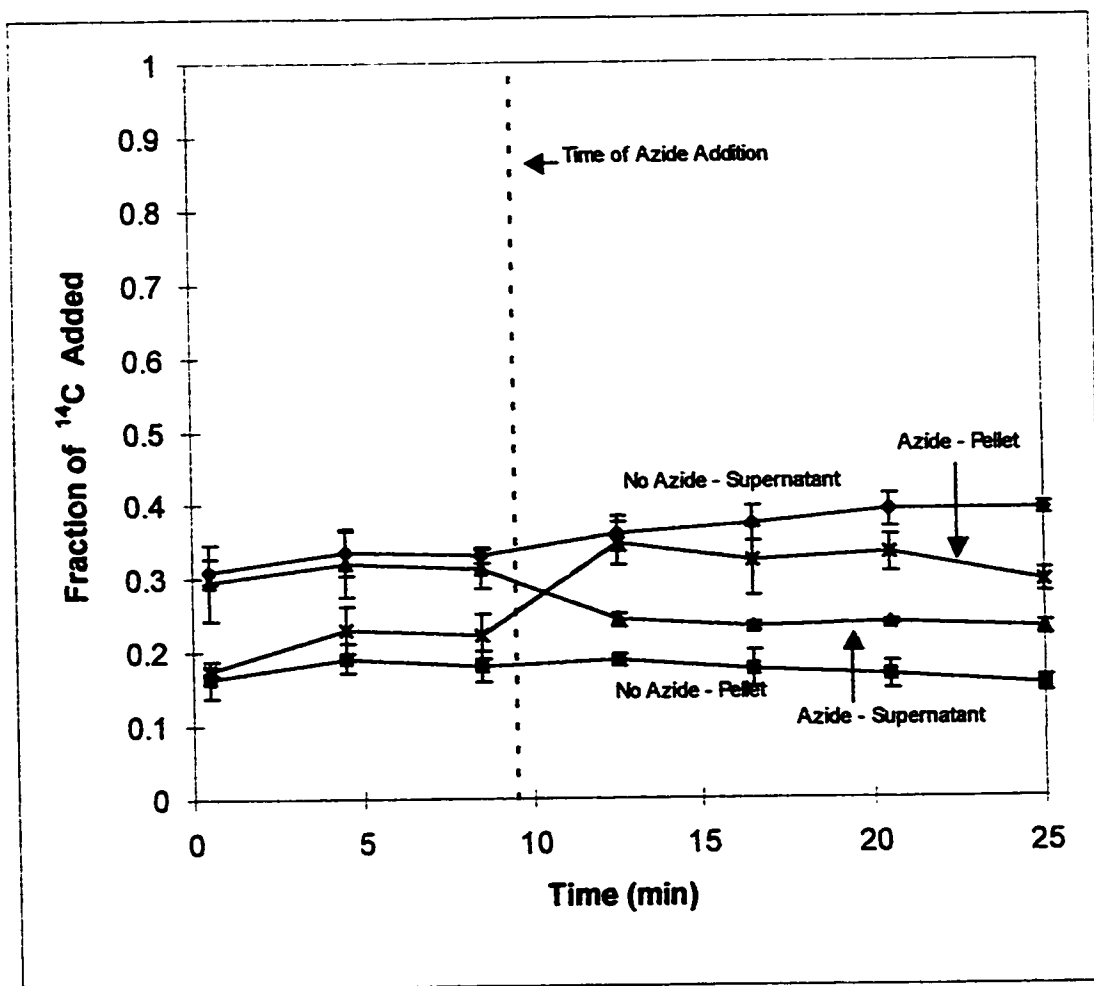


Figure 4.21 Time dependence of liquid phase and cell pellet ^{14}C concentrations for the transport of anthracene in LP6a mutant 1-51.

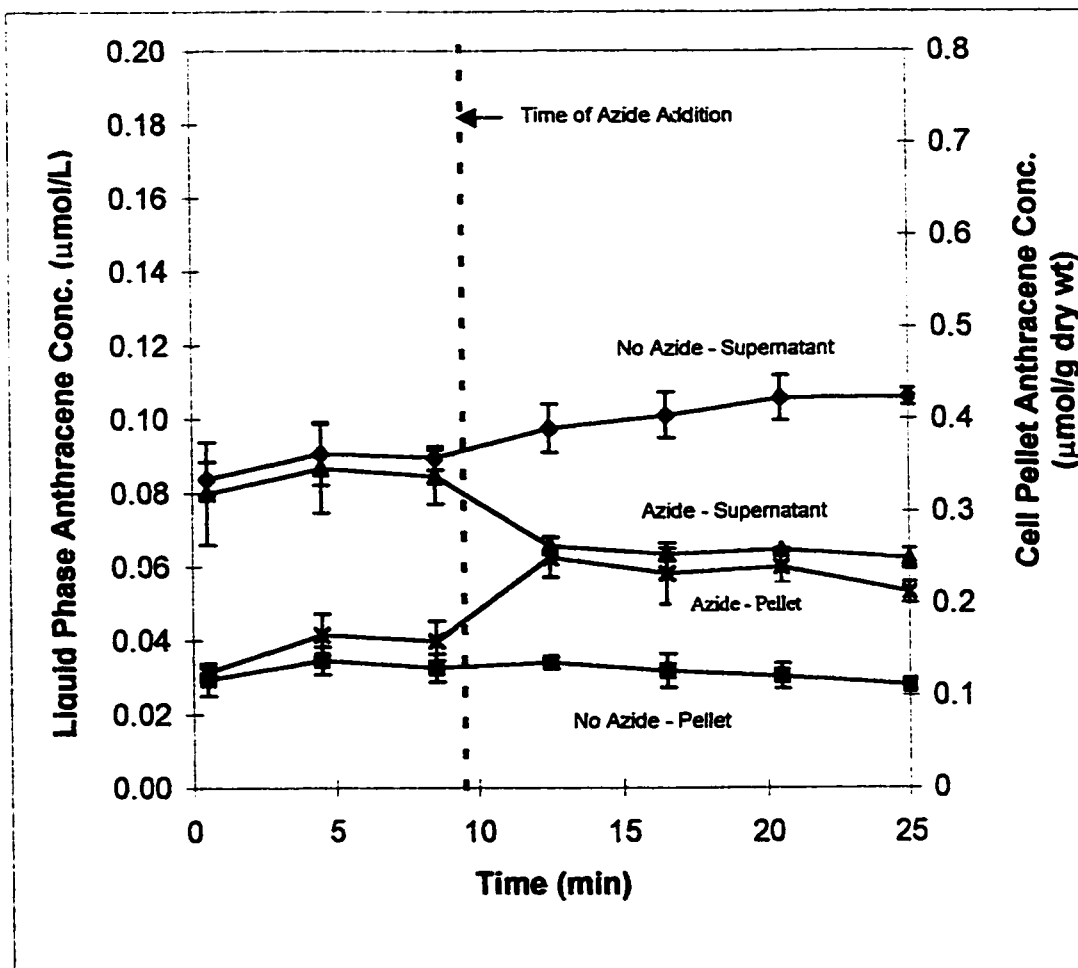


Figure 4.22 Time dependence of liquid phase and cell pellet anthracene concentrations for the transport of anthracene in LP6a mutant 1-51.

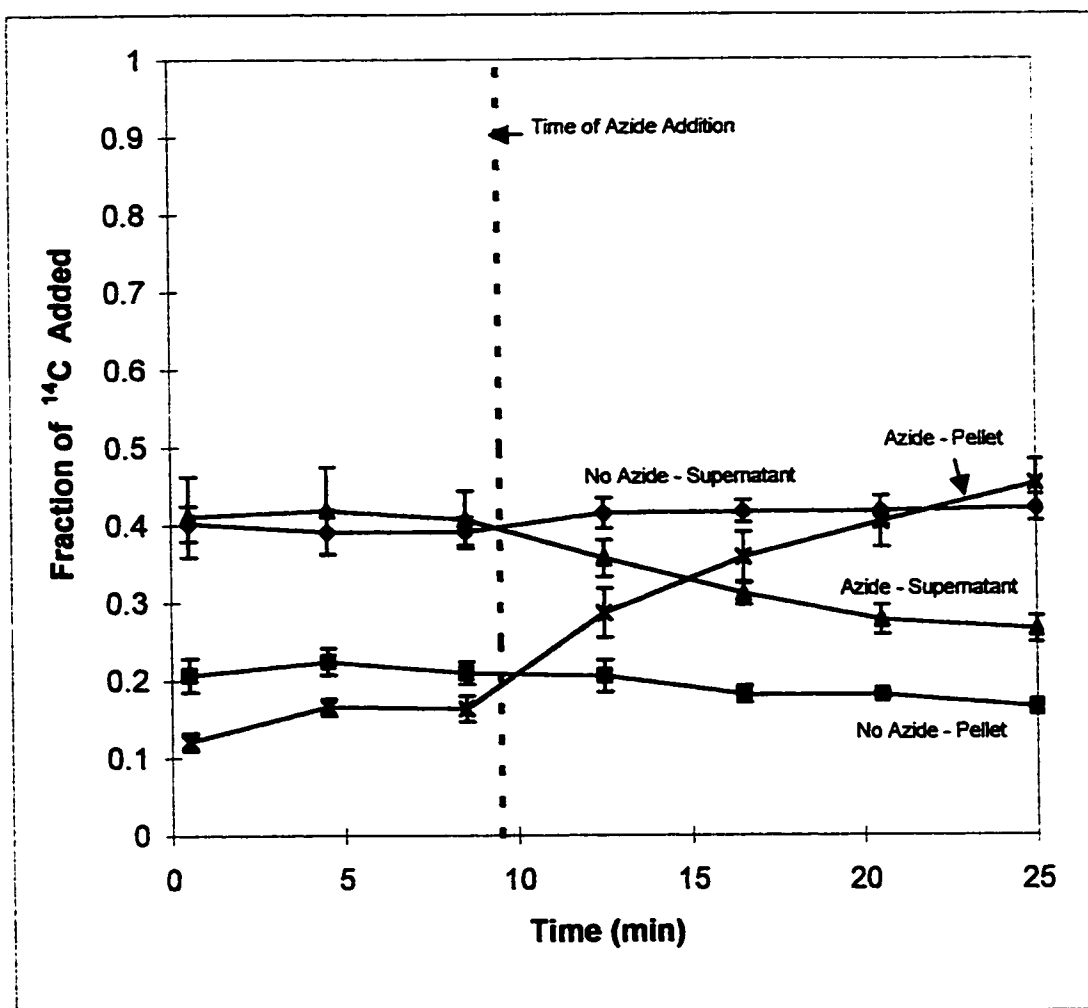


Figure 4.23 Time dependence of liquid phase and cell pellet ^{14}C concentrations for the transport of fluoranthene in LP6a wild-type.

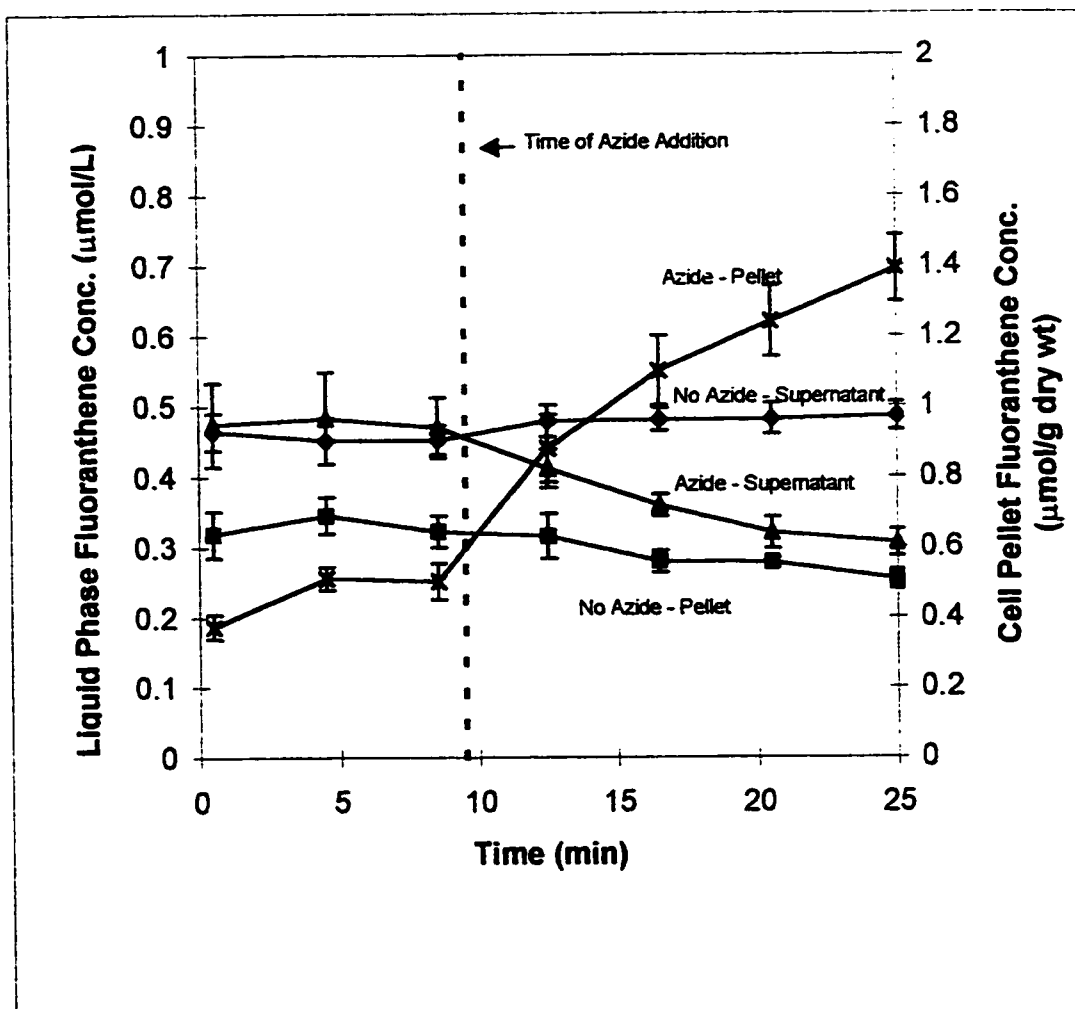


Figure 4.24 Time dependence of liquid phase and cell pellet fluoranthene concentrations for the transport of fluoranthene in LP6a wild-type.

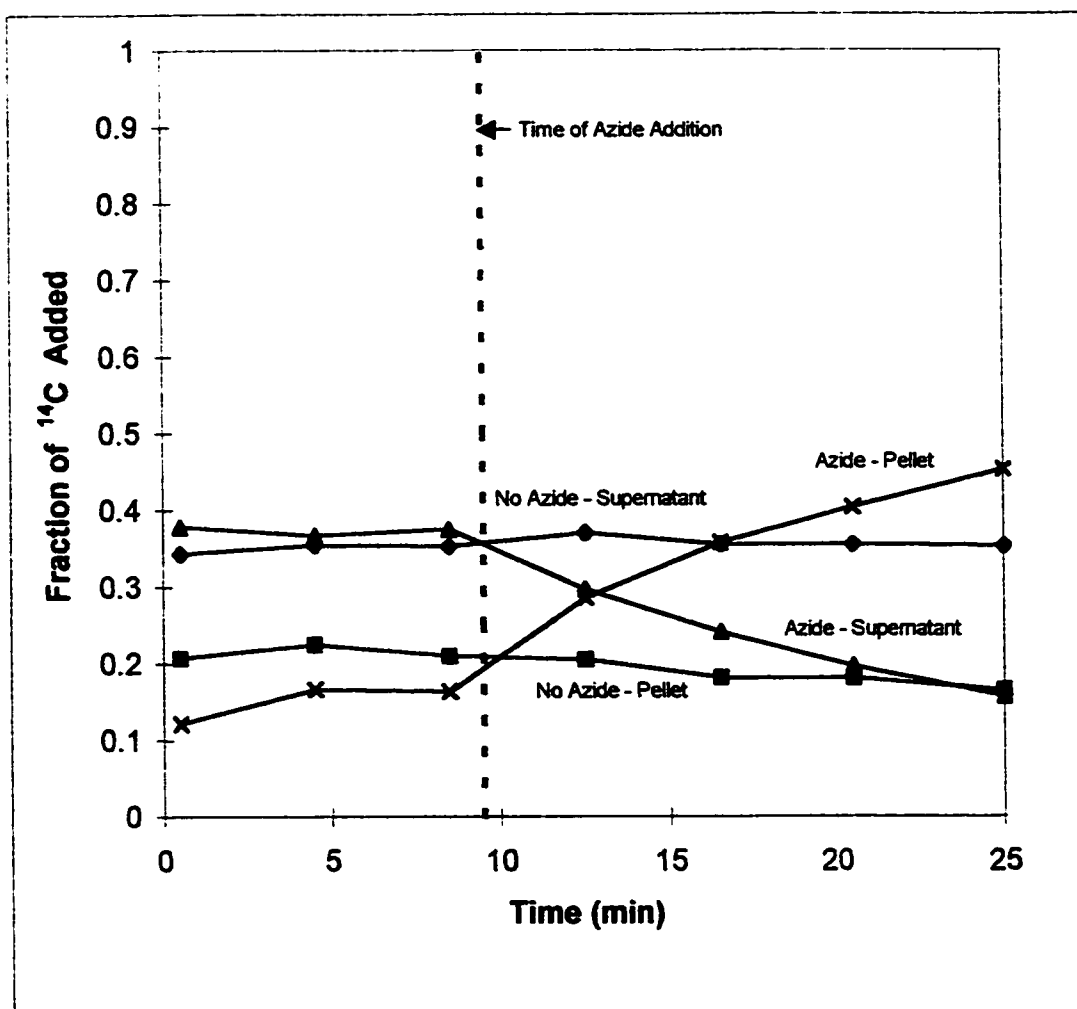


Figure 4.25 Time dependence of liquid phase and cell pellet ^{14}C concentrations for the transport of fluoranthene in LP6a mutant 1-51.

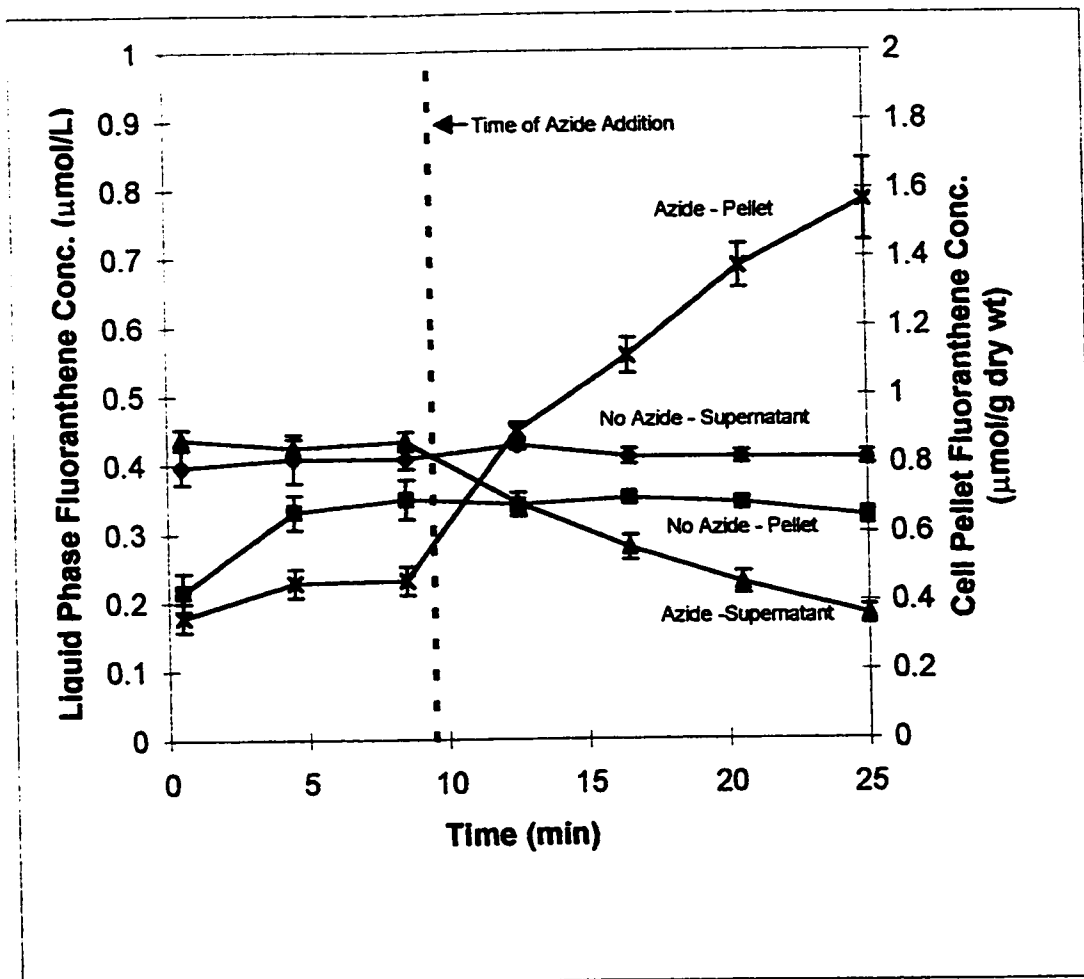


Figure 4.26 Time dependence of liquid phase and cell pellet Fluoranthene concentrations for the transport of fluoranthene in LP6a mutant 1-51.

experiments. Consequentially, there was no increase in supernatant concentrations over time in the absence of azide. Prior to the addition of azide both sets of experiments display identical transport profiles. When 120 mM azide was added at 8.5 min, there was a sudden increase in pellet phase ^{14}C concentration and decrease in supernatant concentration. The transport of fluoranthene in the wild-type strain was essentially identical to transport in the mutant 1-51 strain (Figures 4.25 and 4.26). The similarity is expected given that LP6a is not able to metabolize fluoranthene. For the experiments without azide, the steady-state pellet concentration was $0.60 \pm 0.05 \mu\text{mol}/(\text{g dry wt})$ for the wild-type and $0.68 \pm 0.04 \mu\text{mol}/(\text{g dry wt})$ for the mutant 1-51 strain. For the experiments with azide, after azide addition, the equilibrium pellet concentration increased to $1.4 \pm 0.1 \mu\text{mol}/(\text{g dry wt})$ in the wild-type and $1.6 \pm 0.1 \mu\text{mol}/(\text{g dry wt})$ in the mutant 1-51 strain. Within experimental error, these two values are the same. Thus, both the wild-type and mutant 1-51 strains are able to transport fluoranthene out of the cell by an active efflux mechanism. The transport behaviour in both strains confirms the similarity between the two strains and strengthens the arguments made for the observed trends for the transport of anthracene and phenanthrene in the wild-type strain.

Due to volatility concerns, the experiments on the transport of naphthalene were conducted in closed 35-mL serum vials. The serum vials minimized the headspace and prevented loss of material to the environment through volatilization. To verify that this variation in methods did not alter the observed results, control experiments were conducted. The transport of phenanthrene in LP6a mutant 1-51 was studied in the closed serum vials (Figure 4.27). For this experiment, two tests were performed: one where

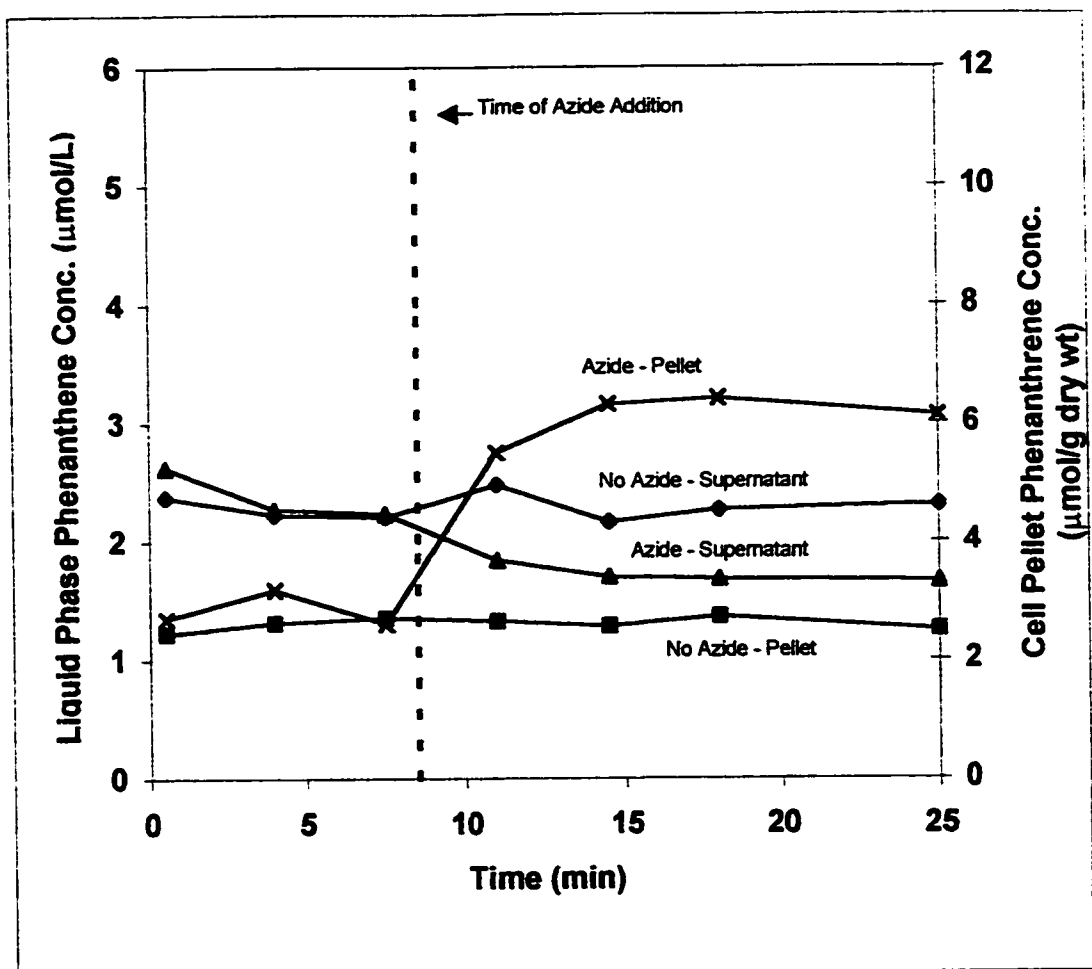


Figure 4.27 Time dependence of liquid phase and cell pellet phenanthrene concentrations for the transport of phenanthrene in LP6a mutant 1-51 in closed serum vials.

30 mM azide was added as a concentrated solution in 0.3 mL of buffer at 8.5 min and one where no azide was added. From the data presented in Figure 4.28, there was an increase in cell pellet concentration and decrease in supernatant concentration when azide was added at 8.5 min. This trend indicates that experiments in the serum vials were able to identify active efflux in LP6a.

The changes in phenanthrene concentrations observed in the experiments conducted in the serum vials were not, however, as large as those observed in the experiments conducted in the 250-mL erlenmeyer flasks (Figures 4.6 and Figure 4.7). In the experiments with the 250-mL flasks, cell pellet phenanthrene concentration after azide addition was 3.6 times that of the pellet concentration when no azide was added. For the serum vials, an increase of 2.5 times was observed. The discrepancy could be a result of the different glassware and sampling equipment used. However, it is uncertain as to how the apparatus would affect results. It is more likely that the discrepancy is due to differences in the physiological state of the cells. It has been noted a number of times in experimentation that LP6a would occasionally accumulate less PAH or transport PAH by active efflux to a lesser extent. This physiological difference was observed most frequently when the bacteria had not been transferred to new plates in some time. Thus, it is unlikely that there is a real discrepancy in partitioning in the different environments. As a result, a comparison between data obtained by both methods is considered to be valid.

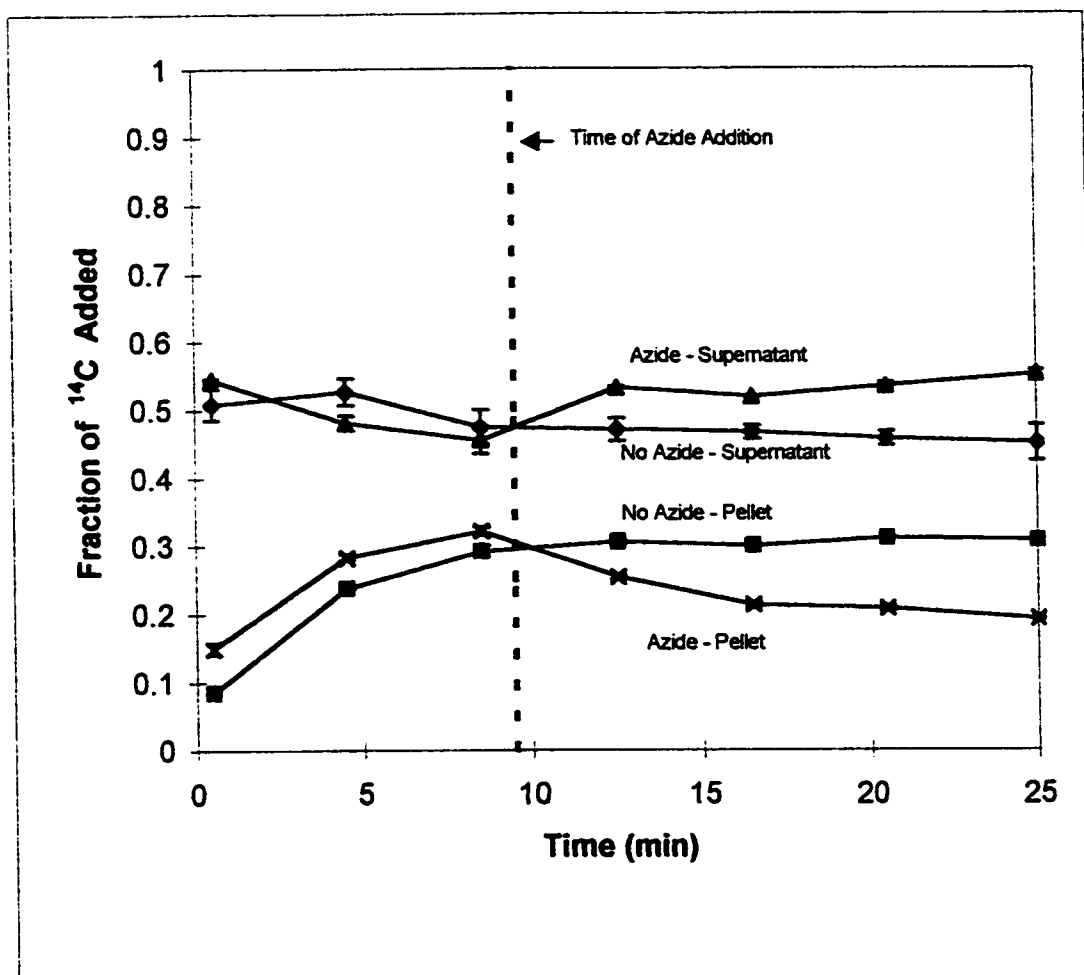


Figure 4.28 Time dependence of liquid phase and cell pellet ^{14}C concentrations for the transport of naphthalene in LP6a wild-type.

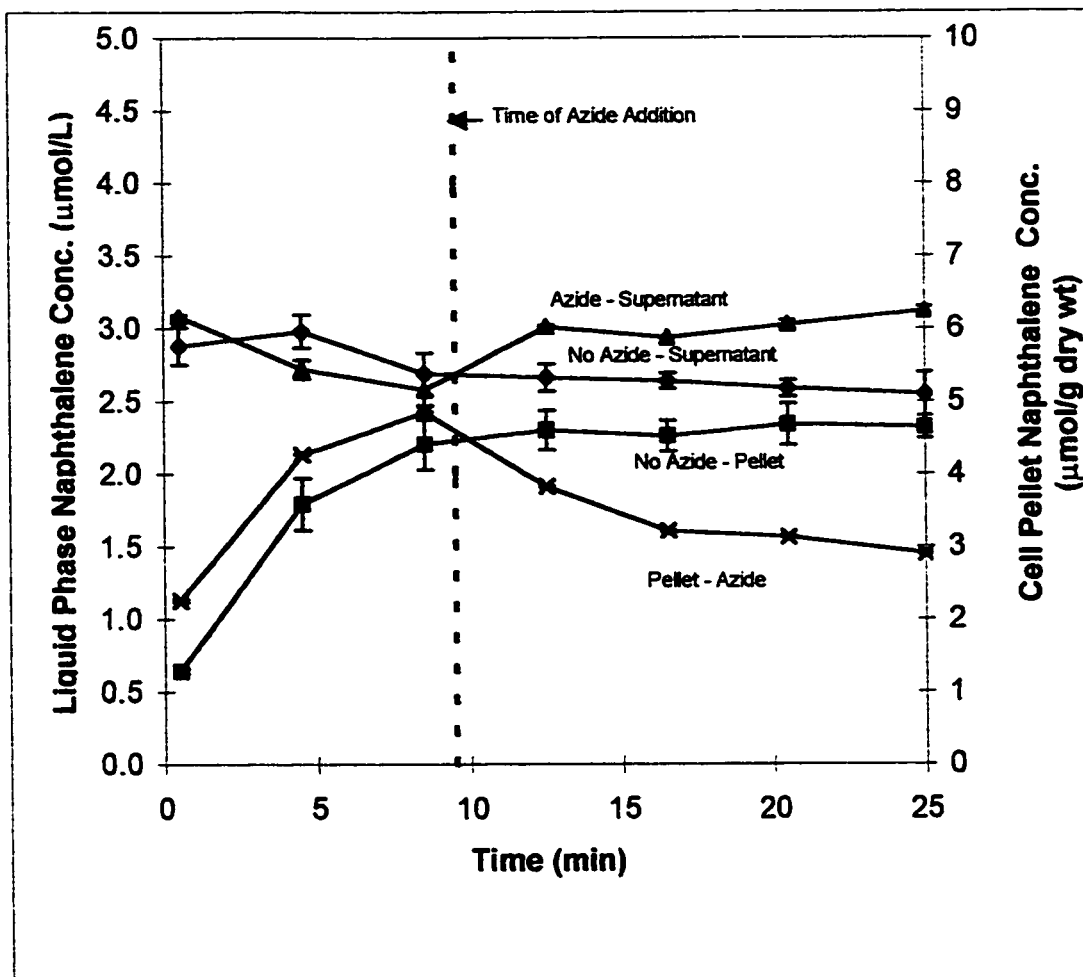


Figure 4.29 Time dependence of liquid phase and cell pellet naphthalene concentrations for the transport of naphthalene in LP6a wild-type.

Having established that it is possible to observe transport properties for LP6a in the serum vials, the transport of naphthalene and toluene were studied. For naphthalene, a concentration comparable to that of phenanthrene was used. Initial attempts at using naphthalene concentrations near the solubility limit of naphthalene resulted in dissolution problems. The naphthalene solidified upon addition to the liquid and slowly dissolved into aqueous phase over the sampling period of 25 min. Figure 4.28 and 4.29 show the transport of naphthalene in the LP6a wild-type at an initial concentration of $5.7 \mu\text{mol/L}$. Experiments were tested in the presence and absence of 30 mM azide added at 9.5 min. Given that naphthalene is metabolized by LP6a wild-type, a similar graph to that for transport of phenanthrene in the wild-type was expected. However, comparison between Figures 4.28 and Figure 4.4 clearly indicates differences. In Figure 4.28 there was no increase in supernatant concentration as naphthalene was metabolized. Another difference between Figures 4.28 and 4.4 is that the cell pellet concentration increased over the first part of the experiment for naphthalene transport whereas for phenanthrene transport it remained constant. It is unlikely that abiotic factors would contribute the observed differences between phenanthrene and naphthalene transport. Naphthalene is significantly more water-soluble than phenanthrene and adsorption and desorption of naphthalene from the glass surfaces would be less significant. Also, naphthalene has a vapour pressure of 36.8 Pa (Mackay and Shiu, 1992). Given the low aqueous naphthalene concentration and the small headspace in the serum vial partitioning effects between the liquid and gas phase would not be significant. The most likely source of the difference in the liquid phase concentration between phenanthrene and naphthalene transport in the LP6a wild-type strain is the efflux pump. In figure 4.4, the immediate

increase in liquid phase concentration indicates that metabolites are quickly leaking out of the cell and into the medium. As a result of the increased polarity of these compounds, they will have decreased permeability across the cell membranes. However, a possible hypothesis is that, given the structural similarity between parent PAH molecules and the metabolites in the early stages of the metabolic pathway (Figures 2.2 and 2.3), it is possible that the efflux pump can transport these compounds out of the cell. Since Figure 4.28 no differences between azide inhibited and non-inhibited experiments upon azide addition, it can be concluded that naphthalene is not subject to active efflux. Thus, as naphthalene is metabolized, the metabolites would remain inside the cell as opposed to being transported out of the cell by active efflux. Thus, there would be no increase in liquid phase ^{14}C concentration over time and the cell pellet ^{14}C concentration would increase as metabolites accumulated in the cell.

The most significant difference between naphthalene transport and transport of phenanthrene, anthracene, and fluoranthene is that there was no change in cell pellet or supernatant concentration upon the addition of azide. This result is clearly emphasized in the graphs for naphthalene transport in the mutant 1-51 strain (Figures 4.30 and Figure 4.31). In this case there is no metabolism to interfere with results. In these graphs, it is apparent that the samples to which azide was added do not differ from those where it was not added. The LP6a mutant 1-51 pellet concentration was $0.803 \pm 0.059 \mu\text{mol}/(\text{g dry wt})$ in the experiments without azide and $0.811 \pm 0.074 \mu\text{mol}/(\text{g dry wt})$ in those with azide at the end of the sampling period. The steady-state supernatant concentration was $2.93 \pm 0.06 \mu\text{mol}/\text{L}$ for the experiments without azide and the equilibrium concentration

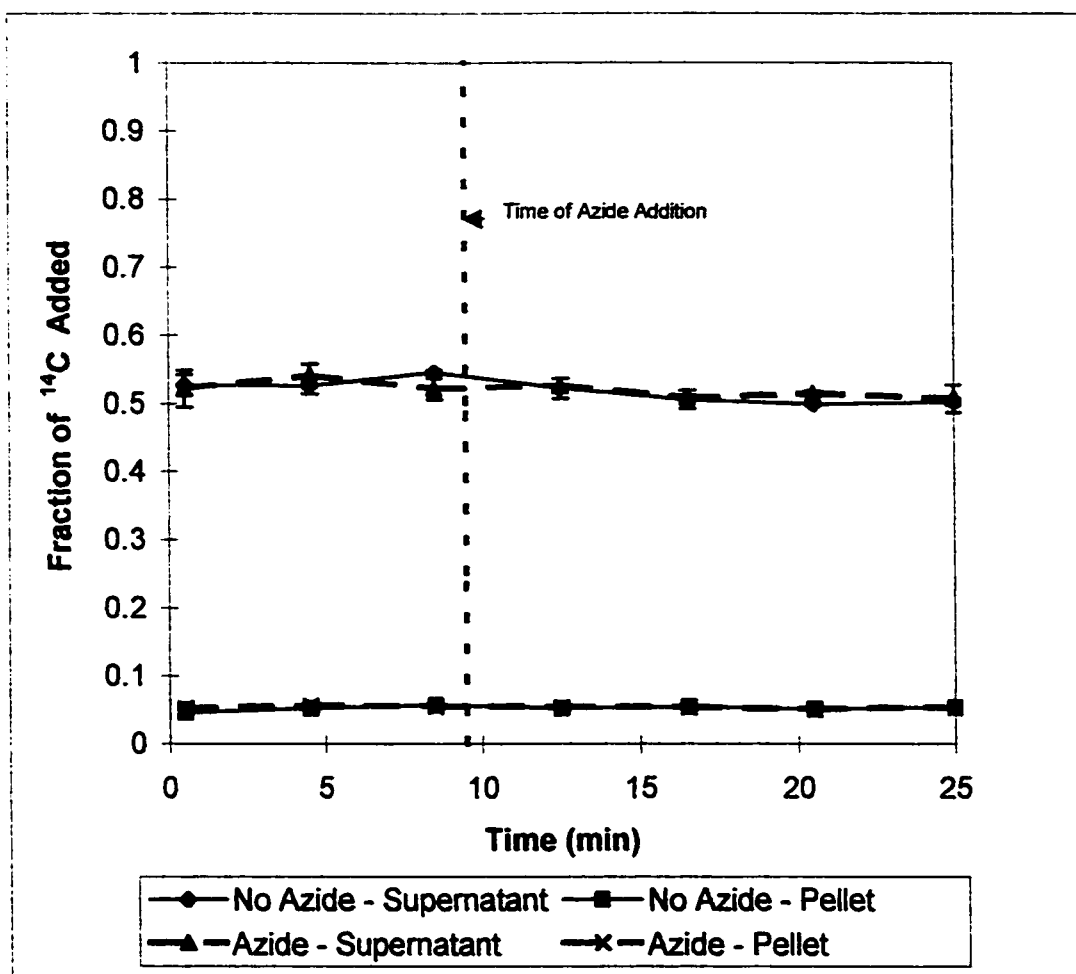


Figure 4.30 Time dependence of liquid phase and cell pellet ^{14}C concentrations for the transport of naphthalene in LP6a mutant 1-51.

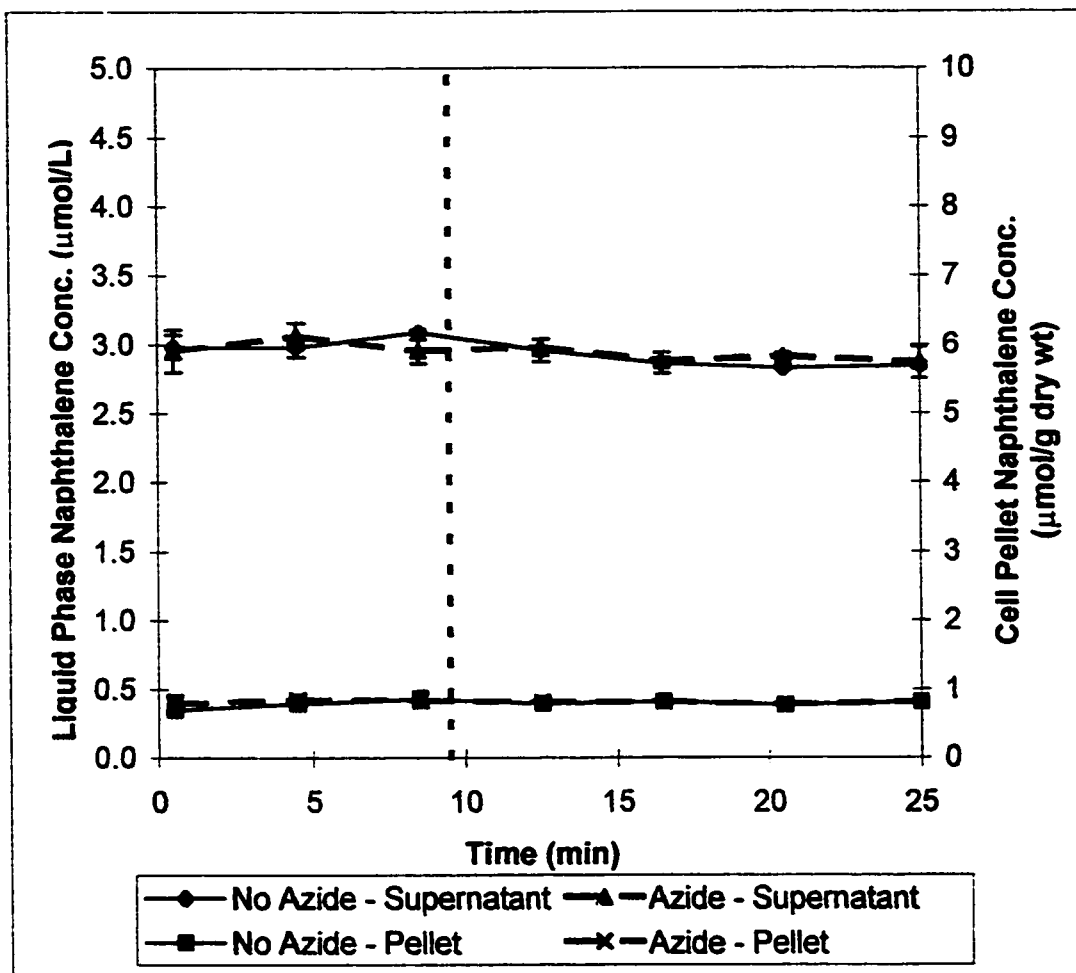


Figure 4.31 Time dependence of liquid phase and cell pellet ^{14}C concentrations for the transport of naphthalene in LP6a mutant 1-51.

was $2.94 \pm 0.09 \mu\text{mol/L}$ for those with azide addition. The experiments for the transport of phenanthrene at different azide concentrations have shown that 30 mmol/L is sufficient to completely inhibit active transport. Thus, the results for naphthalene transport suggest naphthalene transport is not subject to the active efflux mechanism.

To confirm the lack of an efflux mechanism for naphthalene in LP6a, experiments on the transport of naphthalene was conducted in open 250-mL erlenmeyer flasks. Due to the open headspace, volatilization of naphthalene was a factor in analysis of results. The transport of naphthalene in LP6a mutant 1-51 strain is shown in Figure 4.32 on an absolute scale. For this experiment, three tests were done: an abiotic control, one with 120 mM azide added at 8.5 min, and one with no azide. Figure 4.32 shows that there was a continual decrease in supernatant concentration in all three cases over the time period of the experiment. This trend was due to the volatilization of naphthalene. The other significant feature in this graph is the lack of change in naphthalene concentration, in both the liquid and cell pellet phase, upon addition of azide. This observation confirms the lack of an efflux mechanism for naphthalene transport.

4.6 Toluene Transport

Due to the volatility of toluene, experiments on the transport of toluene were conducted in closed 35-mL serum vials. The liquid and cell phase concentrations of toluene in the wild-type strain are shown in Figures 4.33 and Figure 4.34 on a fractional and absolute basis respectively. The transport of toluene in the mutant 1-51 strain is shown in Figure 4.35 and 4.36. Plate cultures of LP6a wild-type and mutant 1-51 strains incubated with

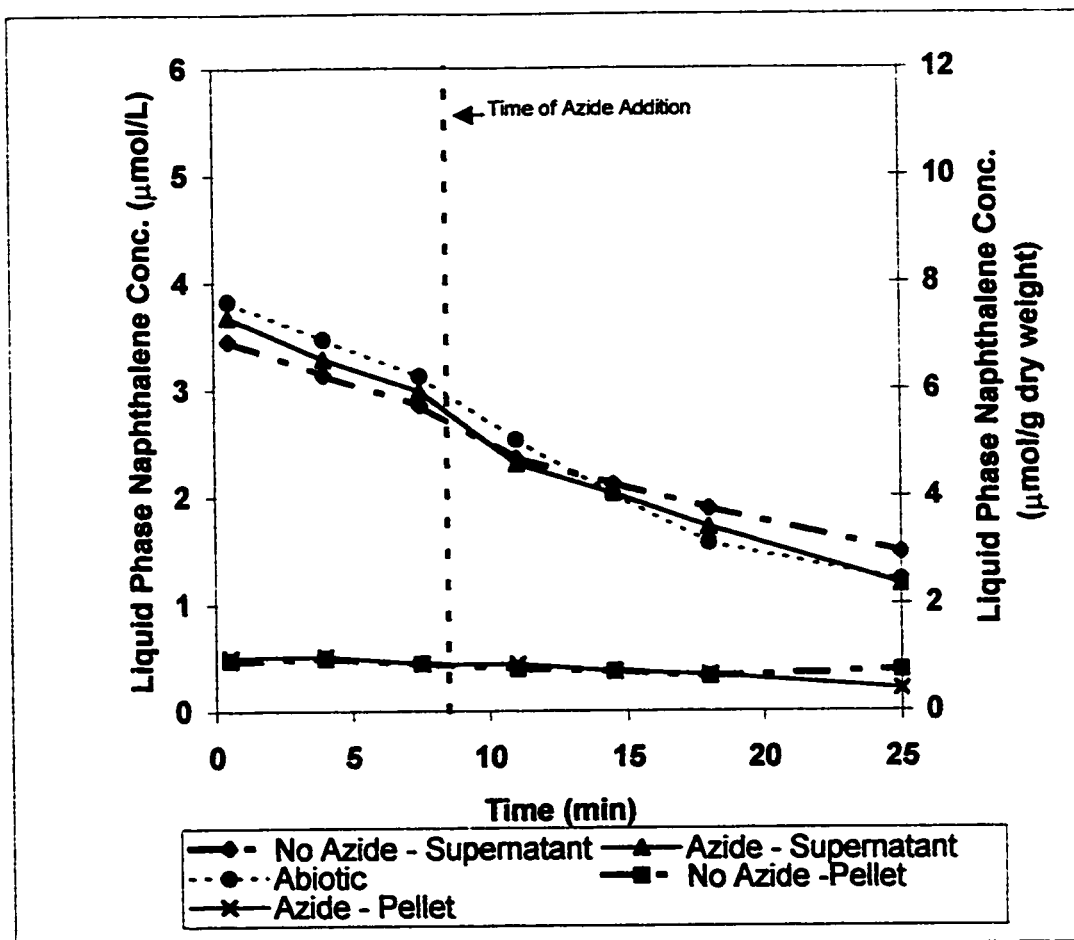


Figure 4.32 Time dependence of liquid phase and cell pellet phase naphthalene concentrations for the transport of naphthalene in LP6a mutant 1-51 in open 250-mL flasks.

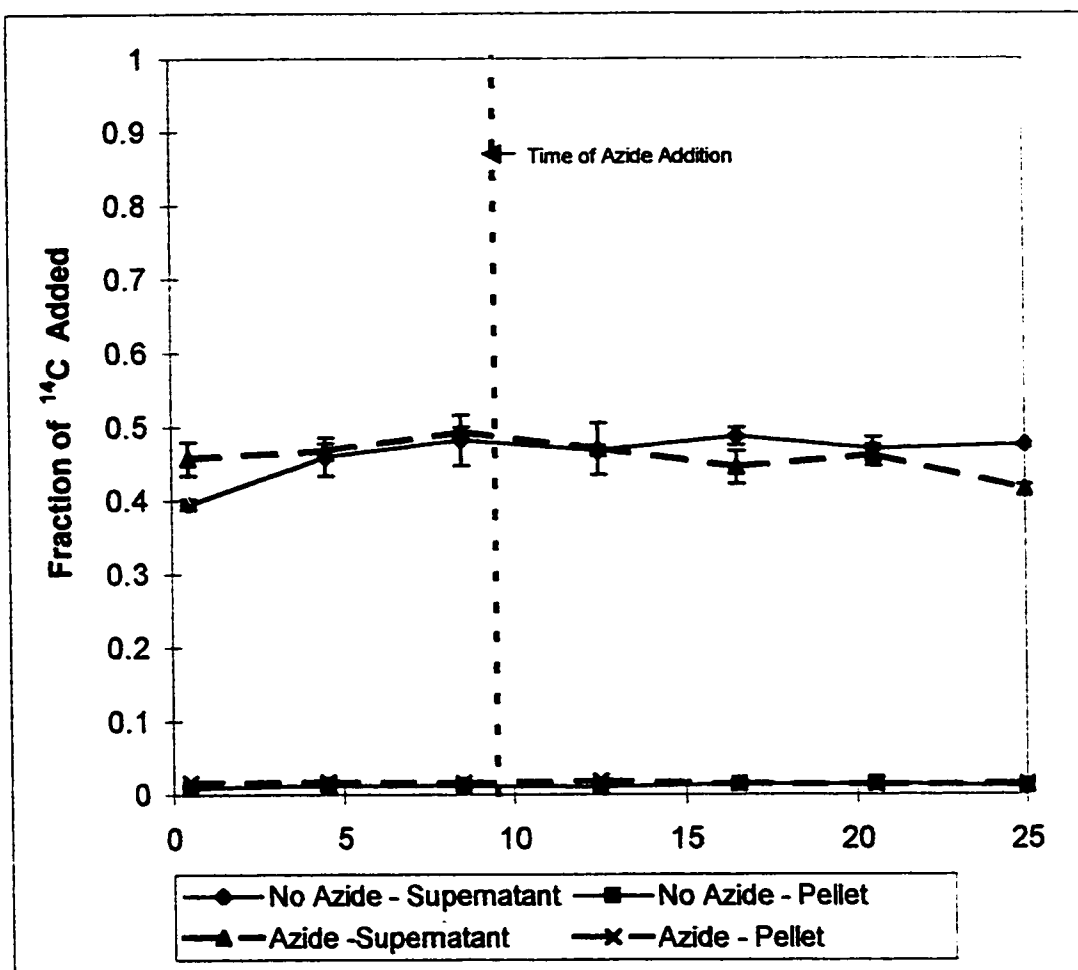


Figure 4.33 Time dependence of liquid phase and cell pellet ^{14}C concentrations for the transport of toluene in LP6a wild-type.

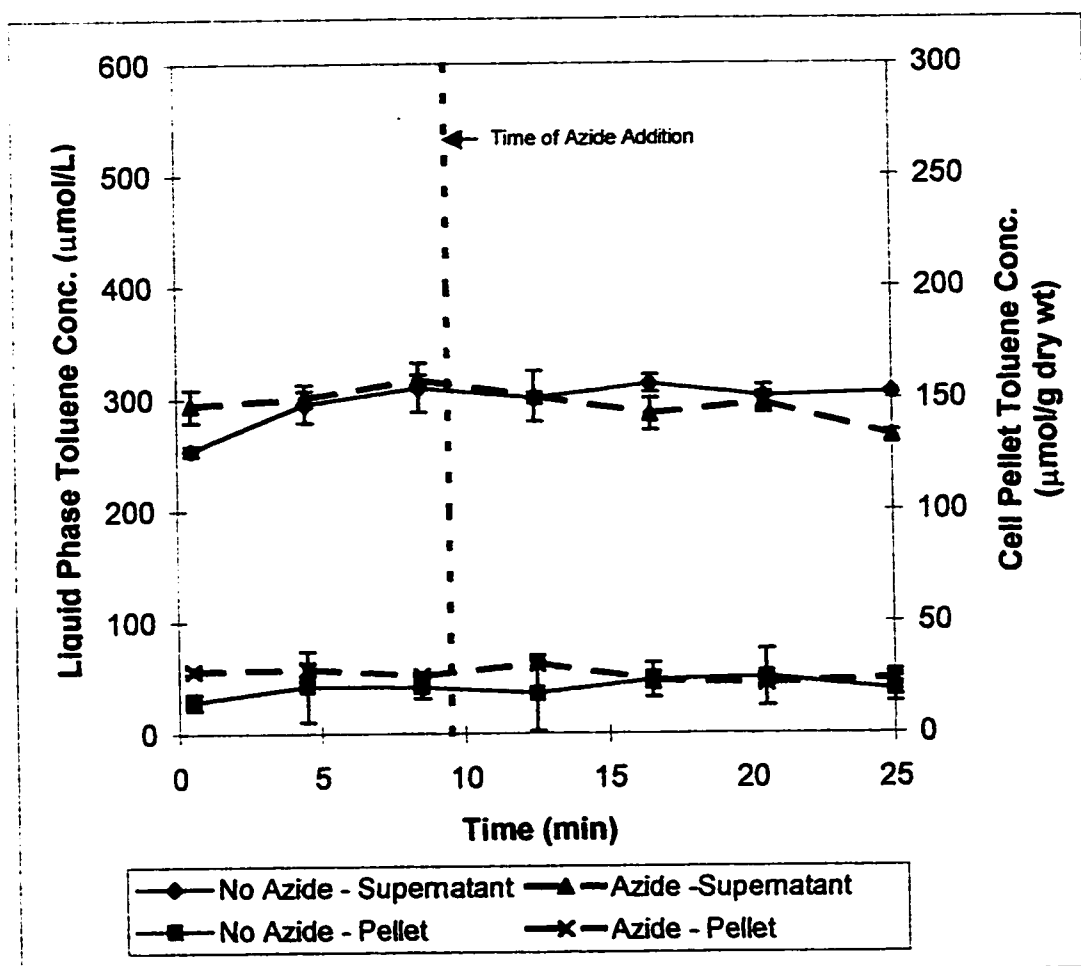


Figure 4.34 Time dependence of liquid phase and cell pellet toluene concentrations for the transport of toluene in LP6a wild-type

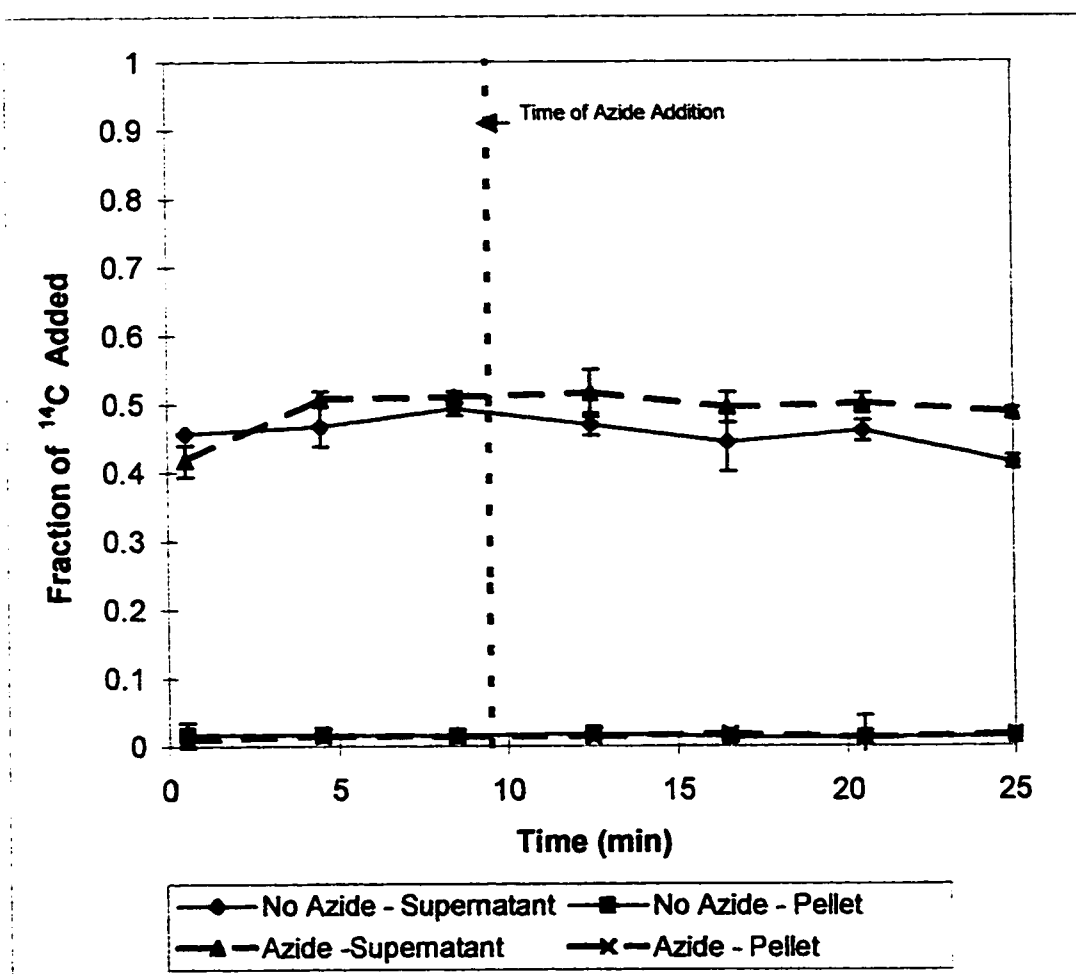


Figure 4.35 Time dependence of liquid phase and cell pellet ^{14}C concentrations for the transport of toluene in LP6a mutant 1-51

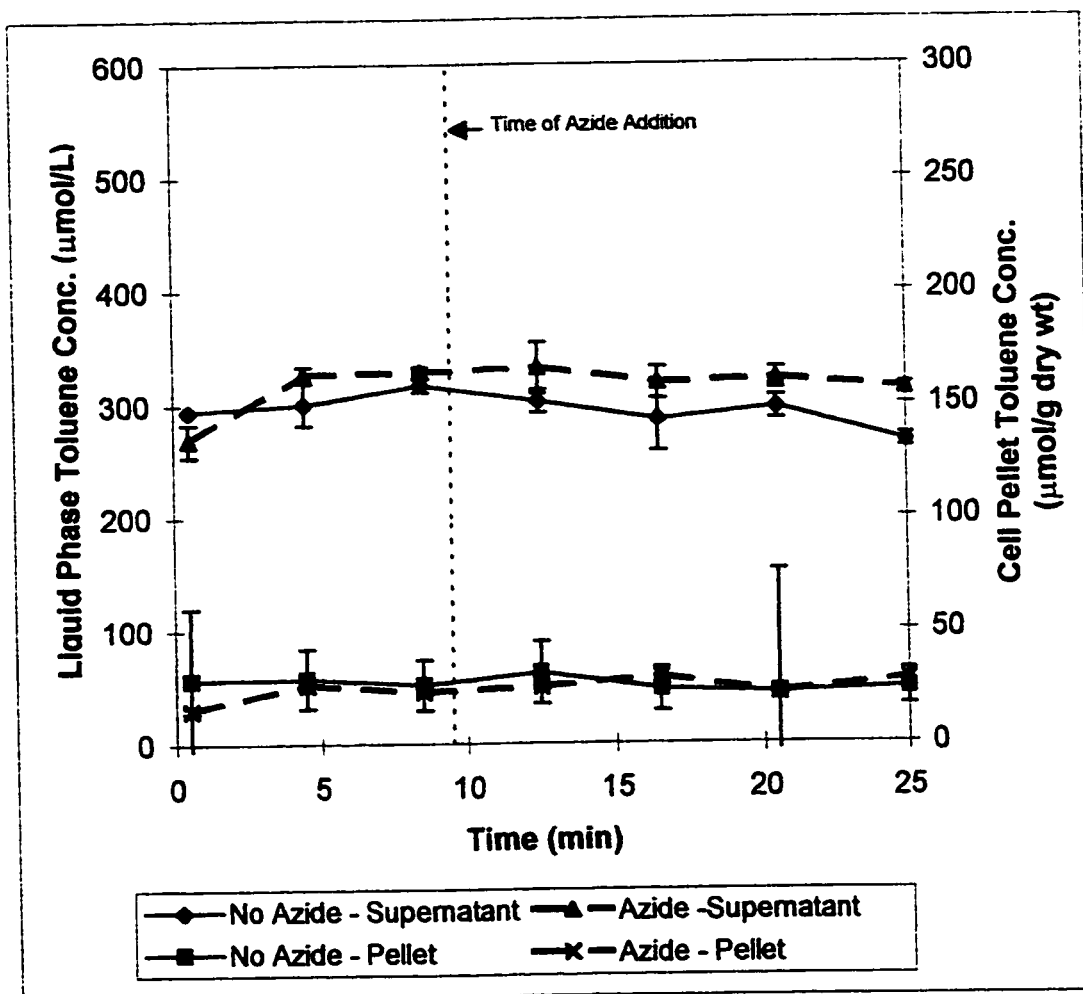


Figure 4.36 Time dependence of liquid phase and cell pellet toluene concentrations for the transport of toluene in LP6a mutant 1-51

toluene vapours indicated a lack of growth over a 1 month period. Thus, it is unlikely that toluene would be metabolized during the transport experiment. As a result, the graphs for the transport of toluene in the wild-type and mutant 1-51 strains were essentially identical. Similar to naphthalene transport, there was no change in supernatant or cell pellet toluene concentrations for both the wild-type and mutant 1-51 strains upon the addition of 30 mM azide. For the wild-type strain, the steady-state pellet toluene concentration was $21 \pm 11 \mu\text{mol}/(\text{g dry wt})$ for the experiments without azide and the equilibrium toluene concentration was $27 \pm 2 \mu\text{mol}/(\text{g dry wt})$ for those with azide addition. For the mutant 1-51 strain, the steady-state pellet toluene concentration was $27 \pm 26 \mu\text{mol}/(\text{g dry wt})$ for the experiments without azide and the equilibrium toluene concentration was $25 \pm 2 \mu\text{mol}/(\text{g dry wt})$ for those with azide addition. Thus, the pellet toluene concentrations are comparable between the two strains under both conditions.

The low partitioning of toluene into LP6a wild-type and mutant 1-51 cells creates ambiguity in the observed results for toluene transport. Toluene is significantly more water-soluble than the PAHs and thus would have a smaller partition coefficient into the cells (Mackay and Shiu, 1992). A comparison of the supernatant and cell pellet toluene concentrations indicates that only 1.5% of the total toluene partitioned into the cells. The 95% confidence interval on the cell pellet concentrations is $20 \pm 10 \mu\text{mol}/(\text{gram dry wt})$ for the wild-type and $26 \pm 23 \mu\text{mol}/(\text{gram dry wt})$ for the mutant 1-51 strain. These values indicate that the pellet toluene concentrations are significantly different from zero. However, the confidence intervals are based on an averaged standard deviation from all the data points. From the graphs for toluene transport, the error bars for the cell pellet

curve, which represent one standard deviation, occasionally include the zero value. Thus, it is likely that an underestimate of the real variance was used in calculating the confidence intervals. As a result, it cannot be concluded that the cell pellet concentrations are significantly different from zero. Thus, the lack of change in concentration upon azide addition could be a result of insufficient analytical precision or the lack of an active efflux mechanism for toluene. The latter result would support the observed behaviour in naphthalene transport.

4.7 Implications of Transport Studies with Different Compounds

The observed results for the transport of the different PAHs indicates a degree of selectivity in the active efflux pump. The more hydrophobic PAHs like phenanthrene, fluoranthene, and anthracene are transported out of the cells by efflux whereas the more water-soluble PAH, naphthalene, was not. This selectivity indicates a fundamental difference between PAH efflux in LP6a and organic solvent and antibiotic efflux in other bacteria: in solvent-tolerant bacteria, a broad specificity efflux pump was observed. Given the observed results for active efflux of PAHs, it is anticipated that LP6a will transport other higher molecular weight PAHs by active efflux. However, the ability of LP6a to remove other lower weight organic solvents from the cell by active efflux is unknown.

The research conducted in this study focused on one bacterium and a limited number of PAHs. Further research is required to compare PAH transport in other PAH-degrading bacteria to that in LP6a. Also, research needs to be done on the transport of other

hydrophobic hydrocarbons, like alkanes, in LP6a and other bacteria. These studies will provide insight into whether the transport of PAHs in LP6a is a phenomenon unique to this bacterium or whether it exists in other bacteria. Experiments with other compounds will give information on the degree of selectivity of this active efflux mechanism, as well as provide an understanding of how bacteria transport other hydrophobic compounds. In particular, it will provide clarity on the similarities or differences between PAH efflux and organic solvent efflux. Further work needs to be done on the mechanism by which the efflux pump operates to try to determine if the energy source is ATP, the proton gradient, or the charge gradient. An understanding of whether the pump spans both membranes and whether it removes PAH from the cytoplasm, periplasm, or the membranes will provide insight into the mode of operation of efflux pumps.

From the transport studies with the different PAHs and on toluene, it was possible to obtain partition coefficients between the aqueous phase and cell pellet phase in the presence of inhibitory levels of azide. Unlike the transport studies with phenanthrene, these values were based on one concentration. When the log of the partition coefficient was plotted against the log of the octanol-water partition coefficient for each compound, a linear trend resulted (Figure 4.37). A linear trend between membrane partitioning and K_{ow} is not surprising since linear correlations have already been discovered for the partitioning of hydrophobic compounds into membrane vesicles (Sikkema et al., 1994). From the research conducted, a relationship of $\log(K)=0.79\log(K_{ow})+0.30$ was obtained, where K is the partition coefficient in L (membrane volume)/L (aqueous volume) between the cell pellet and aqueous phase in the mutant 1-51 strain in the absence of

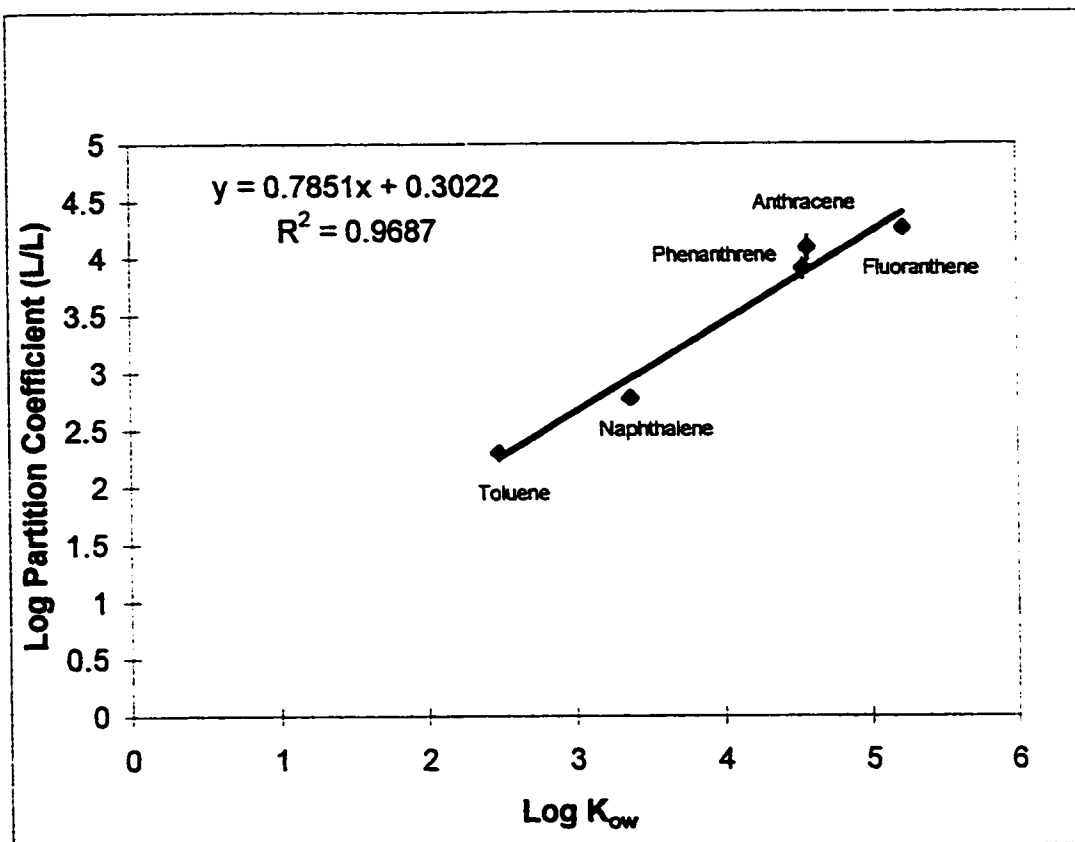


Figure 4.37 Relationship between PAH partition coefficients with LP6a mutant 1-51 in the presence of azide and the corresponding K_{ow} (Mackay and Shiu, 1992).

active efflux. In comparison, Sikkema et al. (1994) reported a correlation of $\log(K)=0.97\log(K_{ow})-0.64$ based on research on the partitioning of a number of organic compounds into single membrane liposomes. Hieppieper et al. (1994) also reported correlations between K_{ow} and membrane partition coefficients for compounds with K_{ow} values between 1 and 5, however, a specific equation was not given.

A direct comparison between the partition coefficients obtained for LP6a and those that were obtained experimentally and mathematically for single membrane liposomes prepared from *E. Coli* phospholipids is not possible (Table 4.5) (Sikkema et al., 1994). If it is assumed that partitioning in LP6a would be twice that of a single membrane system, a reasonable comparison can be made. Based on this assumption, the values obtained in LP6a and those reported by Sikkema et al. (1994) for anthracene and phenanthrene are reasonably similar. However, the values for the remaining compounds are not. In particular, the values of 600 ± 55 and 527 ± 38 obtained for naphthalene are, within error, similar without considering differences in the number of membranes. The values obtained for fluoranthene are even more divergent. Based on the correlation obtained by Sikkema et al. (1994), the calculated value of 26500 for fluoranthene partitioning in single membrane liposomes is significantly larger than the experimentally obtained value of 18300 ± 2000 for partitioning in LP6a.

Table 4.5 Comparison of partition coefficients obtained for LP6a mutant 1-51 strain to those reported by Sikkema et al. (1994) for single membrane liposomes.

Compound	Partition Coefficient (L/L) in LP6a	Partition Coefficient (L/L) obtained by Sikkema et al. (1994)
toluene	200±29	58 (calculated)
naphthalene	600±55	527±38 (experimental)
phenanthrene	12400 ± 1600	4937 ± 86 (experimental)
anthracene	12500 ± 600	4748 (calculated)
fluoranthene	18300 ± 2000	26509 (calculated)

It might be possible to extrapolate from the relationship between K and K_{ow} to predict the partitioning of significantly more hydrophobic PAHs. However, some caution is required since it has been previously observed in membrane vesicles that a linear correlation to K_{ow} no longer applies for compounds with K_{ow} values larger than 5.5. Compounds with K_{ow} values ranging from 5.5 to 9 displayed a constant membrane partition coefficient in liposomes that was independent of K_{ow} (Gobas et al., 1988).

4.8 Metabolite Production

It was previously argued in this thesis that the increasing supernatant ^{14}C concentrations for the transport of phenanthrene in the LP6a wild-type strain (Figure 4.5) were a result of metabolism. This same trend was observed in the transport of anthracene (Figure 4.20) in the wild-type. However, it was not observed in the transport of fluoranthene (Figure 4.24) and toluene (Figure 4.32) in the wild-type. LP6a wild-type is able to degrade phenanthrene anthracene, and naphthalene but it is not able to grow on toluene and fluoranthene as sole carbon sources.

To confirm that the observed trends were a result of metabolite production, liquid-liquid extraction was performed on an abiotic control and on the supernatant of LP6a wild-type and mutant 1-51 cell suspensions incubated at room temperature for 25 min with phenanthrene. This time period represents the end of transport studies. To ensure that all the material was recovered, two extractions with methylene chloride were done. However, due to the high partitioning into the organic phase, one extraction was often sufficient. Also, prior to extractions, the cell suspension was centrifuged to separate the cell fraction. As a result, there was potential for loss of phenanthrene to the walls of the centrifuge tube. To recover this material, the cell pellet was disposed of and the tube rinsed once with water to remove any cells. The tube was then rinsed with methylene chloride to recover the adsorbed phenanthrene. The extracted samples were dried and resuspended in acetonitrile for analysis by HPLC using a UV-vis detector spectroscopy. For UV-vis spectroscopy, a second set of extractions were done at pH 2. By acidifying the liquid, some of the acidic metabolites would be rendered more hydrophobic and would partition more readily into the methylene chloride phase.

The two extractions and the sample from the centrifuge tube were analyzed by HPLC and the results pooled to give a total phenanthrene concentration in the supernatant phase. From the results presented in Table 4.6, the aqueous phase phenanthrene concentration for the abiotic control was $4.4 \pm 0.3 \mu\text{mol/L}$ phenanthrene. Data in Figure 4.3 indicate that during transport studies, the average liquid phase phenanthrene concentration in the abiotic control was $4.3 \mu\text{mol/L}$. Thus, there was approximately 100% recovery of the phenanthrene from the extraction process. Table 4.5 also indicates that the average liquid

phase phenanthrene concentration for the LP6a mutant 1-51 strain was $2.56 \pm 0.8 \mu\text{mol/L}$ when analyzed by HPLC. Figure 4.7 indicates that, during transport studies, the average supernatant phenanthrene concentration for the mutant 1-51 strain in the absence of azide was $2.5 \pm 0.2 \mu\text{mol/L}$ based on a equivalent phenanthrene basis. Thus, there was nearly 100% recovery of phenanthrene in the LP6a mutant 1-51 strain if one assumes that all the ^{14}C in the supernatant of transport experiments was phenanthrene. In contrast to the results for the abiotic control and LP6a mutant 1-51 strain, Table 4.6 indicates that the mean liquid phase phenanthrene concentration for the LP6a wild-type was $0.39 \pm 0.36 \mu\text{mol/L}$ when analyzed by HPLC. Yet Figure 4.5 indicates that after 25 min of incubation, phenanthrene and metabolites concentration in the absence of azide was $5.6 \pm 0.4 \mu\text{mol/L}$. Given that the extractions gave accurate phenanthrene concentrations for the mutant 1-51 strain and abiotic control, it is unlikely to give inaccurate results for the wild-type. Since the supernatant concentration from transport studies is 14 times greater than the value obtained by liquid-liquid extraction and HPLC analysis, it can be concluded that a significant portion of the ^{14}C label in transport studies was metabolites.

Table 4.6 Summary of liquid phase phenanthrene concentrations as determined by HPLC.

Sample	Total Phenanthrene Recovered in Supernatant ($\mu\text{mol/L}$)		
	Abiotic control	LP6a wild-type	LP6a mutant 1-51
1	4.72	0.01	2.74
2	4.13	0.02	3.13
3	4.24	0.83	1.28
4		0.47	3.18
5		0.62	1.99
Average	4.4	0.39	2.5
Standard Deviation	0.3	0.36	0.8

In Table 4.6 there is a large variance in the recovery of phenanthrene for the different biotic samples. Of particular concern are the data for the wild-type strain where an average of 0.39 $\mu\text{mol/L}$ with a standard deviation of 0.36 $\mu\text{mol/L}$ was observed. This variability is likely due to different metabolic states of the cell suspensions. Not all samples were from the same LP6a wild-type cell culture. More importantly, due to the time required to process each sample, some samples were required to sit at room temperature for as much as 1.5 h prior to incubation with phenanthrene. This time period could alter metabolic activity in the wild-type strain. The data for the mutant I-51 strain, however, are not subject to metabolic activity. The variance in results for this strain reflects a combination of variability in technique and human error.

The choice of column and mobile phase for HPLC separation caused all polar compounds to elute as a group at the beginning of the run. Thus, it was not possible to detect individual metabolites at 254 nm on the UV-vis detector used. Thus, extractions were repeated at pH 7 and pH 2 for analysis by UV-vis spectroscopy. Samples were analyzed over a wavelength range of 180 nm to 800 nm. The only significant peak was at 254 nm. Table 4.7 gives the phenanthrene and metabolites concentration based on absorbance at 254 nm. An important distinction is that the absorbance can be a result of phenanthrene or metabolites. UV-vis does not directly distinguish the two. Table 4.7 indicates that for the abiotic control, the liquid phase phenanthrene concentration was $4.7 \pm 0.6 \mu\text{mol/L}$ phenanthrene at pH 2 and $3.5 \pm 0.7 \mu\text{mol/L}$ at pH 7. At a 95% confidence limit, the difference between the value at pH 2 and the value at pH 7 is 1.19 ± 1.12 . This interval

indicates a significance difference between the two values. However, some skepticism is required when the confidence interval on the difference is very near zero. Since it is an abiotic control, there should be no difference in extractions at pH 2 and pH 7. It is more likely that the standard deviations reported are an underestimate of the true variance. The phenanthrene concentrations obtained at the two pH values for the abiotic control also correspond well to the value of $4.4 \pm 0.3 \mu\text{mol/L}$ obtained by HPLC analysis and the aqueous phase phenanthrene concentration of $4.3 \mu\text{mol/L}$ obtained in transport studies on the abiotic control (Figure 4.3). Table 4.7 also indicates that there was an phenanthrene concentration of $2.7 \pm 1.1 \mu\text{mol/L}$ in the supernatant of the LP6a mutant 1-51 at pH 2 and $2.8 \pm 0.6 \mu\text{mol/L}$ at pH 7. The lack of difference between the phenanthrene concentrations at the two pH values for the mutant strain is consistent with the lack of metabolism in the mutant 1-51 strain.

All aromatic absorbances at 254 nm were due to phenanthrene alone in the mutant 1-51 strain. The values obtained by UV-vis for the phenanthrene concentration in the supernatant of the mutant 1-51 strain are consistent with the value of $2.5 \pm 0.8 \mu\text{mol/L}$ obtained by HPLC and with the phenanthrene concentration of $2.5 \pm 0.2 \mu\text{mol/L}$ obtained in transport studies (Figure 4.7). The equivalent phenanthrene and metabolites concentration, as determined by UV-vis spectroscopy, for the LP6a wild-type strain was $3.0 \pm 0.5 \mu\text{mol/L}$ at pH 2 and $1.0 \pm 0.5 \mu\text{mol/L}$ at pH 7. The difference between these two values at a 95% confidence limit is $1.94 \pm 0.80 \mu\text{mol/L}$. Thus, these values are significantly different from each other. At pH 2, more of the acidic metabolites will partition into the methylene chloride phase than at pH 7. Since UV-vis spectroscopy only detects the aromatic absorbance at 254 nm and not individual species, the increase in the

amount of metabolites manifests itself as the observed increase in absorbance at pH 2. Even at pH 7, some metabolites will partition into the organic phase. As a result, there was an increase in the measure concentration of phenanthrene and metabolites concentration when analyzing the supernatant of the wild-type strain by UV-vis over HPLC. A phenanthrene concentration of $0.39 \pm 0.36 \mu\text{mol/L}$ was obtained by HPLC analysis versus an equivalent phenanthrene concentration of $1.01 \pm 0.46 \mu\text{mol/L}$ at neutral pH for UV-vis analysis. Given the large variability though, these values are the same at a 95% confidence interval. Also, the results obtained by UV-vis are significantly lower than the equivalent ^{14}C -phenanthrene concentration of $5.63 \pm 0.40 \mu\text{mol/L}$ obtained in transport studies on the wild-type strain in the absence of azide (Figure 4.6). This discrepancy is due to the inability of extractions to recover all the metabolites. From the results obtained by HPLC and UV-vis, it can be concluded that the increase in supernatant ^{14}C concentrations for the transport of phenanthrene and anthracene in the LP6a wild-type strain in the absence of azide were a result of metabolism.

Table 4.7 Summary of liquid phase phenanthrene concentrations as determined by UV-visible spectroscopy of extract from supernatant samples.

	Conditions of Extraction			
	pH 2		pH 7	
	Average ($\mu\text{mol/L}$)	Standard Deviation	Average ($\mu\text{mol/L}$)	Standard Deviation
LP6a	3.0	0.5	1.0	0.5
LP6a Mutant 1-51	2.7	1.1	2.8	0.6
Abiotic control	4.7	0.6	3.5	0.7

During extractions, there was a material present that emulsified the methylene chloride phase. Whether this material was produced by the cells, or it was lipid materials leached from the cell, or whether emulsification was due to the presence of residual cells in the supernatant is uncertain. Preliminary work indicated that its presence was not affected by prior exposure of the cells by PAH. To determine the effect of this factor on transport, a cell suspension was allowed to incubate for 30 min in the absence of PAH to ensure production of the unknown material and the supernatant was collected by centrifugation. The primary concern was whether this unknown material was a biosurfactant and whether it altered the aqueous PAH concentrations. The equilibrium phenanthrene concentration for an abiotic control of phosphate buffer was compared to that for the supernatant from the cell suspension. To both samples, phenanthrene was added to give an initial concentration of 6.36 $\mu\text{mol/L}$. The data in Table 4.8 indicate that there is no distinction between the two tests at the concentrations used in the transport studies. The liquid phase phenanthrene concentration for the abiotic control was $3.8 \pm 0.2 \mu\text{mol/L}$ and for the supernatant $4.0 \pm 0.2 \mu\text{mol/L}$. The emulsifying agent had no effect on the aqueous solubility of phenanthrene. Thus, the material is unlikely to affect the transport of PAHs.

4.9 Induction Experiments

Previous research on organic solvent tolerance indicated that there are both constitutively expressed and inducible efflux pumps in *Pseudomonas* species. The greatest resistance to the toxic effects of organic solvents and antibiotics was obtained when efflux pumps

were induced (Ramos et al., 1998). The results presented thus far have indicated active efflux in non-induced LP6a wild-type, mutant 1-51, and cured cells. Furthermore, they have indicated rapid metabolism of naphthalene, phenanthrene, and anthracene in the wild-type strain without the need to induce metabolic enzymes. This observation could be a result of a low level of constitutively expressed metabolic enzymes. To determine if induction can enhance transport rates for active efflux, LP6a mutant 1-51 was grown on TSB, washed, and resuspended to an OD₆₀₀ of 1.5 in 100 mL of 0.1 M phosphate buffer. To the cell suspension, phenanthrene was added at a concentration equal to solubility. The cell suspension was allowed to incubate for 2 h at room temperature with the phenanthrene to allow induction to proceed. Following induction, the cells were collected, washed, and resuspended to an OD₆₀₀ of 1 in phosphate buffer so as to study the transport of phenanthrene in the induced cells.

Figure 4.38 compares the transport of phenanthrene in the cells exposed to phenanthrene for 2 h to the previously obtained results for non-induced cells. From the graph, it is apparent that there is no difference between these two tests. Thus, after a 2-h incubation, phenanthrene was not able to induce transport factors. Research by Kieboom et al. (1998) indicated that organic solvent efflux in *P. putida* S12 was induced by toluene 30 min after the toluene addition to cells grown on LB broth. It is possible that another compound is required to induce efflux pumps in LP6a. However, research on organic solvent efflux has shown that a wide range of organic solvents were able induce organic solvent efflux pumps (Kieboom et al., 1998). If organic solvent efflux and PAH efflux are similar, it can be rationalized that a broad range of PAHs should induce PAH efflux.

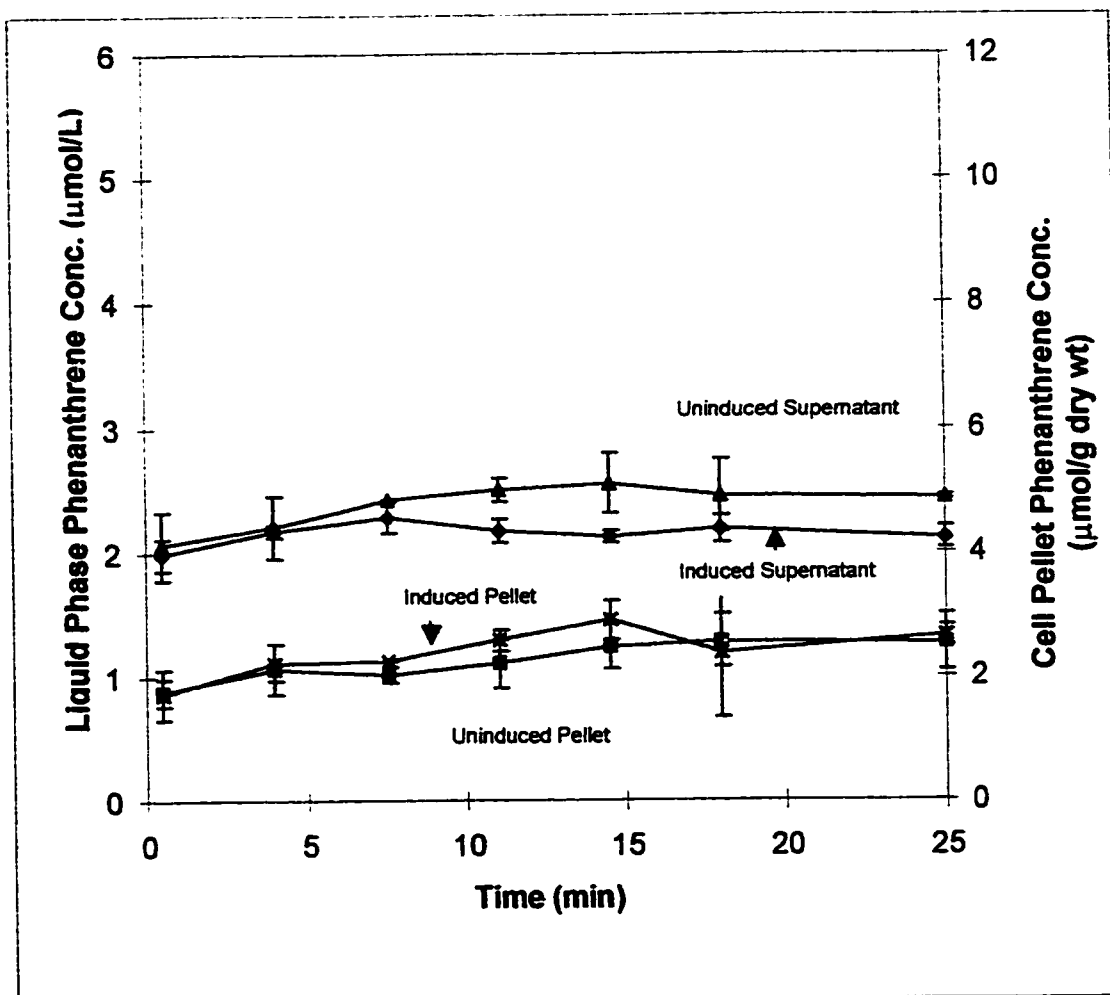


Figure 4.38 Time dependence of liquid phase and cell pellet phenanthrene concentrations for the transport of phenanthrene in induced and non-induced LP6a mutant 1-51 cells.

4.10 Competitive Transport

To look for the presence of a saturatable uptake and efflux system, the effect of a second PAH on the transport of phenanthrene in LP6a mutant was studied. For all experiments, phenanthrene was added at time zero and the second substrate was added at 9.5 minutes. Anthracene was used at a concentration of 0.271 $\mu\text{mol/L}$, fluoranthene at 1.16 $\mu\text{mol/L}$, and naphthalene at 5.66 $\mu\text{mol/L}$. Experiments with naphthalene were conducted in closed serum vials. In some experiments, to study passive transport, 120 mM azide was added 30 min prior to the experiment to ensure complete inhibition of active efflux.

The effect of anthracene addition on passive (azide) and active (no azide) transport is shown in Figure 4.39. For each curve, there were no sudden changes in phenanthrene concentration upon addition of anthracene. For the experiments without azide, the cell pellet and supernatant phenanthrene concentration remained relatively constant over time. For the case where azide was added, there was a constant supernatant concentration and an increasing cell pellet concentration as phenanthrene accumulated to equilibrium levels in the cell. An abiotic control was also tested and the aqueous phenanthrene concentration was also constant over time. Similarly, was no observed effect of fluoranthene (Figure 4.40) or naphthalene (Figure 4.41) on phenanthrene transport. For active efflux, no effect upon naphthalene addition was expected since naphthalene was not subject to active efflux. The lack of saturation of active efflux indicates the high capacity of the transport proteins relative to the solubility of PAHs. For uptake, the lack of effect of all the PAHs is consistent with passive diffusion where transport rates are independent of other compounds at low concentrations. However, given the low

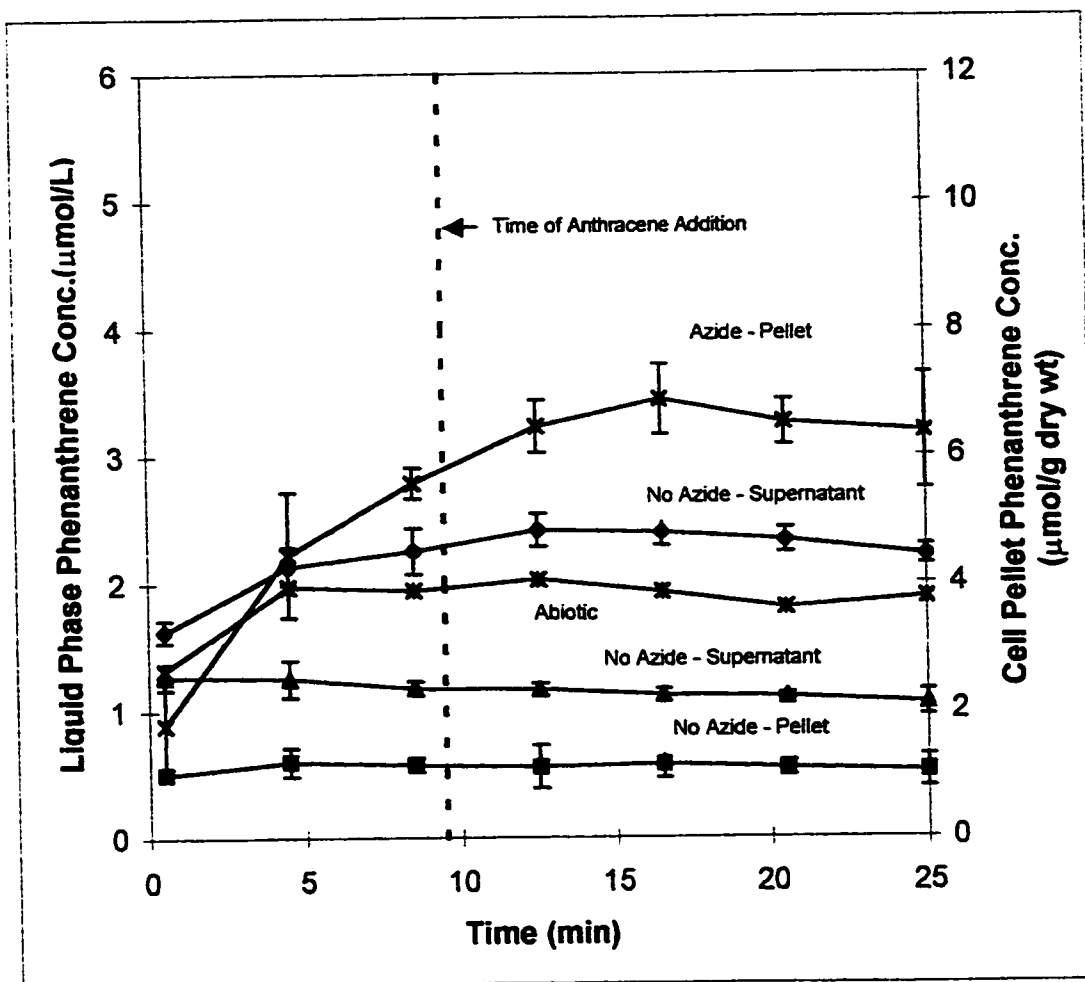


Figure 4.39 Effect of anthracene addition on the transport of ^{14}C phenanthrene in LP6a mutant 1-51.

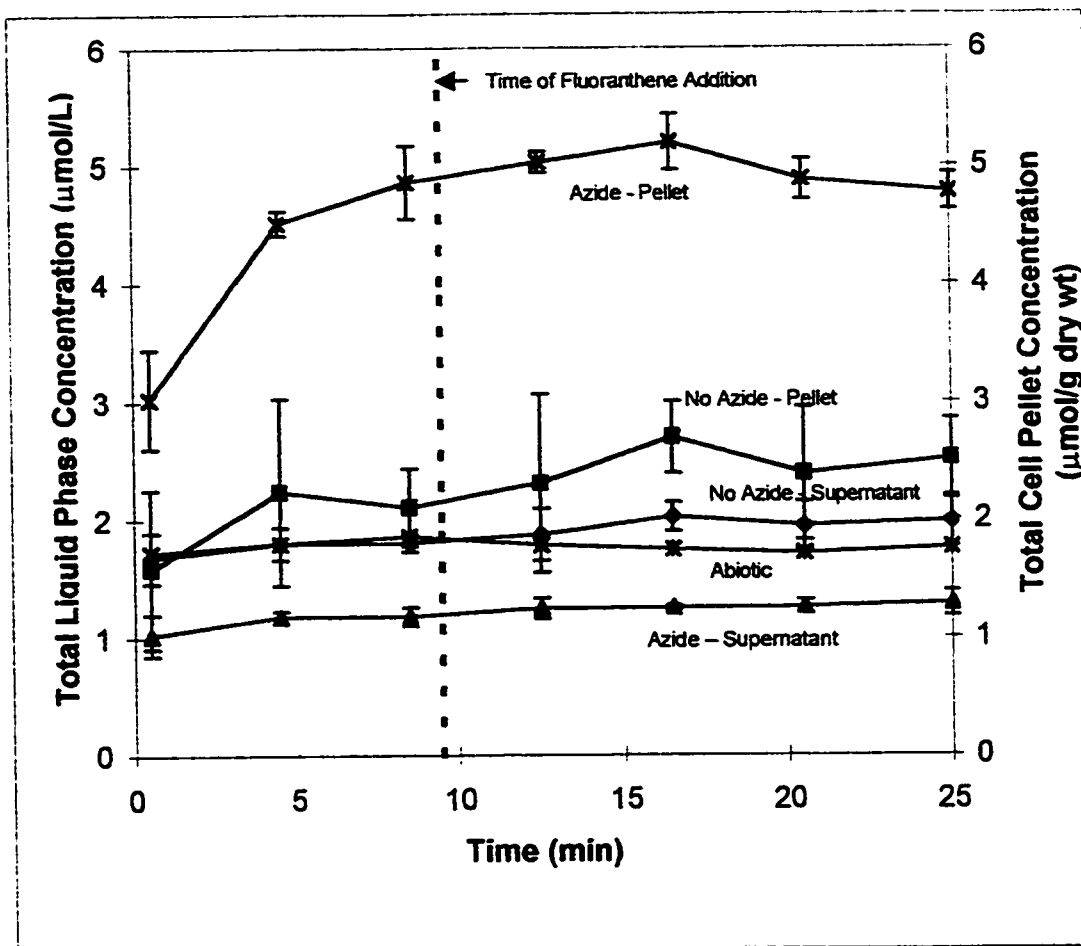


Figure 4.40 Effect of fluoranthene addition on the transport of ^{14}C phenanthrene in LP6a mutant 1-51.

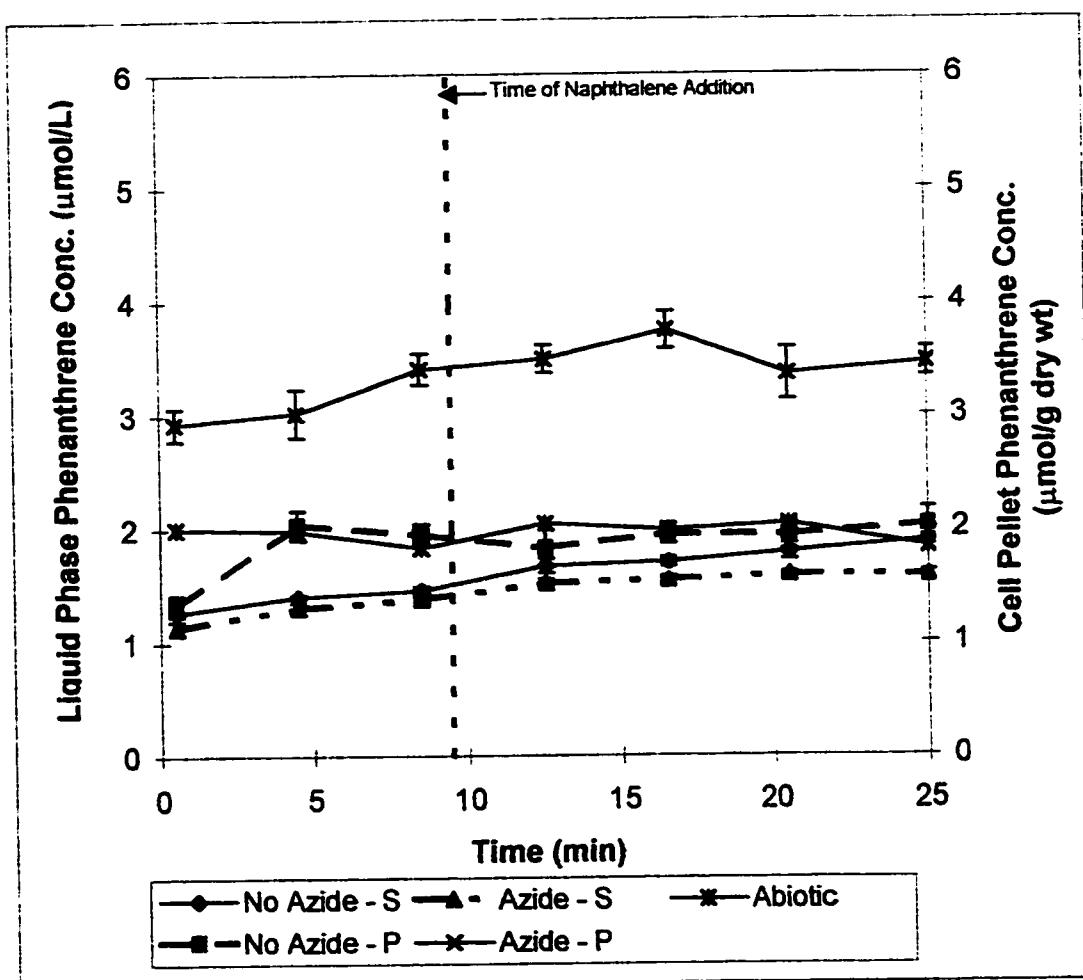


Figure 4.41 Effect of naphthalene addition on the transport of ^{14}C phenanthrene in LP6a mutant 1-51.

solubility of PAHs, facilitated transport cannot be discounted as an uptake mechanism. If there are transport proteins for uptake present, it is possible that they are operating in their linear region even in the presence of a second PAH.

An observation that was of concern was the low cell pellet phenanthrene concentration in Figure 4.39 for the experiments in the absence of azide. From this graph, it appears that there is lower steady-state phenanthrene concentration in the absence of azide as opposed to in the presence of azide. Since these experiments were done in parallel and since LP6a mutant 1-51 is unable to degrade phenanthrene, there should be no biological variability. A reasonable explanation is analytical error. It is possible that errors were made in preparing the cell suspension or in adding insufficient radiolabeled phenanthrene to the flask. However, the reproducibility of the low cell pellet concentration argues against this explanation.

4.11 Modeling Transport

4.11.1 Model Development

The observed results for the transport of phenanthrene in LP6a were used to develop and fit a theoretical model for the mutant strain. Modeling of the mutant strain removed the complication of metabolism from the analysis. Thus, there were three main components to consider: membrane permeability rates for uptake, PAH transport rates by active efflux, and equilibrium partitioning. The approach taken was to model the cell

concentrations. Thus, there were some important concentrations in the cell membrane to consider (Figure 4.42): the concentration at the outer membrane-liquid interface ($y_{om}(x=0)$), the concentration at the outer membrane-periplasm interface ($y_{om}(x=L)$), the periplasmic concentration (C_p), the concentration at the inner membrane-periplasm interface ($y_{im}(x'=0)$), the concentration at the inner membrane-cytoplasm interface ($y_{im}(x'=L)$), and the cytoplasmic concentration (C_c).

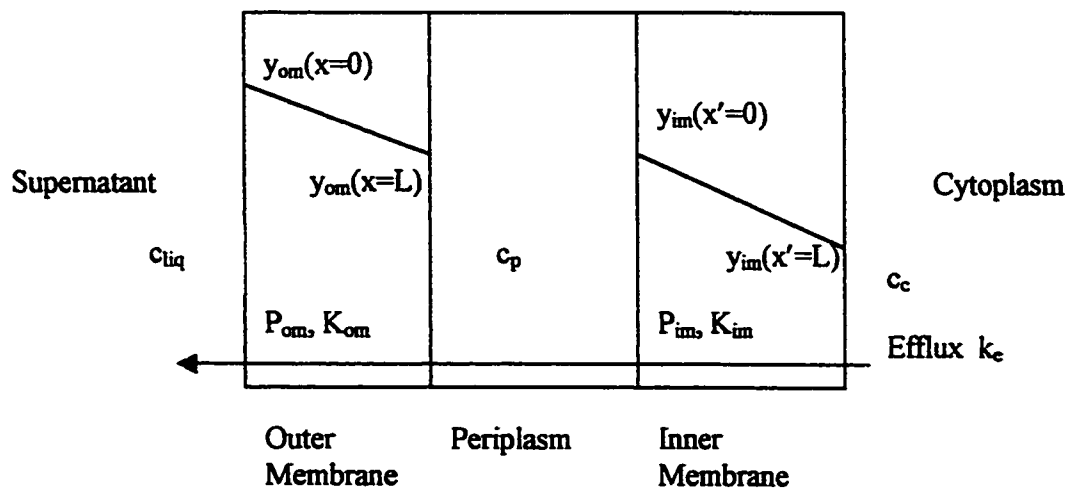


Figure 4.42 Schematic of concentration gradients in bacteria and location of important parameters

Although facilitated transport was not disproven as a possible mechanism, uptake was assumed to proceed by diffusion. Thus, permeability equations were used with two permeability coefficients P_{om} and P_{im} for the outer and inner membrane respectively.

Two flux equations were developed for the flux across the outer membrane (J_{om}) and the

flux across the inner membrane (J_{im}) (equations 4-1 and 4-2). In this equation, A_o and A_i are the surface area of the outer membrane and inner membrane respectively.

$$J_{om} = P_{om} A_o (y_{om}(x = 0) - y_{om}(x = L)) \quad (4-1)$$

$$J_{im} = P_{im} A_i (y_{im}(x' = 0) - y_{im}(x' = L)) \quad (4-2)$$

In using a permeability equation for passive uptake, the non-ideality and surface properties imposed by the membrane structure can be ignored. Fick's law of diffusion implies linear concentration gradients through the cell membrane. However, given the structure of PAHs, they are likely to accumulate at the center of the lipid bilayer causing a localized concentration maximum. This trend was observed for partitioning of benzene (De Young and Dill, 1988) and short alkanes (McIntosh et al., 1980) into membrane vesicles. The permeability coefficient encompasses the diffusion coefficient and all other factors that would otherwise be introduced by a rigorous thermodynamic analysis of the non-linear PAH distribution in the membrane. For the surface area (A), the bacterium was assumed to be a cylinder 1 μm in diameter and 3 μm in length. A membrane thickness (L) of 4 nm was assumed so as to calculate membrane volumes. This value was obtained from neutron diffraction experiments conducted on hexane partitioning into liposomes (White et al., 1981). The thickness of the periplasm is unknown. However, the efflux pump is believed to be made up of three proteins spanning both membranes (Nikaido, 1996). As a result, a reasonable assumption is that the volume of the periplasm will be small relative to the dimensions of the cells so that the outer wall and inner

membrane can be in close proximity to each other. Thus, the surface area of the outer wall and inner membrane can be approximated as being equal.

The second component to consider was equilibrium partitioning. It was assumed that the system was well mixed so that no boundary layers existed at membrane-liquid interfaces. The assumption of a well mixed system applies well to the bulk liquid-outer membrane interface where stirring creates a mixed environment. The assumption does not apply well to the periplasm-membrane and cytoplasm-membrane interfaces where the enclosed volumes restrict mixing. Using this assumption though, it can be concluded that the membrane concentrations at the interfaces were in equilibrium with the corresponding average liquid concentration. It was also assumed that no concentration gradients existed in the periplasm and cytoplasm. Two separate partition coefficients K_{om} and K_{im} were used to describe the partitioning in the outer membrane and inner membrane respectively. When used to predict the total membrane concentration at equilibrium, partition coefficients make no assumptions about the distribution of PAH within the membrane. However, when the same coefficient is used to predict a concentration at a specific point in the membrane, like the interfaces, the assumption is made that the coefficient applies equally well at all points in the membrane. In fact, the coefficient obtained for the total membrane concentration is an average of the partition coefficients at each point in the membrane (equation 4-3).

$$K = \frac{\int_0^L K(x) dx}{L} \quad (4-3)$$

Thus, the non-uniform distribution of PAHs in a membrane is linearized by the use of one partition coefficient for the entire membrane. From these partition coefficients, the membrane interface concentrations are related to liquid phase concentrations by equations 4-4 – 4-7.

$$y_{om}(x=0) = K_{om}c_{liq} \quad (4-4)$$

$$y_{om}(x=L) = K_{om}c_p \quad (4-5)$$

$$y_{im}(x'=0) = K_{im}c_p \quad (4-6)$$

$$y_{im}(x'=L) = K_{im}c_c \quad (4-7)$$

$$y_{avg} = K_{avg}c_{liq} \quad (4-8)$$

The equilibrium concentrations are given by equation 4-8, where C_{liq} is the liquid phase concentration in $\mu\text{mol/L}$ and y_{avg} is the average cell pellet concentration in $\mu\text{mol}/(\text{g dry wt})$. The average partition coefficient K_{avg} is a measure of the partitioning between the aqueous phase and the total cell pellet concentration. However, most of the PAH will reside in the membrane, it is essentially a partition coefficient between the aqueous phase and cell membrane phase. Equation 4-8 is based on the assumption that active efflux has been inhibited and no concentration gradients exist within the cells. From the adsorption isotherm for the mutant 1-51 strain in the presence of inhibitory levels of azide (Figure 4.19), a value of $K_{avg}=5.6 \text{ L}/(\text{g dry wt})$ was obtained. Since the system was assumed to be well mixed, equations 4-4 to 4-7 apply at all times. However, equation 4-8 is only valid at equilibrium when active efflux is fully inhibited.

A mass balance was done on the cell pellet fraction. It was assumed that the volume of the two membranes is the same. Thus, the volume of each membrane is one half of the total membrane volume (V_{mem}). Using this assumption, the total amount of PAH in the cell ($V_{mem}zy_{avg}$) is equal to the sum of the average amount of PAH in each membrane plus the amount in the periplasm (V_pC_p) and cytoplasm (V_cC_c) (equation 4-9).

$$V_{mem}zy_{avg} = \frac{V_{mem}}{2} \frac{(y_{om}(x=0) + y_{om}(x=L))}{2} + \frac{V_{mem}}{2} \frac{(y_{im}(x'=0) + y_{im}(x'=L))}{2} + V_pC_p + V_cC_c \quad (4-9)$$

The variable z is a conversion factor to convert y_{avg} from gram dry weight basis to membrane volume basis. A value of $z=2.2 \times 10^3$ (g dry wt)/L(membrane volume) was obtained from the average dry weight measurement of 365.5 $\mu\text{g/mL}$, the average cell count of 1.94×10^9 CFU/mL (Table 4.1), and the assumptions made on bacterial dimension. For the mass balance on the cell pellet, it was assumed that the periplasmic and cytoplasmic concentrations were very small relative to the membrane concentrations. Thus, from a mass balance perspective an accurate approximation was that all of the PAH resided in the membrane. This is a valid assumption when considering the aqueous solubility of the phenanthrene and the fraction of phenanthrene in the cell pellet phase during transport experiments. From figure 4.8, the cell pellet concentration after azide addition was 10.97 $\mu\text{mol/g dry wt}$ and the liquid phase concentration was 1.36 $\mu\text{mol/L}$. At equilibrium, the phenanthrene concentrations in the periplasm and cytoplasm will be equal to the external liquid phase concentration. Using the data in table 4.1 for cell enumeration and the assumed cell pellet concentrations, it can then be concluded that at

equilibrium, $5.95 \times 10^{-3}\%$ of the phenanthrene was located in the periplasm and cytoplasm of LP6a. Thus, the assumption that the PAH resided primarily in the membranes is valid. Using this assumption and the equilibrium expressions (equations 4-4 to 4-7), equation 4-9 was simplified to equation 4-10.

$$zy_{avg} = \frac{K_{om}C_{liq} + (K_{om} + K_{im})C_p + K_{im}C_c}{4} \quad (4-10)$$

When active efflux was completely inhibited PAH was transported into the cell until equilibrium was reached. At this point, the chemical potential gradient of the PAH was zero and thus there were no concentration gradients in the cell. Thus, $y_{om}=y_{op}$, $y_{ip}=y_{im}$, and $C_{liq}=C_p=C_c$. Using these equalities and equation 4-8 for the average partitioning, equation 4.11 was obtained from equation 4-10. Thus, the average pellet partition coefficient is the average of the two membrane partition coefficients.

$$zK_{avg} = \frac{K_{om} + K_{im}}{2} \quad (4-11)$$

Important information was obtained from the ratio of the equilibrium phenanthrene concentrations in the cell pellet of the azide inhibited case (y_{avg}) to the steady-state pellet concentration for the no azide case (y'_{avg}). Using equation 4-10, which was developed for the mass balance on the cell pellet, equation 4-12 was obtained for the ratio of the pellet concentrations.

$$\frac{y_{avg}}{y'_{avg}} = \frac{K_{om}C_{liq} + (K_{om} + K_{im})C_p + K_{im}C_c}{K_{om}C'_{liq} + (K_{om} + K_{im})C'_p + K_{im}C'_c} \quad (4-12)$$

For the azide inhibited case, there were no concentration gradients in the cell, so $C_{liq}=C_p=C_c$. The equation was further simplified by introducing a parameter α to describe the ratio of the outer membrane partition coefficient to the inner membrane partition coefficient. Using equation 4-11, which relates the individual membrane coefficients to the average membrane coefficient, equation 4-13 was obtained.

$$\alpha = \frac{K_{om}}{K_{im}} = \frac{K_{om}}{2zK_{avg} - K_{om}} \quad (4-13)$$

When these simplifications were introduced into equation 4-12, equation 4-14 was obtained for the ratio of cell pellet concentrations.

$$\frac{y_{avg}}{y'_{avg}} = \frac{2(\alpha + 1)C_{liq}}{\alpha C'_{liq} + (\alpha + 1)C'_p + C'_c} \quad (4-14)$$

When active efflux is present, the cell concentration is at steady-state. Thus, the flux of PAH across the outer membrane is equal to the flux of PAH across the inner membrane in the mutant strain. An equation for the periplasmic concentration in the absence of azide was obtained by setting equation 4-1 equal to equation 4-2. This relationship was simplified by the introduction of a parameter δ to represent the ratio of the outer membrane permeability to the inner membrane permeability (equation 4-15). Using the flux equations (equations 4-1, 4-2), the parameters δ and α , the equilibrium expressions

(equations 4-4 to 4-7), the periplasmic concentration in the absence of azide is thus described by equation 4-16.

$$\delta = \frac{P_{om}}{P_{im}} \quad (4-15)$$

$$C'_p = \frac{\alpha \delta C'_{liq} + C'_c}{\alpha \delta + 1} \quad (4-16)$$

When active efflux is present, the cytoplasmic PAH concentration is likely to be very small. The assumption was made that the cytoplasmic concentration was negligible in comparison to the other contributions to the mass balance. Thus, when all these assumptions and equations were applied to equation 4-14, equation 4-17 describing the ratio of the cell pellets was obtained.

$$\frac{y_{avg}}{y'_{avg}} = \frac{2(\alpha + 1)}{\left(\alpha + \frac{\alpha \delta (\alpha + 1)}{(\alpha \delta + 1)}\right)} \frac{C_{liq}}{C'_{liq}} \quad (4-17)$$

This expression contains two unknown variables, α and δ , which are themselves calculated from three unknown parameters : K_{om} , P_{om} , and P_{im} . From this equation the ratio of the permeability coefficients can be determined if the ratio of the partition coefficients is known.

The unsteady-state component of transport that followed the addition of inhibitors was modeled for the mutant 1-51 strain. Since there was no metabolic activity, there was no generation term to consider in the transport equation. Furthermore, since active efflux

was fully inhibited, there was no movement of material out of the cell during the initial uptake. Thus, there are only uptake and accumulation terms to consider in the transport model. The concentration profile within the membrane will not be linear during the unsteady transport. Thus, an equation for the concentration profile across the membrane is required. If the cell is viewed as a cylinder, then the membrane must be viewed as a hollow cylinder. Since the diameter of the bacterium is assumed to be one third its length, the ends of the cylinder model cannot be ignored. Consequentially, transport in both the radial and lateral directions must be considered. A simpler approach is to approximate the membrane as a finite slab. With this approximation, the surface area can be assumed to be constant throughout the membrane and transport occurs in only one direction across the membrane. Since the membrane thickness is assumed to be approximately 1% of the radius of the cell, there is a small degree of error in assuming a fixed area for transport through the membrane. The concentration profile in the membrane can be defined by equations 4-18 and 4-19.

$$\frac{dy_{om}}{dt} = D_{om} \frac{d^2 y_{om}}{dx^2} = P_{om} L \frac{d^2 y_{om}}{dx^2} \quad (4-18)$$

$$\frac{dy_{im}}{dt} = D_{im} \frac{d^2 y_{im}}{dx^2} = P_{im} L \frac{d^2 y_{im}}{dx^2} \quad (4-19)$$

Equations 4-18 and 4-19 each require two boundary conditions and an initial condition to solve. The initial condition is the solution to the steady-state equations that will be developed shortly. The boundary conditions are given by equations 4-4 – 4-7. However, the liquid phase, periplasmic, and cytoplasmic concentrations are variable during uptake.

Either the periplasmic or cytoplasmic concentration can be defined by the mass balance for the cell pellet (equation 4-10). The liquid phase concentration can be defined by an overall mass balance (equation 4-20).

$$M = VC_i = Wy_{avg} + VC_{liq} + q \quad (4-20)$$

In this equation, VC_i is the initial amount of PAH in μmol added to the flask. The term q accounts for the amount of PAH lost to the equipment. Experiments with abiotic controls at different phenanthrene concentrations indicated a linear relationship between the liquid phase phenanthrene concentration and the amount lost to equipment. Thus, q is defined by equation 4-21.

$$q = 0.0388C_{liq} - 0.0268 \quad (4-21)$$

If it was possible to obtain values or equations for either the cytoplasmic or periplasmic concentrations, the concentration profiles could be fitted to experimental data that represent transport only to obtain values for the permeability coefficients. If it is assumed that the amount in the cytoplasm and periplasm is negligible, the total cell bound PAH is the sum of the amount at each point in the membrane (equation 4-22).

$$Wy_{avg} = A_o \int_0^L y_o(x) dx + A_i \int_0^L y_i(x) dx \quad (4-22)$$

In this equation, W is the weight of cells at an OD_{600} of 1 and can be obtained from data in Table 4.1. A value for δ can be obtained from equation 4-17 if α is known. δ can then be used to eliminate one of the permeability coefficients in equation 4-22. Equation 4-22

would then contain only one unknown, which could be obtained by fitting the equation to experimental data for y_{avg} after azide addition. However, as was previously discussed, the data obtained for the uptake of PAHs after azide addition is a combination of uptake kinetics and the kinetics of azide inhibition. Thus, no suitable data were obtained to fit a model.

The final component of modeling was active efflux. Since it was observed that active efflux was not saturated at the concentrations used (Figure 4.17) and since the cytoplasmic concentration is likely to be small, it was assumed that active efflux was operating in its linear regime. Research on antibiotic efflux indicated that the efflux pumps spanned both membranes (Nikaido, 1996). However, from the research conducted and from literature, it is uncertain if the efflux pumps remove compounds from the cytoplasm or from within the membrane itself. For this work, it was assumed that PAH was removed from the cytoplasm. Thus the rate equation for active efflux was assumed to be a first order reaction equation based on the cytoplasmic concentration and on a rate constant k_e . At steady-state, in the absence of azide, the flux across the outer membrane is equal to the flux across the inner membrane. This equality resulted in the already developed equation 4-16 for C'_p . Additionally, the flux of PAH across the inner membrane is equal to the rate of transport of PAH out of the cell by active efflux (equation 4-23).

$$k_e C_c = J_{im} = P_{im} A_i K_{im} (C'_p - C'_c) \quad (4-23)$$

The mass balance for the pellet concentration (equation 4-10) was rearranged for an expression for C'_c (equation 4-24).

$$C'_c = \frac{4zy'_{avg}(\alpha\delta + 1) - ((2\alpha\delta + 1)K_{om} + K_{im})C'_{liq}}{(\alpha\delta + 2)K_{im} + K_{om}} \quad (4-24)$$

Using equation 4-16, equation 4-23 was rearranged to express the rate constant in terms of the measured pellet concentration (equation 4-25) with substitution of equation 4-24 for C'_c . If P_{om} can be obtained from previous equations, a value for k_e can then be obtained.

$$k_e = \frac{P_{om} A_o K_{om}}{(\alpha\delta + 1)} \left(\frac{C'_{liq}}{C'_c} - 1 \right) \quad (4-25)$$

The initial unsteady-state uptake of PAH in the presence of active efflux can be modeled. Equations 4-18 , 4-19, and 4-22 apply to the initial uptake if the same assumptions are used. There is an initial condition of zero PAH concentration at all points in the membrane. Once again, the boundary conditions are given by equations 4-4 – 4-7. Similar to uptake after azide addition, the liquid phase, periplasmic, and cytoplasmic concentrations are variable during the initial uptake. The cytoplasmic concentration is defined by the transport equation for efflux (equation 4-23). The periplasmic concentration is defined by the mass balance on the cell pellet (equation 4-10). Lastly, the liquid phase concentration can be defined by the overall instantaneous mass balance (equation 4-20).

4.11.2 Model Fitting

For equation 4-17, a comparison of calculated pellet concentration ratios for assumed values of α and δ gives an indication of the relative importance of these two parameters.

Equation 4-17 was rearranged to give equation 4-26.

$$f = \frac{y_{avg} C'_{liq}}{y'_{avg} C_{liq}} = \frac{2(\alpha + 1)}{\left(\alpha + \frac{\alpha\delta(\alpha + 1)}{(\alpha\delta + 1)}\right)} \quad (4-26)$$

Calculated values of f for assumed values of α and δ are plotted in Figure 4.43. Using the experimentally obtained values of $C'_{liq}=2.46 \mu\text{mol/L}$, $C_{liq}=1.38 \mu\text{mol/L}$, $y'_{avg}=2.78 \mu\text{mol}/(\text{gram dry wt})$, and $y_{avg}=10.47 \mu\text{mol}/(\text{g dry wt})$ from Figure 4.7 for the transport of phenanthrene in the mutant 1-51 strain, f was experimentally determined to be 6.74.

Values of δ versus α that give a value of $f=6.74$ are plotted in Figure 4.44. What both these graphs indicate is that there is a narrow range α values that meet the experimentally obtained concentrations for phenanthrene transport. In contrast, there is no limit on δ .

Figure 4.44 shows that if α is increased beyond 0.42, and negative value of δ is required to meet the experimentally observed conditions. Since permeability coefficients cannot be negative, α is bounded by a maximum value of 0.42. Thus, the inner membrane partition coefficient is a minimum of 2.4 times that of the outer membrane. If the ratio of partitioning between the outer membrane and inner membrane is closer to 0.42, then δ will approach a value of zero. In such a situation, the outer membrane permeability will be significantly smaller than the inner membrane permeability and thus will be rate controlling in the transport of phenanthrene. Figure 4.44 also shows that as α approaches zero, δ approaches infinity. Thus, as the outer membrane partition coefficient becomes

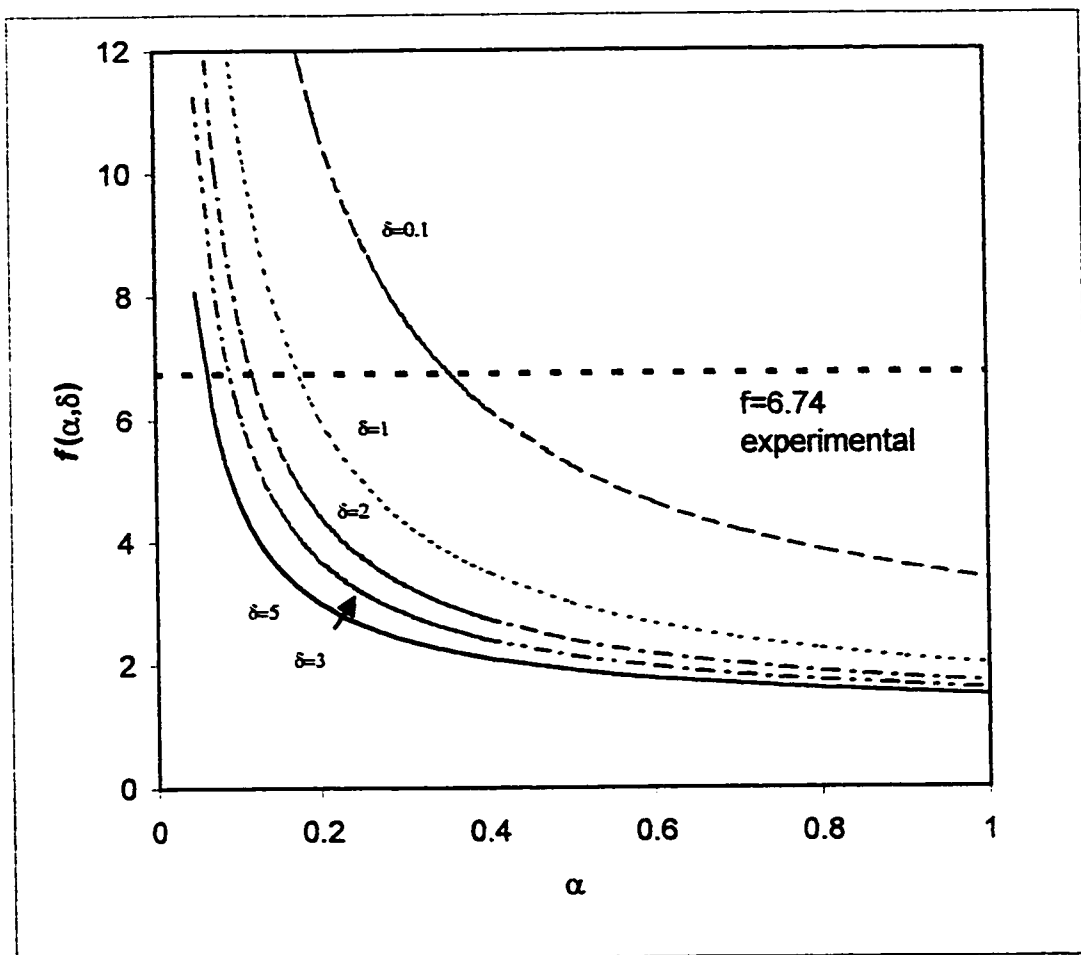


Figure 4.43 Plots of equation 4-26 for a range of values of α and δ

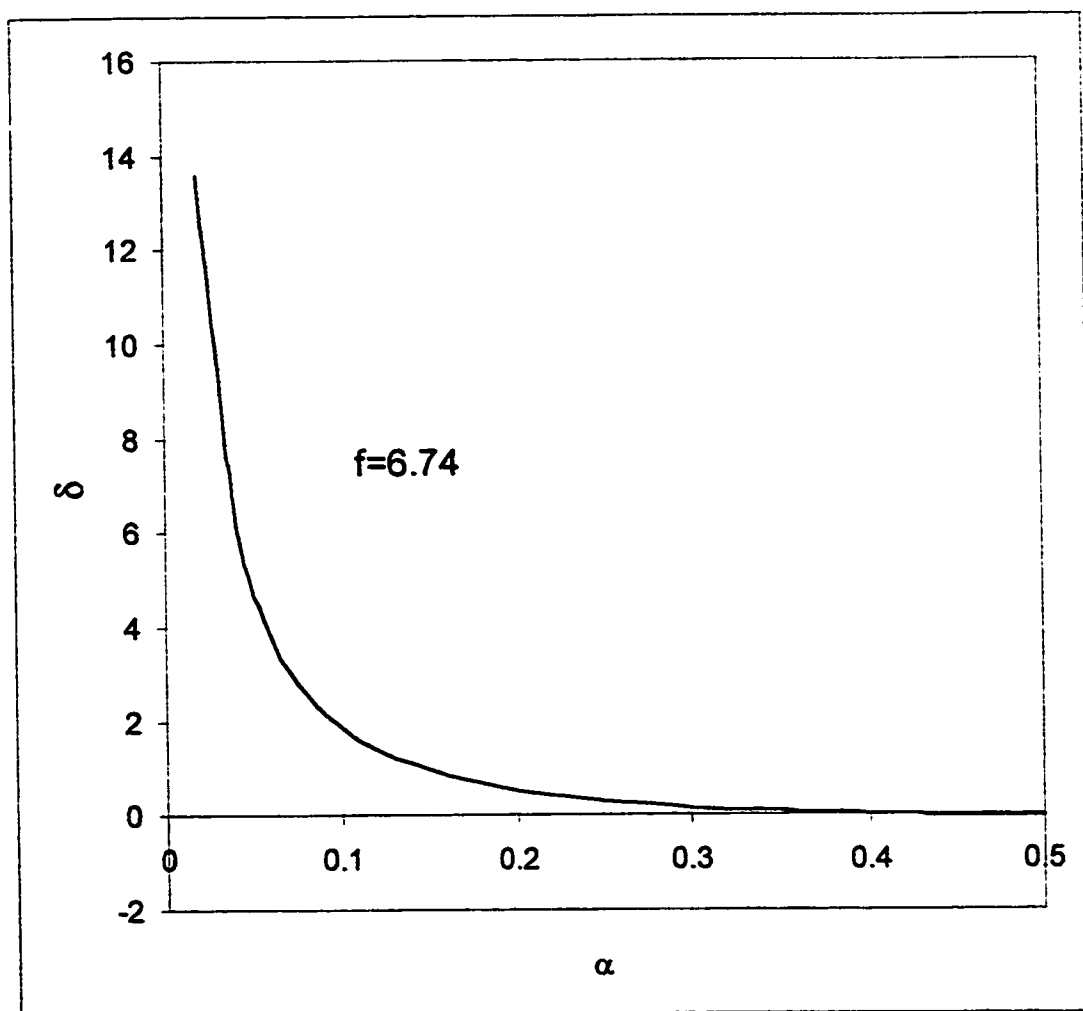


Figure 4.44 Plot of α and δ values that give the experimentally obtained value of $f=6.74$ for phenanthrene transport

negligible, the inner membrane permeability becomes rate controlling. When considering that PAHs partition to the interior of the lipid bilayer, a reasonable argument can be that the two partition coefficients are unlikely to differ by more than an order of magnitude. Thus, a reasonable hypothesis would be that the outer membrane is rate controlling.

Similar graphs can be made for the transport behaviour of fluoranthene and anthracene. From Figure 4.26 for fluoranthene transport in LP6a mutant 1-51, an experimental value of $f=5.23$ is obtained. Similarly, from Figure 4.22 for anthracene transport in LP6a mutant 1-51, an experimental value of $f=2.80$ is obtained. Figure 4.45 gives δ values for assumed values of α for fluoranthene transport. This graph displays a similar trend to Figure 4.43 for phenanthrene transport. Likewise, Figure 4.46 gives δ values for assumed values of α for anthracene transport and this also displays a similar trend to Figure 4.44. In both Figures 4.45 and 4.46, there is no limit imposed on values for δ . Also, in both graphs there is an upper limit placed on α . As α approaches its upper limit, the outer membrane permeability becomes rate controlling. What differs in Figures 4.44, 4.45, and 4.46 is the value of the upper limit for α . For fluoranthene transport, α has an upper limit of approximately 0.6. For anthracene transport, the upper limit is 2.4. While there is insufficient data to formulate a correlation, it does appear that as the aqueous solubility of the PAHs decreases, the maximum ratio of partitioning between the outer and inner membrane increases.

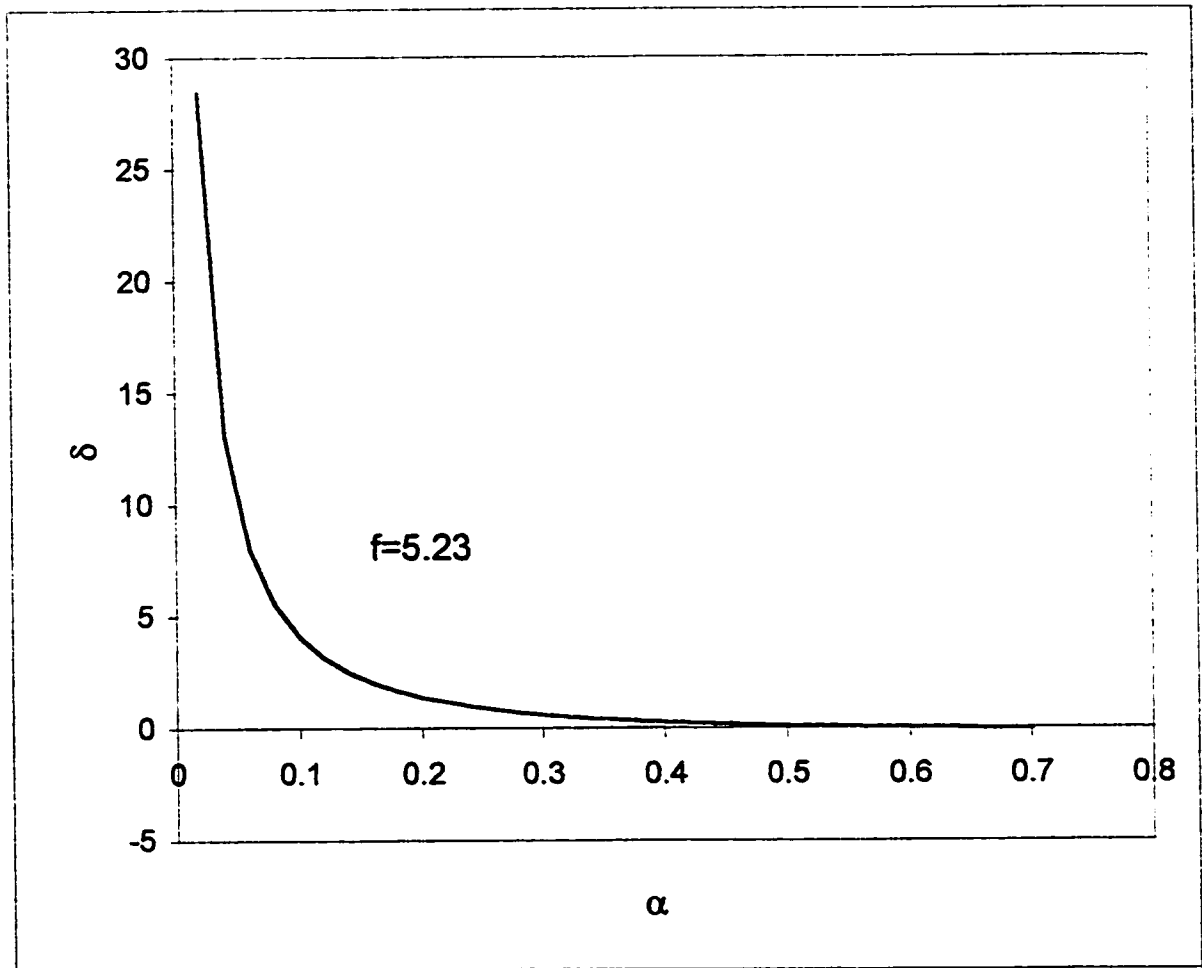


Figure 4.45 Plot of α and δ values that give the experimentally obtained value of $f=5.23$ for fluoranthene transport

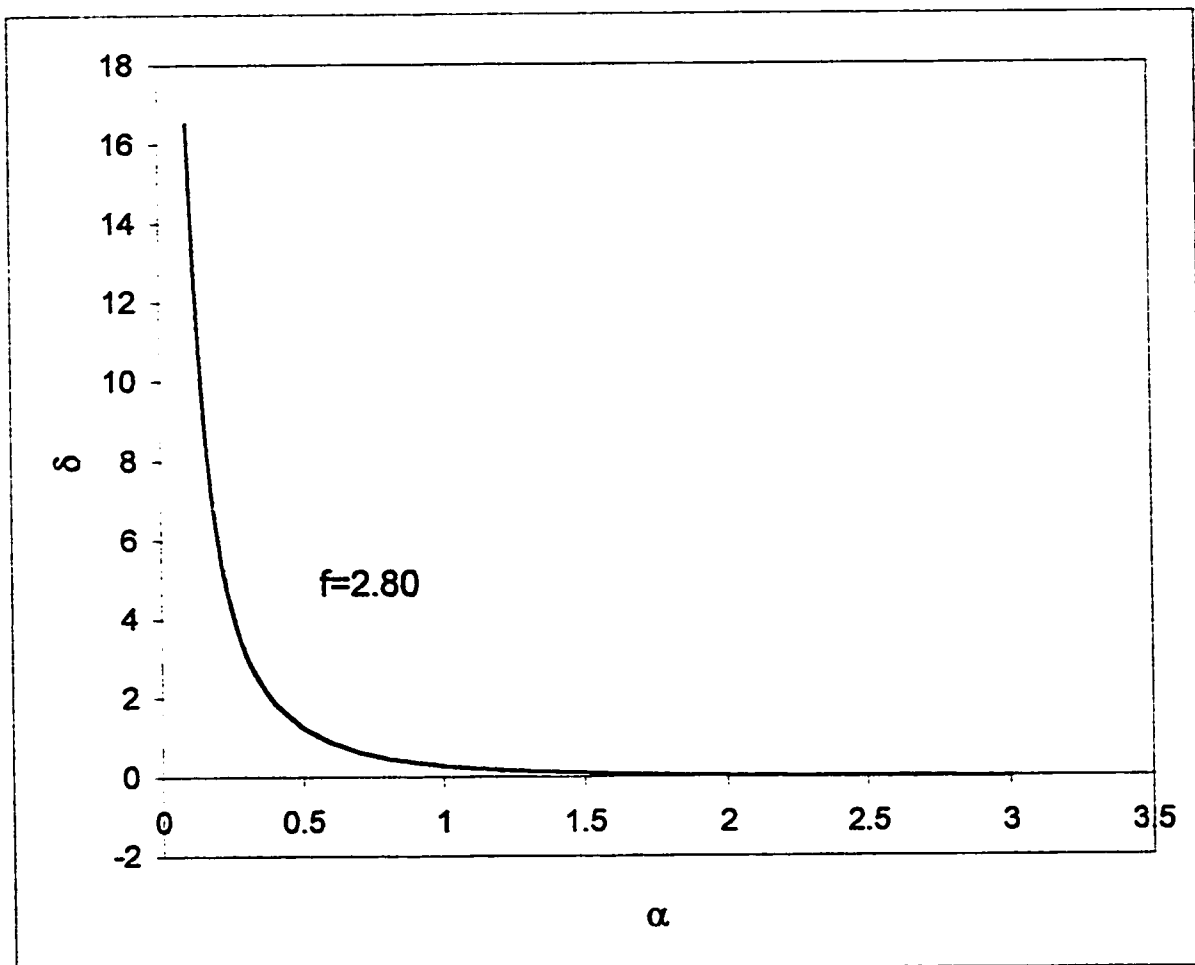


Figure 4.46 Plot of α and δ values that give the experimentally obtained value of $f=2.80$ for anthracene transport

A lower bound on membrane permeability can be obtained by examining the rate at which steady-state is achieved for phenanthrene transport. In Figure 4.7, the steady-state was essentially reached by the time the first data point was obtained. Accounting for the time to process the sample, it can be assumed that the cell concentration goes from zero to a steady-state concentration in a maximum of 2 min. The mean flux of material into the cell can be approximated by equation 4-27.

$$\bar{J}_{\min} = \frac{Wy'_{\text{avg}}}{A_o \Delta t} \quad (4-27)$$

The amount of phenanthrene in the cell (Wy'_{avg}) can be obtained from Table 4.1 and Figure 4.8. A value of $W=0.00751$ g dry weight in 20 mL and a steady-state phenanthrene concentration of $y'_{\text{avg}}=2.78$ $\mu\text{mol/g}$ dry wt were used. The assumed bacterial dimensions give a total cell surface area of 0.42 m^2 in 20 mL for a cell count of 1.9×10^9 cells/mL (Table 4.1). Thus, the minimum average flux of material into the cell is calculated to be $4.1 \times 10^{-4} \mu\text{mol}/(\text{m}^2 \cdot \text{s})$. If the outer membrane is assumed to be controlling, then the concentration at the outer membrane-periplasm interface is negligible. Also, if the outer and inner membrane partition coefficients are assumed to be equal, then a value of $K_{\text{om}}=K_{\text{avg}}=5.6$ L/g dry wt is obtained. From equation 4-4, the membrane concentration at the outer membrane-liquid interface is calculated as being $3.03 \times 10^4 \mu\text{mol}/\text{m}^3$ using an experimentally obtained steady-state liquid phase phenanthrene concentration of $2.46 \mu\text{mol/g}$ dry wt (Figure 4.8) and a calculated value of $z=2.2 \times 10^3$ g dry wt/L membrane volume to convert the concentration from g dry wt basis to membrane volume basis. From equation 4.1 for the flux into the outer membrane, the

outer membrane permeability coefficient can be calculated. Using the assumed values described above, a minimum value of $P_{om}=1.35 \times 10^{-11}$ m/s was obtained. Since the permeability coefficient is approximately equal to the diffusion coefficient divided by the membrane thickness, a minimum value of $D_{eff,om}=5.5 \times 10^{-20}$ m²/s was calculated.

The obtained values for P_{om} and $D_{eff,om}$ are minimum estimates for the resistance in the outer membrane. In comparison, typical values for diffusion coefficients in various liquids and solids are in the range of 10^{-10} to 10^{-12} m²/s (Welty et al., 1984). Thus, the calculated values are extremely low. This comparison could imply that steady-state is achieved on an order of 10^8 times faster than the assumed 2 minutes. If a typical value of 10^{-12} m²/s is assumed for a diffusion coefficient, then steady-state would be established in a time period of 6.57×10^{-6} s. This is extremely quick and transport is unlikely to proceed at that rate. Alternatively, a comparison can be made between the calculated diffusion coefficient and typical values in polymers can indicate that LP6a has a much lower membrane permeability than can be estimated from typical values. The most likely scenario is a combination of the two situations. LP6a has a most likely has a outer membrane permeability lower than that predicted by typical diffusion coefficients but larger than the estimated value of 1.35×10^{-11} m/s. Thus, steady-state is also achieved more quickly than 2 minutes but not as quick as the estimated 6.57×10^{-6} s using typical values.

5.0 CONCLUSIONS AND RECOMENDATIONS

Experiments on the transport of phenanthrene in *Pseudomonas fluorescens* LP6a indicated that phenanthrene was transported into LP6a wild-type, mutant 1-51, and cured strains by passive transport. The specific mechanism of uptake could not be determined as a result of the low solubilities of PAHs. Phenanthrene was also subject to an energy mediated efflux mechanism that could be inhibited by azide, cyanide, and CCCP. A minimum inhibitory azide concentration between 1 and 10 mM was required to inhibit active efflux. An azide concentration of 30 mM was sufficient to completely inhibit active efflux. Further research into the mechanism of active efflux and inhibition may indicate why such a high concentration of inhibitor was required. From the presence of active efflux in the cured strain, it was concluded that the genes for active efflux are chromosomally encoded and potentially not related to PAH degradation.

Research indicated that phenanthrene rapidly partitioned into LP6a, indicating a high permeability of the cell wall and membranes. Experiments at different phenanthrene concentrations showed a linear relationship between liquid phase and cell pellet phenanthrene concentration when active efflux was inhibited. An average partition coefficient of 5.6 g/L was obtained. From the linear relationship, it was concluded that LP6a has a high capacity to accumulate PAH in the membrane. When active efflux was active, there was also a linear relationship between the liquid and cell phase concentrations. A partition coefficient of 0.68 g/L was obtained for the wild-type strain and 0.78 g/L for the mutant 1-51 strain. Comparison of the partition coefficients for

inhibited and non-inhibited cells indicated that active efflux was able to reduce the cell phenanthrene concentration by a factor of seven. Thus, active efflux is effective at maintaining low PAH concentrations in the cell. The linear relationship in the presence of active efflux indicates that both passive transport and active efflux are not saturated at the concentrations used. Thus, active efflux has a high capacity relative to cell concentrations of phenanthrene. Also, passive transport is either proceeding by diffusion or a facilitated transport mechanism that has a high capacity for PAH. Adding more phenanthrene to the system after equilibrium or steady-state is reached would allow for higher liquid and cell concentrations. Such experiments may identify the saturation point for active efflux and may conclude whether uptake is by passive diffusion or facilitated transport.

Attempts to induce active efflux by incubation with phenanthrene indicated no difference in the transport of phenanthrene between induced cells and non-induced cells. Thus, the active efflux mechanism may be constitutively expressed. It was also observed that a low level of PAH metabolism was constitutively expressed in the wild-type strain. Liquid-liquid extraction of the supernatant from transport studies proved that a majority of the phenanthrene was metabolized by the LP6a wild-type over the 25-min time period used in transport studies. Thus, the metabolic enzymes are also constitutively expressed.

Experiments on the transport of other PAHs showed that, in addition to phenanthrene, fluoranthene and anthracene are also subject to active efflux in LP6a. However, naphthalene was not. This selectivity in transport is different from behaviour observed in

other efflux pumps. Organic solvent and antibiotic-resistant bacteria have broad specificity. Organic solvent bacteria are also resistant to antibiotics and vice versa. The results observed for active efflux in LP6a show selectivity, which suggests differences between PAH efflux in LP6a and organic solvent efflux. The experiments on the transport of toluene in LP6a were not conclusive in supporting this hypothesis. Further research needs to be conducted on the possible connection between PAH efflux and solvent and antibiotic efflux to confirm the observed results. This could be explored through transport studies on organic solvents. It could also be investigated through the ability of LP6a to survive in media containing high concentration of organic solvents or antibiotics that are subject to active efflux. The transport of other PAHs by active efflux needs to be further studied to generate a better understanding of the degree of selectivity. Also, a linear relationship was observed between the liquid-cell pellet partition coefficients and the corresponding octanol-water partition coefficients for the different PAHs in the presence of inhibitory levels of azide. Whether this relationship applies to PAHs of higher molecular weights is uncertain.

A mathematical model was developed to predict the PAH concentration in the bacteria. However, given the number of parameters, it was not possible to determine unique values for the permeability and partition coefficients of the outer and inner membranes. However, for anthracene, fluoranthene, and phenanthrene, it was determined that the ratio of partition coefficients (α) was restricted to a narrow range of values whereas the ratio of permeabilities (δ) was not. For phenanthrene, it was determined that α has a maximum value of 0.42 for the transport of phenanthrene. It was also argued that since α

is likely to be closer to 0.42, the outer membrane permeability is rate controlling in the uptake of phenanthrene. Also, a minimum value of 1.35×10^{-11} m/s was calculated for the outer membrane permeability. However, it is likely that the actual value is much larger. It was also determined that α had a maximum value of 0.6 for fluoranthene transport and 2.4 for anthracene transport.

The biggest question that arose from this research was the origin of the efflux pump. The presence of metabolism and active efflux provide two conflicting processes in the LP6a wild-type strain. Due to potential toxic effects of PAHs as a result of membrane expansion, active efflux may be a necessary process to allow the survival of the bacterium. However, it is also possible that the bacterium was originally resistant to the toxic effects of PAHs and later inherited the ability to degrade PAH through receiving a plasmid from another PAH-degrading donor. In such a case, if active efflux can be deactivated by a non-toxic mechanism, the ability of LP6a to degrade PAHs would be greatly enhanced. Given the observed rate of metabolism in the presence of active efflux, LP6a would become a highly effective tool in the remediation of contaminated sites if the active efflux mechanism were removed. Genetic analysis of the genes encoding the efflux mechanism may provide insight into a means by which to interrupt the efflux pump. Also, genetic analysis of the genes would give an idea of the evolutionary origin of this efflux pump. Comparison of the efflux genes in LP6a to those for other efflux pumps, particularly those in organic solvent-tolerant and antibiotic-resistant bacteria, would give an indication of the degree of similarity or difference to other efflux processes.

6.0 REFERENCES

- Alexander, M., Biodegradation and Bioremediation, Academic Press Inc., San Diego, CA, USA, (1994)
- Bateman, J.N., Speer, B., Feduik, L., and Harline, R.A., "Naphthalene association and uptake in *Pseudomonas putida*", Journal of Bacteriology **166** (1986) 155-161.
- Bouchez, M., Blanchet, D., Vandecasteele, J-P, "An interfacial uptake mechanism for the degradation of pyrene by a *Rhodococcus* strain", Microbiology **143** (1997) 1087-1093
- Bouchez-Naïtali, M., Rakatozafy, H., Marchal, R., Leveau, J.Y., and Vandecasteele, J.P., "Diversity of bacterial strains degrading hexadecane in relation to the mode of substrate uptake", Journal of Applied Microbiology **86** (1999) 421-428
- Brock, T.D., Madigan, M.T., Martinko, J.M., and Parker, J., Biology of Microorganisms, 7th Edition, Prentice Hall, Englewood Cliffs, NJ, USA, (1994)
- Cerniglia, C.E., "Microbial metabolism of polycyclic aromatic hydrocarbons", Advances in Applied Microbiology **30** (1984) 31-71
- Cookson, J.T., Jr., Bioremediation Engineering: Design and Application, McGraw Hill Inc., New York, NY, USA (1995)
- Dawson, R.M.C., Elliott, D.C., Elliot, W.H., and Jones, K.M., Data for Biochemical Research, 2nd Edition, Oxford University Press, Oxford, England, (1969)
- De Bont, J.M., "Solvent-tolerant bacteria in biocatalysis", Trends in Biotechnology **16** (1998) 493-499
- De Young, L.R., and Dill, K.A., "Solute partitioning into lipid bilayer membranes", Biochemistry **27** (1988) 5281-5289
- Foght, J.M., and Westlake, D.W.S., "Transposon and spontaneous deletion mutant of plasmid-borne genes encoding polycyclic aromatic hydrocarbon degradation by a strain of *Pseudomonas fluorescens*" Biodegradation, **7** (1996) 353-366
- Gobas, F.A.P.C., Lahittete, J.M., Garofalo, G., and Shiu, W.Y., "A novel method for measuring membrane-water partition coefficients of hydrophobic organic chemicals: comparison with 1-octanol-water partitioning", Journal of Pharmaceutical Sciences **77** (1988) 265-272

Groenewegen, P.E.J., Driessen, A.J.M., Konings, W.N., and de Bont, J.A.M., "Energy-dependent uptake of 4-chlorobenzoate in the *Coryneform* bacterium NTB-1", Journal of Bacteriology **172** (1990) 419-423

Harold, F.M., The Vital Force: A Study of Bioenergetics, W.H. Freeman and Company, New York, NY, USA, (1986)

Heipieper, H.J., Weber, F.J., Sikkema, J., Keweloh, H., and de Bont, J.A.M., "Mechanisms of resistance of whole cells to toxic organic solvents", Trends in Biotechnology **12** (1994) 409-415

Higgins, S.J., and Mandelstam, J., "Evidence for induced synthesis of an active transport factor for mandelate in *Pseudomonas putida*", Biochemical Journal **126** (1971) 917-922

Kaback, H.R., "Molecular biology and energetics of membrane transport", Journal of Cell Physiology **89** (1976) 575-594

Keuth, S. and Rehm, H.-J., "Biodegradation of phenanthrene by *Arthrobacter polychromogenes* isolated from a contaminated soil", Applied Microbiology and Biotechnology **34** (1991) 804-808

Kieboom, J., Dennis, J.J., Zylstra, G.J., and De Bont, J.A.M., "Active efflux of organic solvents by *Pseudomonas putida* S12 Is Induced by Solvents", Journal of Bacteriology **180** (1998) 6769-6772

King, R.B., Long, G.M., and Sheldon, J.K., Practical Environmental Bioremediation: the field guide, Lewis Publishers, Boca Raton, FL, USA (1998)

Davis, K.L., Smith, H.R., and Day, S.M., "A comparative cost analysis: conventional treatment technologies and bioremediation", *Edited by* Schepart, B.S., Bioremediation of Pollutants in Soil and Water, ASTM, Philadelphia, PA, USA (1995)

Li, X., Zhang, L., and Poole, K., "Role of the multidrug efflux systems of *Pseudomonas aeruginosa* in organic solvent tolerance", Journal of Bacteriology **180** (1998) 2987-2991

Locher, H.H., Poolman, B., Cook, A.M., and Konings, W.N., "Uptake of 4-toluene sulfonate by *Comamonas testosteroni* T-2", Journal of Bacteriology **175** (1993) 1075-1080

Mackay, D.M., and Shiu, W.Y., "Estimating the multimedia partitioning of hydrocarbons: the effective solubility approach" In: Hydrocarbon Contaminated Soils and Groundwater **2**, Lewis Publishers Inc., MI, USA (1992)

Manahan, S.E., Hazardous Waste Chemistry, Toxicology, and Treatment, Lewis Publishers, Chelsea, MI, USA (1990)

Magin, R., Niesman, M., and Bacic, G., "Influence of fluidity on membrane permeability" *Edited by Aloia, R., Curtain, C., and Gordon, L., Advances in Membrane Fluidity: Membrane Transport and Information Storage 4, Wiley-Liss, New York, NY, USA, (1990) 221-237*

Marqusee, J.A., and Dill, K.A., "Solute partitioning into chain molecule interphases: monolayer, bilayer membranes, and micelles", Journal of Physical Chemistry **85** (1986) 434-444

Marrink, S.J., and Berendsen, S.J., "Permeation process of small molecules across lipid membranes studied by molecular dynamics simulations", Journal of Physical Chemistry **100** (1996) 16729-16738

McIntosh, T.J., Simon, S.A., and MacDonald, R.C., "The organization of n-alkanes in lipid bilayers", Biochimica et Biophysica Acta **597** (1980) 445-463.

Nikaido, H., and Vaara, M., "Molecular basis of bacterial outer membrane permeability", Microbiological Reviews **49** (1985) 1-32

Nikaido, H., "Permeability of the lipid domains of bacterial membranes" *Edited by Aloia, R., Curtain, C., and Gordon, L., Advances in Membrane Fluidity: Membrane Transport and Information Storage 4, Wiley-Liss, USA, (1990) 165-190*

Nikaido, H., "Multidrug efflux pumps of Gram-negative bacteria", Journal of Bacteriology **178** (1996) 5853-5859

Pinkart, H.C., Wolfram, J.W., Rogers, R., and White, D.C., "Cell envelope changes in solvent-tolerant and solvent-sensitive *Pseudomonas putida* strains following exposure to o-xylene", Applied and Environmental Microbiology **62** (1996) 1129-1132

Pothuluri, J.V., and Cerniglia, C.E., "Microbial metabolism of polycyclic aromatic hydrocarbons", *Edited by Chaudhry, G.R., Biological Degradation and Bioremediation of Toxic Chemicals, Dioscorides Press, Portland, Oregon, USA (1994)*

Ramos, J.L., Duque, E., Godoy, P., and Segura, A., "Efflux pumps involved in toluene tolerance in *Pseudomonas putida* DOT-T1E", Journal of Bacteriology **180** (1998) 3323-3329

Rogers, H., Perkins, H., and Ward, J., Microbial Cell Walls and Membranes, Chapman and Hall, London, England, (1980)

Rosen, B.P., Bacterial Transport, Marcel Dekker Inc., New York, NY, USA, (1978)

Sikkema, J., Poolman, B., Konings, W.N., and De Bont, J.A.M., "Effects of the membrane action of tetralin on the functional and structural properties of artificial and bacterial membranes", Journal of Bacteriology **174** (1992) 2986-2992

Sikkema, J., de Bont, J.A.M., Poolman, B., "Interactions of cyclic hydrocarbons with biological membranes", Journal of Biological Chemistry **269** (1994) 8022-8028.

Sikkema, J., de Bont, J.A.M., Poolman, B., "Mechanisms of membrane toxicity of hydrocarbons", Microbiological Reviews **59** (1995) 201-222

Smith, P.K., Drohn, R.I., Hermanson, G.T., Mallia, A.K., Gartner, F.H., Provenzano, M.D., Fujimoto, E.K., Goeke, N.M., Olson, B.J., and Klenk, D.C., "Measurement of protein using bicinchoninic acid", Analytical Biochemistry **150** (1985) 76-85.

Song, Hsu, F-L., and Au, J. L.-S., "Binding of taxol to plastic and glass containers and protein under in vitro conditions", Journal of Pharmaceutical Sciences **85** (1996) 29-31
Stein, W.D., Transport and Diffusion across Cell Membranes, Academic Press Inc., Orlando, FL, USA, (1986)

Stein, W.D., The Movement of Molecules across Cell Membranes, Academic Press Inc., New York, NY, USA, (1987)

Stelmack, P., "Effects of surfactants on microbial adhesion", Thesis, University of Alberta (1997)

Stringefellow, W.T., and Aitken, M.D., "Competitive metabolism of naphthalene, methylnaphthalenes, and fluorene by phenanthrene-degrading *Pseudomonads*", Applied and Environmental Microbiology **61** (1995) 357-362

Thayer, J.R., and Wheelis, M.L., "Active transport of benzoate in *Pseudomonas putida*", Journal of General Microbiology **128** (1981) 1749-1753

Weber, F.J., and de Bont, J.A.M., "Adaptation mechanisms of microorganisms to the toxic effects of organic solvents on membranes" Biochimica et Biophysica Acta **1286** (1996) 225-245

Welty, J.R., Wicks, C.E., and Wilson, R.E., Fundamentals of Momentum, Heat, and Mass Transfer, 3rd Edition, John Wiley and Sons, Toronto, Canada, (1984)

White, D., The Physiology and Biochemistry of Prokaryotes, Oxford University Press, New York, NY, USA, (1995)

White, S.H., King, G.I., and Cain, J.E., "Location of hexane in lipid bilayers determined by neutron diffraction", Nature **290** (1981) 161-163

Whitman, B.E., Lueking, D.R., and Mihelcic, J.R., "Naphthalene uptake by a *Pseudomonas fluorescens* isolate", Canadian Journal of Microbiology **44** (1988) 1086-1093

APPENDIX A - MEDIA

Burke's Buffer with Glucose and Nitrogen (BBGN) Medium

	(g/L)
KH_2PO_4	0.2
K_2HPO_4	0.8
$\text{MgSO}_4 \cdot 7\text{H}_2\text{O}$	0.2
$\text{CaSO}_4 \cdot 2\text{H}_2\text{O}$	0.1
$\text{FeSO}_4 \cdot 7\text{H}_2\text{O}$	0.005
$\text{Na}_2\text{MoO}_4 \cdot 2\text{H}_2\text{O}$	0.00025
Glucose	10.0
$\text{CH}_3\text{COONH}_4$	1.1
pH	7.6

Bushnell Haas Medium

	(g/L)
MgSO_4	0.2
CaCl_2	0.02
KH_2PO_4	1.0
K_2HPO_4	1.0
NH_4NO_3	1.0
FeCl_3	0.05
pH	7

BYP Medium

	(g/L)
K ₂ HPO ₄	0.5
NH ₄ Cl	1.0
Na ₂ SO ₄	2.0
KNO ₃	2.0
MgSO ₄ ·7H ₂ O	0.2
FeSO ₄ ·7H ₂ O	trace
Proteose Peptone	1.0
Yeast Extract	1.0

Luria Bertani (LB) Medium

	(g/L)
Tryptone	10
Yeast Extract	5
NaCl	10
pH	7.5 (adjusted with NaOH)

0.1 M Phosphate Buffer pH 7

	(g/L)
KH ₂ PO ₄	6.65
K ₂ HPO ₄	13.35

APPENDIX B – SAMPLE CALCULATIONS

B1: Dry Weight

$$\text{Dry Weight per mL} = \frac{(\text{Weight of (Plate + Bacteria)} - \text{Weight of Plate} - \text{Weight of abiotic})}{\text{Assay Volume}}$$

B2: Cell Counts

Five grids of a 25 grid Petroff Hauser Counting Chamber were counted. The four corners and the centre grids were selected.

$$\# \text{ of cells/mL} = \frac{(\text{Sum of Counts}) * 5}{V} * \frac{1}{f}$$

Example:

$V=2E-5$ mL (Volume of Counting Chamber)

$f=0.1$ (sample diluted by a factor of 10)

Count 1: 120

Count 2: 119

Count 3: 115

Count 4: 113

Count 5: 113

of Cells =

$$\frac{(120 + 119 + 115 + 113 + 113) * 5}{2E-5} * \frac{1}{0.1} = 1.45 \times 10^9 \frac{\text{Cells}}{\text{mL}}$$

B3: Protein Assay

$$\text{Amount of Protein in Sample: } p = (mA + b) \frac{V_2}{V_1} \frac{1}{f}$$

m : slope of calibration curve

b : intercept of calibration curve

A : absorbance at 562 nm

p : amount of protein ($\mu\text{g/mL}$)

V_1 : volume of sample assayed (1mL)

V_2 : volume of standard assayed (0.1 mL)

f : dilution factor

Parameters for m and b obtained from calibration curve for protein standards (protein content plotted versus absorbance)

Example:

$$m = 383 \mu\text{g/mL}$$

$$b = -60.8 \mu\text{g/mL}$$

Sample Absorbance: 0.657

$$f = 0.1$$

$$V_1 = 1.000 \text{ mL sample}$$

$$V_2 = 0.100 \text{ mL BSA std}$$

Amount of Protein =

$$(0.657 * 383 \frac{\mu\text{g}}{\text{mL}} - 60.8 \frac{\mu\text{g}}{\text{mL}}) \frac{0.100 \text{ mL}}{1.000 \text{ mL}} * \frac{1}{0.1} = 191 \frac{\mu\text{g}}{\text{ml}}$$

B4: Amount of ^{14}C -labeled and non-labeled PAH added

$$V_1 = \frac{\text{Desired dpm}}{(2.2 \times 10^6 \frac{\text{dpm}}{\text{mL}}) \alpha C_1}$$

V_1 : Volume of radiolabeled PAH added to flask

α : activity of ^{14}C radiolabeled PAH ($\mu\text{Ci}/\mu\text{mol}$)

C_1 : Concentration of ^{14}C -PAH stock solution ($\mu\text{mol/L}$)

$$V_2 = \frac{C_i(V_i + V_1) - C_1V_1}{(C_2 - C_i)}$$

V_i : Volume in Flask

V_2 : Volume of Non-labeled PAH

C_2 : Concentration of non-labeled PAH standard ($\mu\text{mol/L}$)

C_i : Desired initial liquid phase concentration ($\mu\text{mol/L}$)

Example:

Desired dpm = 1×10^5 dpm

C_1 = 233.1 $\mu\text{mol/L}$

a = 19.5 $\mu\text{Ci}/\mu\text{mol}$

C_2 = 6253.6 $\mu\text{mol/L}$

C_i = 6.36 $\mu\text{mol/L}$

V_i = 20.0 mL

$$V_1 = \frac{1 \times 10^5 \text{ dpm}}{2.2 \text{E}6 \frac{\text{dpm}}{\mu\text{Ci}} * 19.5 \frac{\mu\text{Ci}}{\mu\text{mol}} * 233.1 \frac{\mu\text{mol}}{\text{L}}} = 10.0 \mu\text{L}$$

$$V_2 = \frac{6.36 \frac{\mu\text{mol}}{\text{L}} * (20.0 \text{ mL} + 0.010 \text{ mL}) - 233.1 \frac{\mu\text{mol}}{\text{L}} * 0.010 \text{ mL}}{(6253.6 - 6.36 \frac{\mu\text{mol}}{\text{L}})} = 20.0 \mu\text{L}$$

Thus, 20.0 μL of non-labeled PAH is mixed with 10.0 μL ^{14}C -labeled PAH and added to the flask to give an initial concentration of 6.36 $\mu\text{mol/L}$ with 100 000 dpm

B5: Liquid Scintillation Counts

$$\text{Fractional Amount} = \frac{\frac{(\text{Sample} - \text{BKG})}{V}}{\frac{\text{Stock}}{V_i}}$$

Sample: dpm for sample

BKG: dpm of Background

V: Volume of Sample Taken

Stock: Total dpm added to Flask as determined by liquid scintillation counting

V_f: Volume of Liquid in Flask

Example:

Sample Reading: 500 dpm

Background Reading: 20 dpm

Stock Reading: 100 000 dpm (total amount added to flask)

V=0.5 mL

V_f=20 mL

$$\text{Fractional Amount} = \frac{\frac{(500 - 20 \text{dpm})}{0.5 \text{mL}}}{\frac{100000 \text{dpm}}{20 \text{mL}}} = 0.192$$

Liquid Phase PAH Concentration = Fractional Amount * *C_i*

C_i: Initial Liquid Phase Concentration added

Example:

C_i=6.36 μmol/L

Fractional Amt=0.192

Liquid Phase PAH Concentration =

$$0.192 * 6.36 \frac{\mu\text{mol}}{\text{L}} = 1.22 \frac{\mu\text{mol}}{\text{L}}$$

Cell Pellet PAH Concentration = Fractional Amount * *C_i* / *W*

W: Dry weight for cell suspension at OD₆₀₀=1

Example:

Fractional Amount= 0.192

$$W=375.5 \mu\text{g/mL}=0.3755 \text{ g/L}$$

$$C_i=6.36 \mu\text{mol/L}$$

Cell Pellet PAH Concentration =

$$\frac{0.192 * 6.36 \mu\text{mol} / \text{L}}{0.3755 \text{ g} / \text{L}} = 3.25 \frac{\mu\text{mol}}{\text{g}}$$

B6: Partition Coefficient

Partition coefficient for phenanthrene obtained from linear fit to the data at different concentrations. For the wild-type data in the absence of azide, a straight line was fit to the liquid concentration data for the first three time points to obtain a y-axis (time zero) intercept for the liquid phase concentration in the absence of metabolism.

Partition coefficients for other PAHs obtained according to the formula below

$$K = \frac{y_{avg}}{C_{liq}}$$

y_{avg} : Average cell pellet PAH concentration

C_{liq} : Average liquid phase PAH concentration

B7: HPLC Analysis

$$\text{PAH Concentration} = \frac{\text{Area}_1}{\text{Area}_2} C_2$$

Area_1 : area count of sample

Area_2 : area count of standard

C_2 : concentration of standard

$$\text{PAH Concentration} = \frac{A_1}{A_2} C_2$$

A_1 : Absorbance of sample

A_2 : Absorbance of standard

C_2 : Concentration of standard

B8: Liquid Extractions

$$\text{PAH Conc} = \frac{(C_{e1} + C_{e2})V_a}{V_s} + \frac{C_a V_a}{V_t} \frac{V_{t1}}{V_{t2}}$$

C_{e1} : Concentration of 1st extraction from UV-vis spectroscopy or HPLC

C_{e2} : Concentration of 2nd extraction from UV-vis spectroscopy or HPLC

C_a : Concentration of extraction of centrifuge tube

V_a : Volume of acetonitrile to resuspended dried sample after evaporation of methylene chloride

V_{t1} : Volume of methylene chloride used to rinse centrifuge tube

V_{t2} : Volume of methylene chloride sampled from centrifuge tube

V_s : Volume of supernatant used for extractions

V_t : Total volume of cell suspension

Example

V_t = 20.0 mL

V_s = 10.0 mL

V_{t1} = 3.00 mL

V_{t2} = 2.00 mL

V_a = 0.500 mL

C_{e1} = 65.7 µmol/L

C_{e2} = 1.35 µmol/L

C_a = 36.4 µmol/L

PAH Concentration=

$$\frac{(65.7 + 1.35 \frac{\mu\text{mol}}{L}) * 0.500\text{mL}}{10.0\text{mL}} + \frac{(35.4 \frac{\mu\text{mol}}{L}) * 0.500\text{mL}}{20.0\text{mL}} \frac{3.00\text{mL}}{2.00\text{mL}} = 4.68 \frac{\mu\text{mol}}{L}$$

B9 : Statistical Analysis

$$95\% \text{ Confidence interval} = \text{average} \pm t_{0.975, n-1} \frac{s}{\sqrt{n}}$$

95% Confidence Interval on Difference=

$$(x_1 - x_2) \pm t_{0.975, n_1 + n_2 - 2} s_p \sqrt{\frac{1}{n_1} + \frac{1}{n_2}}$$

$$s_p = \sqrt{\frac{(n_1 - 1)s_1^2 + (n_2 - 1)s_2^2}{n_1 + n_2 - 2}}$$

APPENDIX C – STATISTICAL ANALYSIS

Table C.1: Comparison of 95% confidence intervals for cell enumeration of LP6a wild-type and mutant 1-51 strains at the 95% confidence limit

	LP6a		LP6a Mutant 1-51	
	Lower 95%	Upper 95%	Lower 95%	Upper 95%
Plate Count (CFU/mL)	1.74x10 ⁹	2.12x10 ⁹	1.62x10 ⁹	2.27x10 ⁹
Protein (µg/ml)	166	208	165	208
Dry Weight (µg/mL)	298	450	292	462

Table C.2 : Comparison of equilibrium and steady-state phenanthrene concentrations in LP6a Mutant 1-51 at the 95% confidence limit

	No Azide			Azide			Difference Between Concentrations
	Average	s	n	Average	s	n	
Liquid Conc. (µmol/L)	2.5	0.2	5	1.4	0.02	3	1.1±0.3
Pellet Conc. (µmol/L)	2.8	0.3	4	11.0	0.5	3	8.2±0.7

Table C.3 : Comparison of equilibrium and steady-state anthracene concentrations in LP6a Mutant 1-51 at the 95% confidence limit

	No Azide			Azide			Difference Between Concentrations
	Average	s	n	Average	s	n	
Liquid Conc. (µmol/L)	0.096	0.006	7	0.064	0.002	3	0.032±0.008
Pellet Conc. (µmol/L)	0.13	0.01	7	0.23	0.002	3	0.10±0.03

Table C.4 : Comparison of equilibrium and steady-state fluoranthene concentrations in LP6a wild-type at the 95% confidence limit

	No Azide			Azide			Difference Between Concentrations
	Average	s	n	Average	s	n	
Liquid Conc. ($\mu\text{mol/L}$)	0.47	0.02	7	0.31	0.02	3	0.16 ± 0.04
Pellet Conc. ($\mu\text{mol/L}$)	0.60	0.05	7	1.4	0.10	3	0.80 ± 0.10

Table C.5 : Comparison of equilibrium and steady-state fluoranthene concentrations in LP6a mutant 1-51 at the 95% confidence limit

	No Azide			Azide			Difference Between Concentrations
	Average	s	n	Average	s	n	
Liquid Conc. ($\mu\text{mol/L}$)	0.41	0.02	7	0.18	0.010	3	0.22 ± 0.02
Pellet Conc. ($\mu\text{mol/L}$)	0.68	0.04	6	1.6	0.119	3	0.92 ± 0.120

Table C.6: Comparison of equilibrium and steady-state naphthalene concentrations in LP6a mutant 1-51 at the 95% confidence limit

	No Azide			Azide			Difference Between Concentrations
	Average	s	n	Average	s	n	
Liquid Conc. ($\mu\text{mol/L}$)	2.9	0.06	7	2.9	0.1	21	0.0 ± 0.09
Pellet Conc. ($\mu\text{mol/L}$)	0.79	0.06	7	0.81	0.08	21	0.02 ± 0.08

Table C.7: Comparison of equilibrium and steady-state toluene concentrations in LP6a wild-type at the 95% confidence limit

	No Azide			Azide			Difference Between Concentrations
	Average	s	n	Average	s	n	
Liquid Conc. ($\mu\text{mol/L}$)	297	11	7	294	12	7	3 ± 14
Pellet Conc. ($\mu\text{mol/L}$)	21	11	7	27	2	7	6 ± 9

Table C.8: Comparison of equilibrium and steady-state toluene concentrations in LP6a mutant 1-51 at the 95% confidence limit

	No Azide			Azide			Difference Between Concentrations
	Average	s	n	Average	s	n	
Liquid Conc. ($\mu\text{mol/L}$)	295	14	7	316	12	7	21 ± 16
Pellet Conc. ($\mu\text{mol/L}$)	27	26	7	24	2	7	2 ± 2

Table C.9: 95% Confidence Intervals for Cell Pellet Toluene Concentrations in LP6a in the absence of azide

	Lower 95%	Upper 95%
Wild-type	11	30
Mutant 1-51	3.6	49

Table C.10: Comparison of pellet phenanthrene concentrations in LP6a mutant 1-51 at different azide concentrations to no azide at 95% confidence limit

Azide Concentration	Pellet Concentration ($\mu\text{mol/g}$)			Difference to no azide
	Average	s	n	
None	2.8	0.22	4	
1 mM	1.9	0.32	4	-0.9 ± 0.5
11 mM	7.2	0.37	3	4.4 ± 0.6

Table C.11: Comparison of pellet phenanthrene concentrations in LP6a mutant 1-51 at different azide concentrations at 95% confidence limit

Azide Concentration	Pellet Concentration ($\mu\text{mol/g}$)			Difference
	Average	s	n	
30 mM	8.9	0.7	3	
120 mM	11	1	3	2.1 ± 1.1

Table C.12 : Comparison of pellet phenanthrene concentrations in LP6a mutant 1-51 for different inhibitors at 95% confidence limit

	Pellet Concentration ($\mu\text{mol/g}$)			Difference
	Average	s	n	
10 mM Cyanide	6.4	0.7	3	
11 mM Azide	7.2	0.9	3	0.8 ± 1.9

Table C.13: Comparison of pellet phenanthrene concentrations in LP6a mutant 1-51 for different inhibitors at 95% confidence limit

	Pellet Concentration ($\mu\text{mol/g}$)			Difference
	Average	s	n	
50 μM CCCP	11	1	3	
120 mM Azide	11	1	3	0.55 ± 1.66

Table C.14: Comparison of Pellet Phenanthrene Concentrations in LP6a Mutant 1-51 for Induced and Non-Induced Cells at 95% Confidence Limit

	Pellet Concentration ($\mu\text{mol/g}$)			Difference
	Average	s	n	
Non-Induced	2.6	0.6	4	
Induced	2.5	0.5	4	-0.1 ± 0.9

Table C.15: 95% Confidence Intervals for phenanthrene Partition Coefficients in LP6a in the absence of azide

	Lower 95%	Upper 95%
Wild-type	0.50	0.85
Mutant 1-51	0.50	0.91

Table C.16: Comparison of calculated pellet phenanthrene concentration from model to 95% Confidence Interval for experimental results in LP6a mutant 1-51

	Pellet Concentration ($\mu\text{mol/L}$)		
	Calculated	Experimental	
		Lower 95%	Upper 95%
Steady-state	1.9	1.7	2.4
Equilibrium	8.5	9.8	12.1

Table C.17: Comparison of phenanthrene supernatant concentrations as analyzed by UV-vis from extractions at different pH

	pH 2			pH 7			Difference
	Average	s	n	Average	s	n	
LP6a	3.0	0.5	5	1.0	0.5	4	2.0±0.8
LP6a Mutant 1-51	2.7	1.1	5	2.8	0.6	5	-0.1±1.3
Abiotic control	4.7	0.6	4	3.5	0.7	4	1.2±1.1

Table C.18: Comparison of Supernatant Concentrations from extractions to those obtained by transport studies at 95% Confidence Limit

		Average	s	n	Difference from Transport Data
Abiotic control	Transport	4.4	0.1	7	
	UV-vis	3.5	0.7	4	-0.9±0.6
	HPLC	4.4	0.3	3	-0.01±0.26
LP6a	Transport	5.6	0.4	3	
	UV-vis	1.0	0.5	4	-4.62±0.86
	HPLC	0.39	0.36	5	-5.24±0.74
LP6a Mutant 1-51	Transport	2.5	0.2	5	
	UV-vis	2.8	0.6	5	0.3±0.5
	HPLC	2.5	0.8	5	-0.01±0.71